Organochloride Mediated Oxidation Reactions Induced by Ionizing Radiation

Dissertation

for the purpose of obtaining the degree of doctor
at Delft University of Technology,
by the authority of the Rector Magnificus Prof.dr.ir. T.H.J.J. van der Hagen,
chair of the Board for Doctorates,
to be defended publicly on
Thursday 20, March 2025 at 12.30

by

Juncheng LIU

Master of Chemistry, Beijing Normal University, China
Born in Tianjin, China

This dissertation has been approved by the promotors.

Composition of the doctoral committee:

Rector Magnificus	chairperson
Dr. R. Eelkema	Delft University of Technology, promotor
Dr. ir. A. G. Denkova	Delft University of Technology, promotor

Independent members

Prof. dr. J. H. van Esch	Delft University of Technology
Prof. dr. L. Siebbeles	Delft University of Technology
Prof. dr. Z. Liu	Peking University
Dr. M. Verdoes	Leiden University
Dr. K Djanashvili	Delft University of Technology

The research described in this thesis was performed in the Advanced Soft Matter (ASM) group of the department of Chemical Engineering and the Application of Radiation and Isotope (ARI) group of the department of Radiation Science and Technology, Faculty of Applied Sciences, Delft University of Technology, the Netherlands. The Chinese Scholarship Council partly financial supports this research.

The cover is partially generated by AI with major modification by Wankun Zhang and Juncheng Liu

ISBN: 978-94-6384-732-2

Printed in the Netherlands

Fortes fortuna adjuvat
Fortune favors the bold
命运厚爱勇敢之人

CONTENTS

Introduction 1

Cancer is among the leading causes of death worldwide. In 2022, there were almost 20 million new cases and 9.7 million cancer-related deaths globally. It is estimated that by 2040, the annual incidence of new cancer cases could rise to 29.9 million, with 15.3 million associated deaths.[1] The management of cancer presents a growing challenge, particularly in developing countries with large aging populations. Surgery, radiotherapy and chemotherapy are commonly applied treatments against cancer. Surgery is typically the first option for localized, accessible tumors, while chemotherapy is crucial for treating metastatic cancers. Radiotherapy is broadly classified into external beam radiotherapy, brachytherapy, and radionuclide therapy; the first two target locally advanced tumors, while the last one targets metastases. These therapies are often used in combination. For instance, external beam radiotherapy and consolidation chemotherapy are administered following surgery to control tumor regression. Combining cytotoxic drugs with radiation can lead to a variety of synergistic effects: the administration of one agent apparently increases the effect of another, such as reoxygenation after drug treatment therefore increasing radiation sensitivity, or more rapid cell proliferation after radiation and greater chemosensitivity. This multimodal approach generally leads to improved therapeutic outcomes,[2] with higher overall survival rates compared to single treatment, although accompanied by increased side effects.[3]

There is a growing need in cancer treatment to reduce the side effects of therapy in order to improve patients' well-being and enhance their quality of life after recovery. Reducing the side effects of cancer therapy could allow older and vulnerable individuals, who may not tolerate these side effects well, to receive proper treatment. Targeted drug delivery offers a promising approach to minimizing these side effects by caging the drugs until they reach the tumor, thereby reducing toxicity to healthy tissues. In response to specific stimuli present in the tumor, the drugs are released to target and damage cells in the affected area.

Ionizing Radiation-Targeted Drug Release

The concept of ionizing radiation-targeted drug release or activation was proposed at the end of the 20th century by Wilson et al., when studies on water radiolysis were well-developed, and researchers were seeking more efficient combinations of radiation and

drugs.[4, 5] Bioreductive prodrugs, such as nitroarylmethyl-functionalized nitrogen mustard, were of interest because the reduction of these prodrugs, initiated by radiation in hypoxic regions, could activate the cytotoxin.[6] However, nitroarylmethyl was not used as a radiation-sensitive group[7-9] due to its passive activation by cellular reductases and the low reducing capacity of radiation at clinically relevant doses. These limitations necessitate that radiation-sensitive prodrugs should react selectively with species generated from water radiolysis, releasing highly potent cytotoxins upon activation. In the past decade, several highly radiation-sensitive functional groups have been developed,[10-14] and highly toxic drugs have been used as the released agents.[15-17] These release systems have demonstrated efficient cell killing *in vitro* and *in vivo* upon exposure to clinically relevant doses of radiation, indicating the promising application of radiation-targeted drug release in combination with chemo-radiation therapy.

Research Goals

The research goal of this Thesis is to apply ionizing radiation-initiated reactions on radiation-targeted drug release. These reactions can work in cell culture media and are therefore promising for application *in vivo*. Specifically, we are interested in:

i. The mechanism of organochloride-mediated oxidation initiated by ionizing radiation.
ii. Does polymeric organochloride functionalize similar as small molecular organochloride?
iii. Development of substrates that can release drugs upon oxidation.

In this way, we aim to provide a new method to release drugs in response to radiation.

Outline of the Thesis

This Thesis focuses on organochloride-mediated oxidation reactions induced by ionizing radiation and explores the application of the oxidation reactions in targeted drug release.

In **Chapter 2**, we provide a comprehensive introduction to the principles of water radiolysis and the role of radiation-initiated reactions in targeted drug release. We discuss the reactivities of reactive species formed from water radiolysis and their compatibility with biological systems. Finally, we review recent progress in radiation-induced drug release in the context of combining radiotherapy and chemotherapy.

In **Chapter 3**, we demonstrate that stilbene derivatives can be oxidized by irradiating aqueous solution containing an organochloride. This was the first observation of organochloride-mediated oxidation. We identified the oxidizing species to be the peroxyl radicals. An amphiphilic block copolymer, using stilbene as the linker between two blocks, can be cleaved by this oxidation. Drug-loaded micelles composed of the polymer showed efficient drug release upon exposure to a clinical dose of irradiation in a phosphate-buffered solution containing chloroform.

In **Chapter 4**, we show that thioether compounds can be oxidized by the peroxyl radical. To reduce the toxicity of small molecular organochlorides, organochloride groups were attached covalently to the backbone of a hydrophilic polymer. The polymeric organochloride functioned similarly to small molecular organochloride, thereby extending the range of organochloride options.

In **Chapter 5**, we propose a reaction network for the formation pathway of the peroxyl radical and develop a mathematical model to simulate the yield of the peroxyl radical depending on organochloride and oxygen concentrations. Experiments using a thioether as a reductant to quantify peroxyl radical formation showed good agreement with the simulated data, verifying the proposed network.

In **Chapter 6**, we find that a boronic acid-caged drug can be oxidized by the peroxyl radical, resulting in efficient decaging reactions and drug release. The oxidation can be catalyzed by *N*,*N*-dimethylaniline derivatives to achieve a higher radiolytic yield of the decaging reaction. The prodrug demonstrated similar tumor cell-killing effects upon exposure to a clinical dose of irradiation compared to the parent drug.

Finally, we summarize our findings and provide an outlook on the potential future applications of organochloride-mediated oxidation reactions in anti-cancer therapy.

References

(1) International Agency for Research on Cancer. https://www.iarc.who.int

(2) Gordon Steel, G.; Peckham, M. J. Exploitable Mechanisms in Combined Radiotherapy-Chemotherapy: The Concept of Additivity. *Int. J. Radiat. Oncol. Biol. Phys.* **1979**, *5*, 85-91.

(3) Herskovic, A.; Martz, K.; Al-Sarraf, M.; Leichman, L.; Brindle, J.; Vaitkevicius, V.; Cooper, J.; Byhardt, R.; Davis, L.; Emami, B. Combined Chemotherapy and Radiotherapy Compared with Radiotherapy Alone in Patients with Cancer of the Esophagus. *N. Engl. J. Med.* **1992**, *326*, 1593-1598.

(4) Wilson, W. R.; Tercel, M.; Anderson, R. F.; Denny, W. A. Radiation-Activated Prodrugs as Hypoxia-Selective Cytotoxins: Model Studies with Nitroarylmethyl Quaternary Salts. *Anti-Cancer Drug Design* **1998**, *13*, 663-685.

(5) Wardman, P. Electron Transfer and Oxidative Stress as Key Factors in the Design of Drugs Selectively Active in Hypoxia. *Curr. Med. Chem.* **2001**, *8*, 739-761.

(6) Kriste, A. G.; Tercel, M.; Anderson, R. F.; Ferry, D. M.; Wilson, W. R. Pathways of Reductive Fragmentation of Heterocyclic Nitroarylmethyl Quaternary Ammonium Prodrugs of Mechlorethamine. *Radiat. Res.* **2002**, *158*, 753-762.

(7) Bonnet, M.; Hong, C. R.; Wong, W. W.; Liew, L. P.; Shome, A.; Wang, J. L.; Gu, Y. C.; Stevenson, R. J.; Qi, W.; Anderson, R. F.; et al. Next-Generation Hypoxic Cell Radiosensitizers: Nitroimidazole Alkylsulfonamides. *J. Med. Chem.* **2018**, *61*, 1241-1254.

(8) Wang, J. L.; Foehrenbacher, A.; Su, J. C.; Patel, R.; Hay, M. P.; Hicks, K. O.; Wilson, W. R. The 2-Nitroimidazole EF5 Is a Biomarker for Oxidoreductases That Activate the Bioreductive Prodrug CEN-209 under Hypoxia. *Clin. Cancer Res.* **2012**, *18*, 1684-1695.

(9) Wilson, W. R.; Hicks, K. O.; Pullen, S. M.; Ferry, D. M.; Helsby, N. A.; Patterson, A. V. Bystander Effects of Bioreductive Drugs: Potential for Exploiting Pathological Tumor Hypoxia with Dinitrobenzamide Mustards. *Radiat. Res.* **2007**, *167*, 625-636.

(10) Li, T. Y.; Pan, S. J.; Gao, S. Q.; Xiang, W. T.; Sun, C. X.; Cao, W.; Xu, H. P. Diselenide-Pemetrexed Assemblies for Combined Cancer Immuno-, Radio-, and Chemotherapies. *Angew. Chem. Int. Ed. Engl.* **2020**, *59*, 2700-2704.

(11) Ma, N.; Xu, H.; An, L.; Li, J.; Sun, Z.; Zhang, X. Radiation-Sensitive Diselenide Block Co-Polymer Micellar Aggregates: Toward the Combination of Radiotherapy and Chemotherapy. *Langmuir* **2011**, *27*, 5874-5878.

(12) Ding, Z.; Guo, Z.; Zheng, Y.; Wang, Z.; Fu, Q.; Liu, Z. Radiotherapy Reduces N-Oxides for Prodrug Activation in Tumors. *J. Am. Chem. Soc.* **2022**, *144*, 9458-9464.

(13) Fu, Q.; Li, H.; Duan, D.; Wang, C.; Shen, S.; Ma, H.; Liu, Z. External-Radiation-Induced Local Hydroxylation Enables Remote Release of Functional Molecules in Tumors. *Angew. Chem. Int. Ed.* **2020**, *59*, 21546-21552.

(14) Geng, J.; Zhang, Y.; Gao, Q.; Neumann, K.; Dong, H.; Porter, H.; Potter, M.; Ren, H.; Argyle, D.; Bradley, M. Switching on Prodrugs Using Radiotherapy. *Nat. Chem.* **2021**, *13*, 805-810.

(15) Fu, Q.; Gu, Z.; Shen, S.; Bai, Y.; Wang, X.; Xu, M.; Sun, P.; Chen, J.; Li, D.; Liu, Z. Radiotherapy Activates Picolinium Prodrugs in Tumours. *Nat. Chem.* **2024**, *16*, 1348-1356.

(16) Fu, Q.; Zhang, S.; Shen, S.; Gu, Z.; Chen, J.; Song, D.; Sun, P.; Wang, C.; Guo, Z.; Xiao, Y.; et al. Radiotherapy-Triggered Reduction of Platinum-Based Chemotherapeutic Prodrugs in Tumours. *Nat. Biomed. Eng.* **2024**.

(17) Yang, C.; Yang, Y.; Li, Y.; Ni, Q.; Li, J. Radiotherapy-Triggered Proteolysis Targeting Chimera Prodrug Activation in Tumors. *J. Am. Chem. Soc.* **2023**, *145*, 385-391.

2 The Role of Ionizing Radiation-Initiated Reactions in Targeted Delivery of Chemotherapeutics

Abstract

Ionizing radiation induced drug release has drawn significant attention recent years in combined chemo-radiation therapy with the purpose to reduce the systemic toxicity of chemotherapeutics. Radiation acts both for radiotherapy and as the targeting stimulus. To understand radiation-induced drug activation and to design new radiation-sensitive chemotherapeutics, it is important to become familiar with the underlying concepts and mechanisms. Here, we provide an overview of the crucial process of water radiolysis by ionizing radiation, the mechanism and kinetics of the generation of reactive species, and reactivity of these species with cellular components and chemical functional groups, to give insight into selective drug activation in complex cellular environments. We then discuss recent progress on radiation induced drug release focusing on the reaction of reactive species with drug caging groups and the yield of released drugs. We aim to bridge the gap between basic chemical processes in water radiolysis and its relevance for drug release, and provide suggestions on the design of radiation sensitive prodrugs or nanocarriers.

Availability and Contributions

This chapter is a review article by Liu, J.; Denkova, A. G.; Eelkema, R. currently in preparation for submission.

J.L. conducted the literature search, designed the figures and schemes and wrote the first draft. A.D. and R.E. secured the funding and corrected the manuscript.

Introduction

Surgery, chemotherapy, and radiotherapy are the primary treatments for malignant tumors. These therapies, with distinct mechanisms, are often used in combination to enhance therapeutic efficacy and minimize side effects.[1] External-beam radiotherapy employ high-energy photons, such as X-rays or gamma-rays, to treat tumors, while radionuclide therapy typically uses beta-minus particles. Radiotherapy kills cancer cells either by direct interaction between radiation and DNA, or indirectly by creating reactive species that then damage DNA. Photons and beta-minus particles rely mostly on indirect damage through radical formation, accounting for around 70% of the induced DNA damage. High linear energy transfer (LET) particles such as alpha particles induce mostly direct DNA damage, which is often clustered and therefore, difficult to repair.

Chemotherapy uses cytotoxic drugs to treat localized tumors or metastasized cancer, inducing cell death or inhibiting proliferation. However, the systemic administration of chemotherapeutics in many cases causes severe side effects to normal tissues, thereby limiting the dose of the administered drug, affecting patient wellbeing and often limiting treatment duration. Enhancing the effectiveness of cancer therapy involves either increasing the effects on tumors or reducing the impact on surrounding tissues.[2] Stimuli-response drug release offers a way to reduce the side effects to healthy tissues. Nanocarriers and prodrugs targeting internal stimuli (e.g., pH[3], tumor hypoxia[4] and enzymes[5]) and external stimuli (e.g., near-infrared light[6] and ultrasound[7]) have been extensively studied to treat various types of cancers.[8]

A combination of radiotherapy and systemic drug administration leads to a variety of treatment consequences.[9,10] For example, treating a tumor with radiation results in more rapid cell proliferation, thereby making the tumor more sensitive to chemotherapeutics. Ionizing radiation-triggered drug release offers significant opportunities in combining radiotherapy and chemotherapy. Unlike traditional chemoradiation therapy, radiation-triggered drug release can exploit the different therapeutic mechanisms of the two treatments, potentially reducing the systemic toxicity of anti-tumor drugs and enhancing overall treatment efficacy. Various drug carriers have been reported for ionizing radiation-initiated drug release system, including metal-organic frameworks (MOFs), covalent

organic frameworks[11] (COF), polymeric nano-aggregates[12] and prodrugs. Besides, radiation-induced versions of photodynamic therapy[13-15] (PDT) and photothermal therapy (PTT) have also been reported. The interaction of these therapies with various cell lines or tumors has been discussed in recent reviews.[16,17] Different from radiation-initiated PDT effects, where heavy elements with high cross sections are employed to convert the energy from radiation to photosensitizer, activation of prodrugs relies on chemical reactions with species generated from radiolysis of water, since most prodrugs (organic compounds) do not absorb radiation to any significant degree.

The successful design of radiation-triggered drug release systems requires an understanding of the generation of radiolytic species and their interaction with different organic molecules used to trigger release. In this review, we will start with the fundamentals of radiation chemistry, discussing the physical processes and chemical reactions taking place from sub-picoseconds to pseudo-steady-state microsecond time scales. On the microsecond time scale, scavengers and prodrugs are able to react with species from water radiolysis (e.g., aqueous electron, hydroxyl radical and hydrogen peroxide). We will discuss the radiolytic yields and reactivity of these species and reason which species are more relevant for triggering drug release. As the drug release has to be performed in the tumor microenvironment, the compatibility and limitations of these species will be discussed to give an expectation of the yield of released drug. Finally, we will discuss boundary conditions of radiation-initiated drug release systems, illustrated by recently published examples. Through this review, we aim to shift attention from the current applications of radiation-initiated drug release to a deeper understanding from the perspective of radiation chemistry.

The Basic of Radiation Chemistry

Interactions of ionizing radiation with water

Before discussing the radiation-initiated chemical processes of drug release from prodrugs and nanocarriers, it is essential to briefly introduce the fundamentals of radiation chemistry in aqueous solutions. A key characteristic of ionizing radiation is that the interaction of radiation with matter depends on the atomic makeup of the matter and much less on the

molecular structure.[18] Therefore, radiation energy is absorbed by the molecules present in the system in proportion to their relative abundance, and energy absorption is most likely to result in the ejection of an electron and the ionization of the molecule. In the case of irradiation of dilute aqueous solutions ([solute] < 0.1 M), broadly speaking only water molecules are ionized, and any subsequent radiation-initiated reactions are mediated by the products of water radiolysis.[19] Therefore, understanding the radiation chemistry of water radiolysis is crucial for designing radiation-activated prodrugs.[20,21]

Figure 2.1 outlines the physical process and following chemical process of the ionization of water. The primary ionizing processes are the interactions of high energy photons (such as gamma-rays and X-rays) or charged particles (such as electrons, protons and alpha-particles) with water, causing ionization (reaction **1**) or electronic excitation (reaction **2**). The H_2O^+ produced in reaction **1** undergoes an ion-to-molecule reaction with another water molecule to form ·OH and hydronium ion (reaction **3**), while the ejected electron from reaction **1** may cause a secondary ionization and, in the end, can be trapped by surrounding water to form a so-called aqueous electron (e_{aq}^-, reaction **5**). The H_2O* (excited water) disassociates to ·OH and ·H (reaction **4**). Reactions **1**-**5** take place on a time scale of 10^{-16} to 10^{-12} seconds, after which the radicals start to diffuse randomly. At the start of the diffusion process (10^{-12} s), the radicals may encounter one another and undergo reaction **6**-**12** (10^{-12} to 10^{-7} s). Next, the species diffuse homogeneously in the solution and react with solutes (e.g., prodrugs or scavengers) within 10^{-4} seconds. After that, all the radicals are quenched or recombined to form molecular products.

Amongst all products formed during water radiolysis, the species suitable to initiate chemical reactions (e.g., activating prodrugs) are e_{aq}^-, ·OH, ·H and H_2O_2. The radiolytic yield of H^+ is too small to induce a significant pH change in biological systems, and is thereby not suitable for such applications. However, prodrugs and other scavengers can only react with these species that remain on the $>10^{-7}$ seconds time scale, as the kinetics of prodrug and reactive species, k_p[prodrug] (rate constant k_p multiplied by the prodrug concentration), is generally below 10^7 s^{-1} (*vide infra*),[22] which makes them too slow to react with species at time scales of 10^{-12} to 10^{-7} s. This means that the yield of reactive species

after 10^{-7} s into the water radiolysis process determines the expected yield of activated drugs.

Radiolytic yield of reactive species

The interaction of ionizing radiation with water results in multiple water molecules being ionized or excited by a single ionizing event. Linear energy transfer (LET) describes the energy absorbed by water as a function of travelled distance of incident radiation, which determines the number of ionizations along the track. For low-LET radiation (photons and high-energy electrons), ionizations are widely spread along the track, and the diffusion pattern of radicals resembles a spur (tiny regions with high concentrations of radicals, **Figure 2.1**). Since ionizing events are far away from each other, radical recombination is limited, resulting in a higher yield of radical products (e.g., e_{aq}^-, ·H, and ·OH) in favor of molecular products (e.g., H_2 and H_2O_2). Conversely, high-LET radiation tends to produce more of the molecular products and less of the radical products,[23,24] since ionizing events distribute close to each other thus facilitating radical recombination.

The dose of radiation is given by grey (Gy) where 1 Gy equals 1 joule of energy absorbed by 1 kilogram of mediate (1 Gy = 1 J/Kg). The radiolytic yields of various species for low-LET radiation after 10^{-7} s of the ionizing process, known as their G-values, are listed in **Table 2.1**.[25-27] Clinical administration of concurrent chemoradiation therapy follows fractionation regimen.[28,29] Long-course chemoradiotherapy generally delivers 40-60 Gy in ca. 30 fractions over 5-6 weeks, while short course combination therapy delivers ca. 25 Gy in 4-5 fractions over 3 weeks.[30] Under these conditions, it is expected that approximately 1 μM of reactive species are generated.

Table 2.1. G-values for water radiolysis for low-LET radiation.

Ref	G (μM/Gy)[a]			
	e_{aq}^-	·OH	·H	H_2O_2
25	0.28	0.30	0.063	0.063
26	0.27	0.28	0.057	0.064

[a]The unit is transferred from molecules/100eV, 1 molecule/100 eV = 0.103 μM/Gy[31]

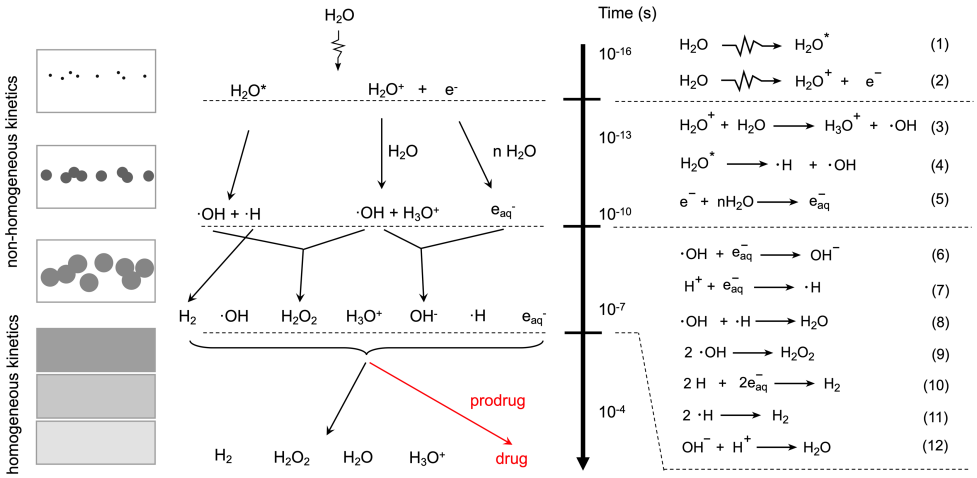

Figure 2.1. Time dependent events of water radiolysis and the reactions. Adapted from reference.[32] The grey area indicates the distribution of radicals: at time scale from 10^{-16} to 10^{-7} seconds, the radicals distribution looks like spurs where reactions undergo non-homogeneous kinetics; at time scale $>10^{-7}$ radicals distribute homogeneously in solution.

The Reactivity of Water Radiolysis Products

In this section, we will discuss the products of water radiolysis relevant for triggering prodrug activation. These species include radical products such as e_{aq}^-, ·OH, and H·, as well as the molecular product H_2O_2. Given the reactivity of these species with a broad range of substrates, we will discuss the reaction rates of each species with various typical substrates or functional groups. The rate constants are listed in **Figure 2.2** and **2.3**, summarized from a comprehensive compilation.[33] Here, we will focus on the reactions of reactive species with (1) compounds abundant in cellular components and (2) functional groups that have been used recently to design radiation sensitive prodrugs. By comparing these reaction rates, the readers can roughly predict which reaction will dominate in a given system such as the tumor microenvironment, providing considerations for prodrug design.

Aqueous electrons

The aqueous electron is a strong reductant with a reduction potential of –2.9 V (*vs*. H^+/H_2), which readily reduces metal ions to lower oxidation states (equation **13**). For example, e_{aq}^- can reduce Cu(II) to Cu(I) at a diffusion-controlled rate (k = 3.3×10^{10} $M^{-1}s^{-1}$). In aqueous

solutions, e_{aq}^- interacts with organic compounds primarily through two mechanisms[34,35]: (1) dissociative electron capture (equation **14**) and (2) addition reactions to π-bonds (equation **15**). A common reaction involving e_{aq}^- is the electron capture by a carbon-halogen bond, resulting in the release of an anion and a carbon-centered radical (for chloroform, $k = 3\times10^{10}$ $M^{-1}s^{-1}$). Additionally, the aqueous electron can perform one-electron reduction of thiols (e.g., cysteine, $k = 1.2\times10^{10}$ $M^{-1}s^{-1}$) or disulfides (e.g., oxidized glutathione, $k = 3.7\times10^{9}$ $M^{-1}s^{-1}$) through dissociative electron transfer mechanisms, leading to the formation of thiol radicals. Although low energy electrons (< 3 eV) are reported to damage DNA, e_{aq}^- is relatively inert to DNA backbones (deoxyribose, $k = 1.0\times10^{7}$ $M^{-1}s^{-1}$) but can add to the double bond of bases (guanine, $k = 1.4\times10^{10}$ $M^{-1}s^{-1}$; adenine, $k = 9.0\times10^{9}$ $M^{-1}s^{-1}$; cytosine, $k = 1.3\times10^{10}$ $M^{-1}s^{-1}$; thymine, $k = 1.8\times10^{10}$ $M^{-1}s^{-1}$). It is important to note that e_{aq}^- reacts with molecular oxygen at a diffusion-controlled rate, to form a peroxyl anion known as superoxide. Superoxide is a highly reactive reductant, which is readily scavenged by superoxide dismutase in living organisms.

$$e_{aq}^- + M^{n+} \longrightarrow M^{(n-1)+} \quad (13)$$

$$CR{-}X + e_{aq}^- \longrightarrow {\cdot}CR + X^- \qquad X = F, Cl, Br, I \quad (14)$$

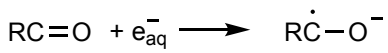

$$RC{=}O + e_{aq}^- \longrightarrow R\dot{C}{-}O^- \quad (15)$$

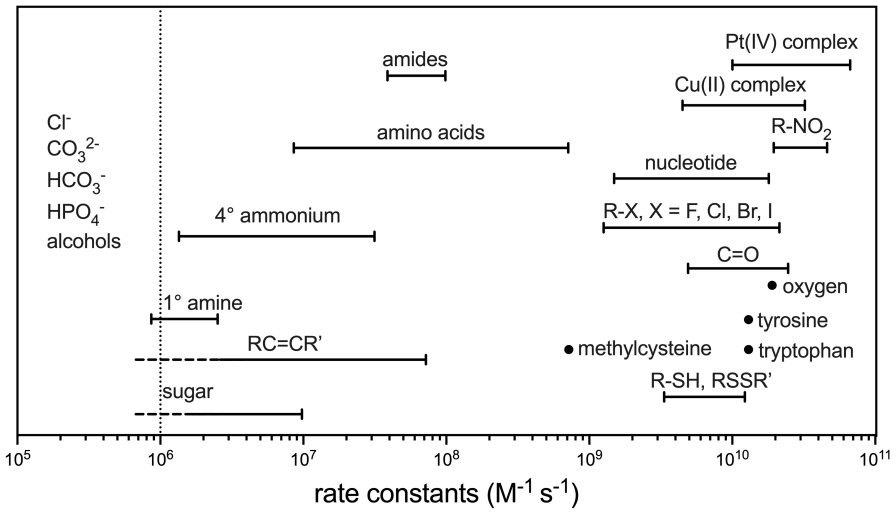

Figure 2.2. Second-order rate constants for reactions of aqueous electrons in aqueous solutions.[33,36] Species on the left of the dashed line can be considered as unreactive.

Hydroxyl radical

Hydroxyl radical reacts with most organic substrates at close to diffusion-controlled rates. The main reaction types of ·OH with substrates include (1) addition to double bonds, (2) hydrogen abstraction and (3) electron transfer. In biological systems, ·OH undergoes addition reactions at the double bonds of the base moieties of nucleotides[37] (equation **16**) with near diffusion-controlled rate constants: guanine (k = 9.2×10^{10} M^{-1}s^{-1}), adenine (k = 6.1×10^{10} M^{-1}s^{-1}), cytosine (k = 5.6×10^{10} M^{-1}s^{-1}) and thymine (k = 1.8×10^{10} M^{-1}s^{-1}). Additionally, ·OH participates in hydrogen abstraction reactions at the sugar moiety (equation **17**), such as glucose (k = 1.5×10^{10} M^{-1}s^{-1}) and ribose (k = 1.5×10^{10} M^{-1}s^{-1}). Given the relatively high concentration of nucleotides in cells and the rapid reaction rate of ·OH with most biological molecules, the design of prodrugs or activation systems targeting ·OH should incorporate functional groups that are either present in significantly higher concentrations than nucleotides or have a much higher reaction rate with ·OH. The last section will present a few examples using ·OH as the triggering agent.

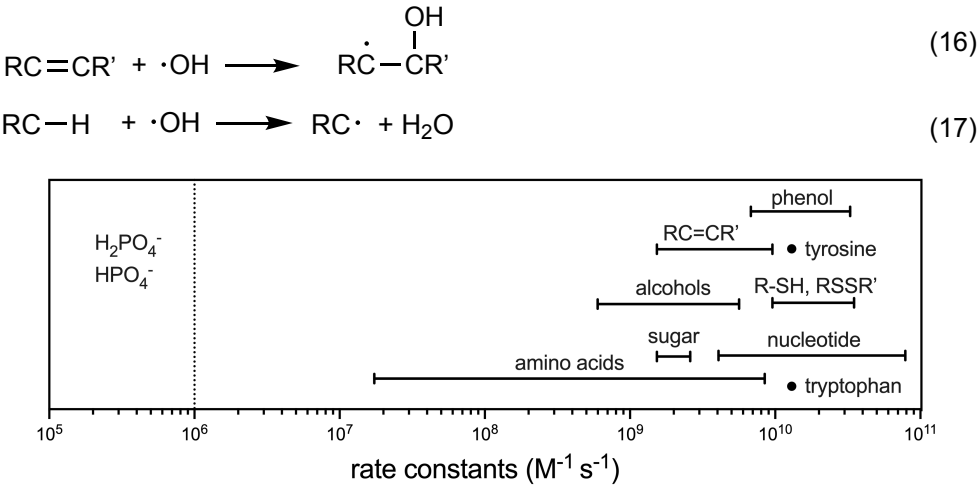

Figure 2.3. Second-order rate constants for reactions of hydroxyl radical in aqueous solution.[33]

Hydrogen radical

The hydrogen radical (H·) is the conjugate acid of e_{aq}^-, with a pKa of 9.1. The typical reaction of H· with organic compounds is hydrogen abstraction, which occurs at a significantly lower rate compared to reactions with ·OH.[33] Under physiological conditions, e_{aq}^- is considered the dominant reductant, which is attributed not only to the lower G-value of H· compared to e_{aq}^- but also to the fact that the reaction rates of H· with most organic compounds are 1 to 3 orders of magnitude lower than those of e_{aq}^-.

Hydrogen peroxide

Hydrogen peroxide is present in most cells at concentrations ranging from a few micromolar in normal cells to sub-millimolar in cancerous or inflamed cells.[38,39] This widespread presence makes H_2O_2 a popular stimulus for activating prodrugs or nanocarriers.[40,41] However, the radiolytic production of H_2O_2 under low-LET radiation has a very low yield (0.07 μM/Gy), which will lead to radiation-induced concentrations that are comparable to typical intracellular levels. Consequently, designing prodrugs that rely on H_2O_2 generated by low-LET radiation is quite challenging. As far as we know, there are no examples published that use H_2O_2 generated from water radiolysis. In contrast, high-LET

radiation produces somewhat higher yields of H_2O_2 (e.g., 0.13 μM/Gy for 3.4 MeV alpha beams)[42,43], making it useful to consider in combination with alpha radionuclide therapy.

Reactivity of Radiolytic Species in Biological Systems

As discussed in the previous section, both e_{aq}^- and ·OH can react with a wide variety of cellular components. In this section we will discuss the selectivity of these species to cellular components and radiolytic species-sensitive molecules. Let us consider a drug that is caged by a radiolytic species-sensitive functional group. The prodrug is designed to react with e_{aq}^-. In a biological system containing this prodrug, upon exposure to ionizing radiation, the prodrug molecule will compete with all cellular components to react with the radiation-generated e_{aq}^-. The fraction (f) of e_{aq}^- reacting with the prodrug relative to the overall scavenging by cellular components can be used to quantify the reactivity of the prodrug in a biological system.[44]

f is given by:

$$f = k_p[\text{functional group}] / \sum (k_i[S_i])$$

and the generated concentration of activated functional group is given by:

$$[\text{activated functional group}] = [e_{aq}^-] \times f$$

where k_p is the rate constant of e_{aq}^- with functional group, k_i is the reaction rate of the ith cellular component S_i with e_{aq}^-, $[e_{aq}^-]$ is the yield of aqueous electrons at a given dose of radiation. The sum represents all the scavenging reactions of e_{aq}^- within cells, including the reaction with the prodrug. In 1978, Hunt et al. estimated this sum to be 3.4×10^8 s^{-1} in mammalian cells without prodrugs.[45] This estimation is based on several assumptions, such as the homogeneous distribution of all reactants within cells. However, certain scavengers, such as bases in DNA, are concentrated in the nucleus and are not homogeneously distributed, suggesting that the actual value might be lower. Considering a few homogeneously distributed e_{aq}^- scavengers in cancerous tissues, such as glutathione (intracellularly 1-10 mM[46] and 20-40 μM outside cells[47,48], $k = 4.5\times10^9$ $M^{-1}s^{-1}$), cysteine (ca.

0.3 mM in blood[49,50], $k = 1.2\times10^{10}$ $M^{-1}s^{-1}$), and oxygen (on average 16.3 μM[51] in tumor microenvironment, $k = 1.9\times10^{10}$ $M^{-1}s^{-1}$), and using the previously mentioned reaction rates, the sum is 0.40×10^{7} s^{-1} (outside cells). In this context, k_p[functional group] should be at least comparable to this value to ensure substantial activation of the prodrug by e_{aq}^-. In the case of a prodrug designed to react with ·OH, the competition between the prodrug and cellular components for ·OH is less favorable, since sugars, which are unreactive to e_{aq}^-, can rapidly react with ·OH. Considering some homogeneously distributed ·OH scavengers in cells, such as cysteine ($k = 3.4\times10^{10}$ $M^{-1}s^{-1}$), glucose (ca. 5.5 mM[52], $k = 1.5\times10^{9}$ $M^{-1}s^{-1}$), and glutathione ($k = 1.4\times10^{10}$ $M^{-1}s^{-1}$), the total scavenging rate is 1.91×10^{7} s^{-1}. This rate is more than four times higher than that of e_{aq}^-, making the design of prodrugs targeting ·OH significantly more challenging than those targeting e_{aq}^-.

Overall, due to the low radiolytic yield of e_{aq}^- and ·OH and their poor selectivity toward most cellular components, radiation-sensitive molecules should have the following characteristics to facilitate effective activation: (1) significantly higher reactivity than the combined scavengers, as the concentration of radiation-sensitive molecules is much lower than that of scavengers (tens of micromolar for prodrugs versus a few millimolar for scavengers), the reaction rate should be at least one order of magnitude higher than that of the scavengers; (2) good solubility to ensure a homogeneous reaction with reactive species; and (3) the drug should be effective (toxic) at applied concentrations.

Discussion of Radiation-Initiated Drug Release

In the previous section, we discussed the selectivity of e_{aq}^- and ·OH toward radiation-sensitive molecules in biological systems. In this section, we will discuss examples where different functional groups have been designed to react with e_{aq}^- and ·OH. After exposure to ionizing radiation, the reactions of radiolytic species with these functional groups induce molecular changes in the parent molecule, leading to drug release. By critically reviewing published papers from a radiation chemistry perspective, we aim to provide insights and inspiration for designing effective radiation-initiated drug release systems.

Carbonyl compounds

Shibamoto et al.[53] were among the first to work on this problem, reporting prodrug OFU001 (**Figure 2.4a**) which was constructed by protecting the anti-tumor drug 5-fluorouracil (5-FU) at the N(1) position using a 2-oxoalkyl group. Under X-ray irradiation, the formed e_{aq}^- added to the carbonyl group to form a π^* anion radical, which is further thermalized to the σ^* orbital with a weak C-N bond, followed by the dissociation of the C-N bond and the release of 5-FU. Release of 5-FU was substantially enhanced under irradiation in hypoxic conditions, with a G-value of 0.19 μM/Gy, while the G-value was 0.010 μM/Gy in aerobic conditions, underlining the scavenging propensity of molecular oxygen. With the decent radiolytic yield of 5-FU, the authors tested the cytotoxicity of the prodrug under irradiation with X-rays. OFU001 showed much lower toxicity compared to 5-FU, and the cell surviving fraction dropped significantly in the group of OFU001 with 30 Gy of irradiation under hypoxic conditions. However, it should be noted that they performed the experiments by firstly irradiating prodrug in Eagle's minimum essential medium (MEM) which was then added to the cells, which is not clinically applicable. Although there has been follow-up research using the carbonyl group as a drug caging group,[54] the activation efficiency in biological systems is far below what is expected. This negative result may be caused by competition reactions of various cellular components in tissues, reducing the utility of the carbonyl group as a prodrug cage. In other words, the de-caging reactions of prodrugs should out-compete the scavenging reactions in biological system to make the drug release efficient.

Azido compounds

Azides (RN_3) are known to be reduced to amines (RNH_2) by reductants such as H_2S, H_2, and phosphines.[55] Tanabe et al.[56] showed that the reduction can also be triggered by reducing species from hypoxic water radiolysis such as e_{aq}^-. They designed a prodrug where 5-fluoro-2'-deoxyuridine (5-FuUrd) was protected by an azido methyl group (**Figure 2.4b**). Upon reacting with e_{aq}^-, the azido group was reduced to the amino compound and the formed methylamino group underwent a hydrolysis reaction to release 5-FdUrd. The G-value of the reaction was 0.16 μM/Gy. A549 cells first treated with N3-FdUrd and irradiated for 6 Gy showed significant difference on cell viability ($P < 0.05$) compared with the N3-FdUrd negative group. The reactivity of azido group increases when it is connected

with electron-withdrawing group. Geng et al.[57] demonstrated that sulfonyl azides and 2,3,5,6-tetrafluorophenyl azides can be reduced to amines under hypoxic irradiation. The *p*-azido-2,3,5,6-tetrafluorobenzyl caging group can be reduced to an aniline which subsequently undergoes 1,6-self-immolation to release doxorubicin (Dox) (**Figure 2.4c**). The radiolytic yield of the drug was approximately 5 μM after exposure to 60 Gy of X-irradiation (ca. 0.083 μM/Gy).

N-oxides

N-oxide derivatives, such as tirapazamine, were initially used as effective hypoxia-targeting agents due to their efficient reduction by cellular reductases.[58] The so-formed benzotriazinyl radical perform hydrogen abstraction from DNA, leading to strand breaks. Ding et al.[59] creatively applied N-oxide derivatives in radiation-activated prodrug therapy. They hypothesized that the e_{aq}^- generated from water radiolysis could reduce N-oxides to tertiary amines (**Figure 2.4d**). They suggested that the e_{aq}^- first occupies the π orbital of the N-oxide by a tunnelling effect. Additionally, N-oxides with extended π systems affected the reactivity of e_{aq}^- to N-oxide. Through structural screening, they identified aniline N-oxides and aromatic heterocyclic N-oxides as promising groups for the reaction, with G-values close to the G-value of e_{aq}^- in phosphate buffered saline (PBS). Anti-tumor drugs such as camptothecin (CPT), which contain heterocyclic tertiary amines, were used as drug candidates in this study. The IC_{50} of the prodrug NO-CPT was 22-fold lower than that of CPT against the CT26 cell line. Tumor-bearing mice treated with NO-CPT and fractionated radiotherapy (4 Gy per fraction) showed significantly greater tumor growth suppression.

Nitroaryl compounds

Kriste et al.[60] reported prodrug activating method using reduction of nitroaryl methylquaternary ammonium salt by e_{aq}^- (**Figure 2.4e**). The formed nitro radical anion undergoes rearrangement to break C-N bond of a quaternary ammonium salt, resulting in the release of a tertiary amine derivative. They used the chlormethine nitrogen mustard as the model drug. For the protecting group, they examined a series of nitrophenyls and nitroheterocycles and found the kinetics of fragmentation reactions varied by more than 4 orders of magnitude independent of reduction potential. 2-Nitropyrrole provided efficient chlormethine release with G-value of 0.67 μM/Gy in deaerated water with 0.1 M sodium

formate buffer and 5 mM sodium phosphate (pH = 7.0). However, the toxicity of such series of prodrugs were only 1.3 to 5.6 times lower than the corresponding drug, limiting the application potential of this such type of prodrug cage.

Quaternary ammonium

Generally, quaternary ammonium salts such as tetrabutylammonium ion are unreactive to aqueous electrons (**Figure 2.2**). However, Guo et al.[61] reported that *p*-acetylbenzyl substituted ammonium salts had a much higher reactivity towards aqueous electrons because of their high electron affinity, with reduction resulting in the cleavage of the *p*-acetylbenzylic bond. The cleavage reaction also worked on a carfilzomib (CFZ)-based prodrug QA-CFZ (**Figure 2.4f**). In vitro experiments showed the G-value of carfilzomib activation is ca. 0.16 μM/Gy in PBS. Tumor-bearing mice showed larger tumor growing suppression in the group treated with QA-CFZ and 4 Gy of X-irradiation.

The same group reported another prodrug activation method using the reaction of e_{aq}^- with picolinium derivatives (**Figure 2.4g**).[62] The positive charge of picolinium makes it more reactive than picolyl- or quinolinyl- substitution. The formed electrically neutral radical underwent rearrangement to release the parent drug. The G-value of released drug was 0.137 μM/Gy in phosphate buffer (PB, pH 7.4) which was close to the G-value of e_{aq}^-. An antibody-drug conjugate (ADC) consisting of a fibroblast activation protein-targeted antibody and monomethyl auristatin E (MMAE) was synthesized using such a functional group as the linker. The ADC reached maximum tumor accumulation on the second day, at this point radiation was applied. The radiolytic yield of released MMAE was 0.035 μM/Gy. Tumor-bearing mice treated with ADC and radiation showed lower tumor volume but similar body weight compared to single treatment groups. This example demonstrated that although the radiolytic yield of drugs in tissue was lower than that in PB because of the scavenging reactions we discussed in the last section, the tumor-killing efficiency was still significantly higher than when only using radiotherapy.

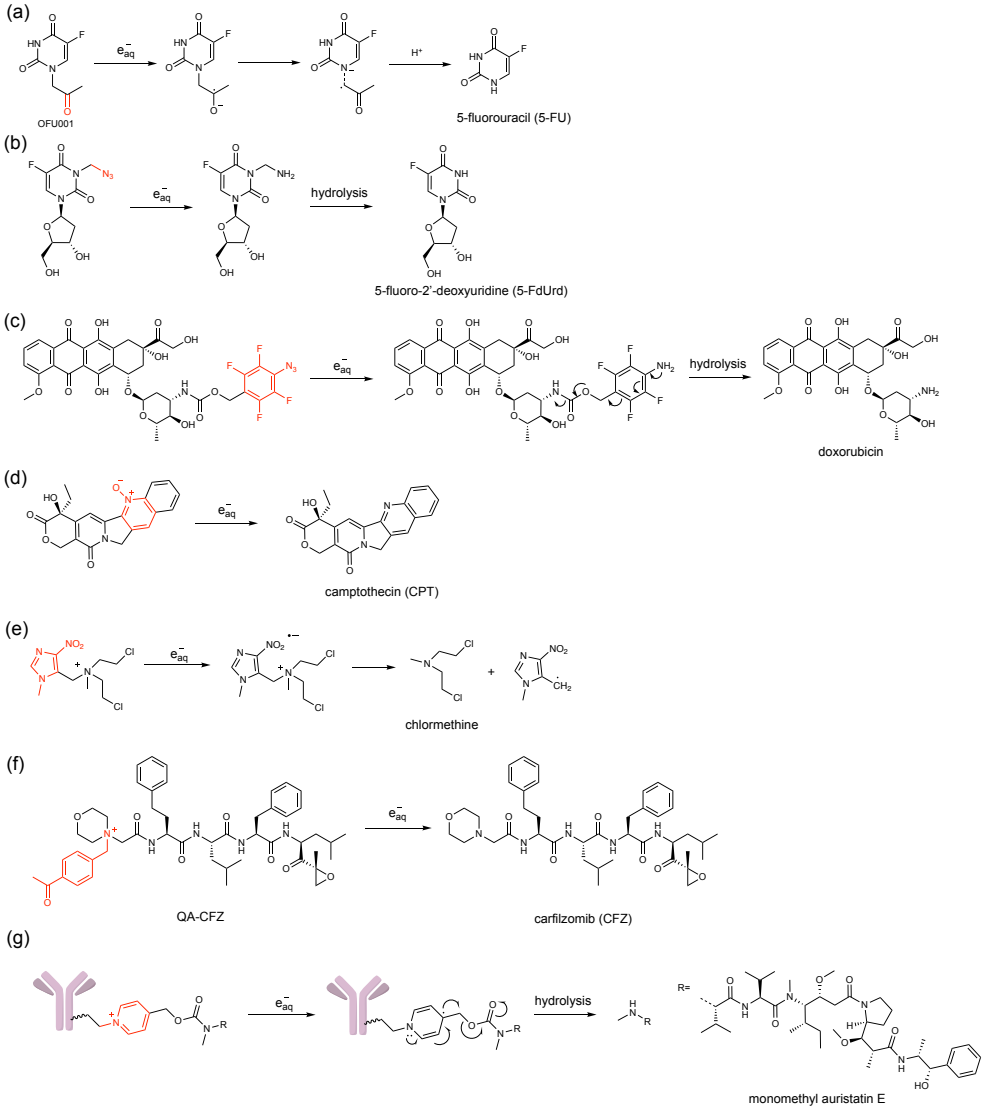

Figure 2.4. Prodrug activation induced by aqueous electrons: (a) activation of 2-oxoalkyl-caged 5-FU via cleavage of C-N bond induced by aqueous electrons; (b) reduction of azido methyl group by aqueous electrons followed by hydrolysis and releasing 5-FdUrd; (c) reduction of 2,3,5,6-tetrafluorophenyl azide followed by the hydrolysis of a self-immolative carbamate linker to release Dox; (d) reduction of N-oxide to release camptothecin; (e) reduction of 2-nitropyrrole induced C-N bond cleavage and the release of chlormethine; (f) aqueous electrons induced decaging of *p*-acetylbenzyl ammonium to release carfilzomib; (g) cleavage of the C-N bond of a picolinium and the rearrangement of the resulting compound to release monomethyl auristatin E.

Metal ions

The one-electron reduction of metal ions by aqueous electrons presents significant opportunities for researchers to investigate hyporeduced metal ions. Akisawa et al.[63] reported that, under hypoxic irradiation of an aqueous solution containing Cu(II), azide and acetylene, an azide-alkyne coupling reaction occurred (**Figure 2.5a**). This reaction was catalyzed by Cu(I), which was formed through the reduction of Cu(II) by e_{aq}^-. They also demonstrated that, due to the deep penetration of X-rays, the reaction could still be initiated even though the reacting vessels were inserted in pork meat. Wang et al.[64] reported a palladium pre-catalyst composed of Pd(II)$(OAc)_2$ and a porous organic polymer (**Figure 2.5b**). Under irradiation in water, the reduction of Pd(II) to Pd(0) occurred, which then catalysed the Tsuji-Trost hydrolysis of allyloxycarbonyl-caged Dox. Notably, they measured the G-value of the released drug to be 2.75 μM/Gy, approximately 10 times higher than that of e_{aq}^-. This finding suggests that the strategy of activating metal catalysts under irradiation can overcome the low-yield limitation of primary species, thereby enhancing radiation-induced reactions. Fu et al.[65] demonstrated that a Pt(IV) complex could be reduced by e_{aq}^-, leading to the dissociation of axial ligands and a Pt(II) complex (**Figure 2.5c**). Using physiological stable prodrug oxaliPt(IV)-$(OAc)_2$, and the treatment with prodrug and 4 Gy X-rays showed enhanced cell killing efficiency to a series of cell lines including HCT116, LoVo, Ls513, and HT29. Furthermore, since the ligands are cleaved when Pt(IV) is reduced to Pt(II), they designed an antibody-drug conjugate, OxaliPt(IV)-ADC using Pt(IV) as the linker of monoclonal anti-HER2 antibody trastuzumab and a cleavable MMAE as the axial ligand. Upon irradiation, the reduction of Pt(IV) led to the release of two types of anti-tumor drug, OxaliPt(IV) and MMAE. Mice bearing BGC823 or MC38 cells treated with ADC and X-rays showed better treatment effect while having no side effects (neither body weight loss nor abnormalities in major organs) when compared with control groups.

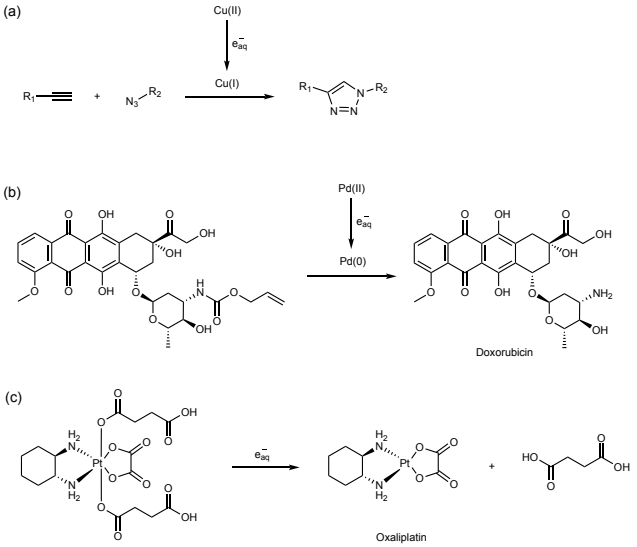

Figure 2.5. Radiation induced reduction of medal ions to lower valent state under hypoxic conditions. (a) azide-alkyne click reaction catalyzed by radiation generated Cu(I); (b) Pd(0) catalysed hydrolysis of allyloxycarbonyl-caged Dox where the Pd(0) is generated by reaction of Pd(II) and e_{aq}^-; (c) reduction of Pt(IV) complex by e_{aq}^- and the cleavage of the ligand.

Dihydroxylbenzyl compounds

Fu et al.[66] reported a dihydroxylbenzyl caged prodrug where the hydroxylation by hydroxyl radical could result in the cleavage of the protecting group. The di-substituted hydroxyl group makes the benzene ring more electron-rich thus facilitating the electrophilic substitution by hydroxyl radical. A prodrug comprised of this group and the anti-tumor drug MMAE showed efficient drug release with a G-value of 0.04 μM/Gy. Cancer cells (4T1 cell line) treated with 10 nM prodrug and 4 Gy X-ray demonstrated significantly lower viability compared with prodrug or treatment only with radiation.

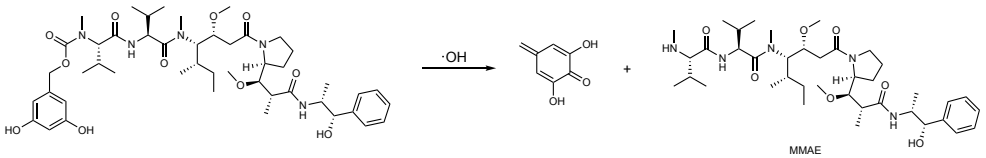

Figure 2.6. Hydroxylation of dihydroxylbenzyl group induced cleavage of self-immolative carbamate group.

Radiation induced reactions to trigger drug release from polymers

Organic selenium compounds are reported to show response to reductants or oxidants in living systems and have been used in redox-responsive drug carriers.[67-71] Ma et al.[72] first applied the diselenide group in the design of an ionizing radiation sensitive drug carrier (**Figure 2.7a**). They hypostasized that the cleavage of the diselenide bond was initiated by hydroxyl radicals, which was confirmed using electron spin resonance. They incorporated the diselenide group in a polyethylene glycol poly urethane block co-polymer (PEG-PUSeSe-PEG) which formed nano-aggregates in aqueous solution. Upon 5 Gy of X-rays irradiation, the nano-carrier could release up to 40% of the encapsulated doxorubicin. Using diselenide as the reactive group, the same group later reported radiation-sensitive hydrogels and liposomes.[73] However, the applied dose was 500 Gy to break the hydrogels, which were too high to use in clinic. As a homologue of selenium, tellurium is also sensitive to redox stimuli.[74] Cao et al.[75] reported an amphiphilic polymer containing organic tellurium bond in the hydrophobic block (**Figure 2.7b**). In response to only 2 Gy gamma irradiation, the micelles formed from the polymer swelled from 30 nm to around 200 nm as the oxidation of tellurium made the hydrophobic core more hydrophilic. This unique property made the polymer promising for application in radiation triggered drug release.

Disulfide bonds are reported to undergo one-electron reduction reactions leading to disulfide bond cleavage and exchange reactions. Tanabe et al.[76,77] demonstrated that disulfide bonds incorporated within an oligoDNA-ampliphile could react with e_{aq}^- (**Figure 2.7c**). The generated disulfide radical anion ($RSSR'^{\cdot -}$) decomposes into a sulfide anion (RS^-) and thiyl radical ($RS^{\cdot}$). The sulfide anion underwent disulfide exchange reaction with another molecule of disulfide. With this reaction, they designed a DNA amphiphile with a disulfide bond as the linker of the hydrophobic and hydrophilic block.[78] The polymer formed micelles in water with drugs encapsulated in the hydrophobic region. Under hypoxic X-irradiation, the disulfide exchange resulted in the disassembly of the micelle and release of the payload. A549 cell line treated with camptothecin-loaded micelles and 9 Gy X-irradiation under hypoxic conditions showed higher toxicity than without radiation.

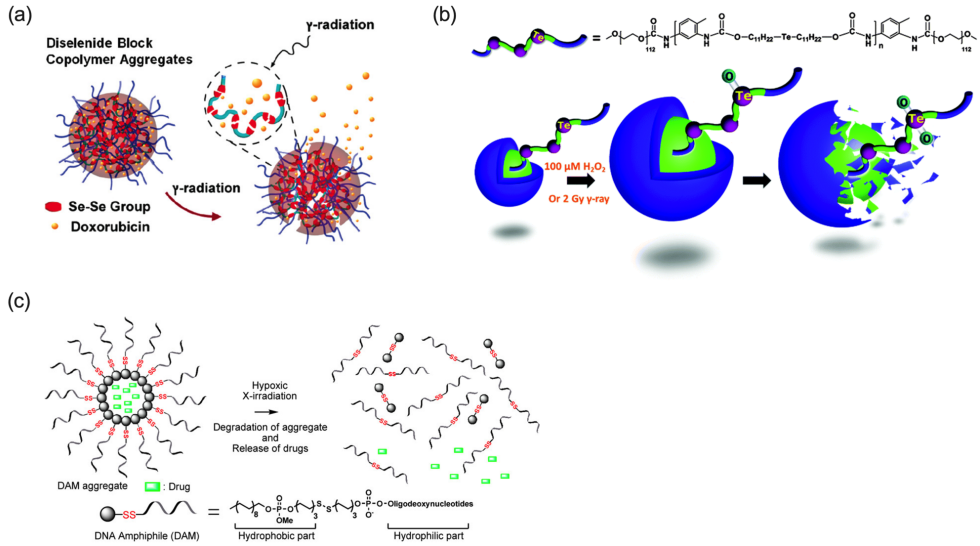

Figure 2.7. Radiation induced micelle disassembly. (a) gamma radiation induced oxidative cleavage of diselenide bond, adapted from reference[72], copyright 2011 American Chemical Society; (b) radiation induced oxidation of tellurium containing polymer, adapted from reference[75], copyright Clearance Cemter, inc.; (c) hypoxic X-irradiation induced disulfide exchange reaction, adapted from reference[78], copyright 2011 American Chemical Society.

Conclusions

Ionizing radiation-induced drug release offers a unique way to reduce the side effects chemotherapeutic drugs. In this concept, radiation acts both as radiotherapy and as an external stimulus to trigger drug release. The deep penetrating characteristic of radiation makes this strategy work on tissues deep inside the body. Radiation induced drug release is mediated by reactive species generated from water radiolysis. The challenges associated to this concept are the low radiolytic yield of the reactive species (a few micromolar per irradiated dose), and the side reactions of these species with a wide range of biological substances. Significant progress has been made in recent years to develop efficient releasing systems that can response to clinical doses of radiation. Most of the reactive species generated in water radiolysis have been studied to trigger drug release. Hydroxyl radicals, as the most abundant species from water radiolysis, suffer from the high reactivity to most cellular components, making it only work on highly sensitive functional groups

such as diselenide, organotellurium and dihydroxylbenzyl compounds. Aqueous electrons have drawn more attention than other species because of the relatively higher yield and selective reactivity towards a few functional groups such as N-oxide, organoazides, carbon-halogen bond, and picolinium groups. Moreover, the reduction of metal ions by aqueous electrons brings new approaches of activating drug in cancerous tissues, and associated metal-catalyzed reactions may potentially enable drug release effects that exceed the maximum yield of radiolysis products.

References

(1) Denkova, A. G.; Liu, H.; Men, Y.; Eelkema, R. Enhanced Cancer Therapy by Combining Radiation and Chemical Effects Mediated by Nanocarriers. *Adv. Therap.* **2020**, *3*, 1900177.

(2) Begg, A. C.; Stewart, F. A.; Vens, C. Strategies to Improve Radiotherapy with Targeted Drugs. *Nat. Rev. Cancer* **2011**, *11*, 239-253.

(3) Xu, X. D.; Wu, J.; Liu, Y. L.; Yu, M. Y.; Zhao, L. L.; Zhu, X.; Bhasin, S.; Li, Q.; Ha, E.; Shi, J. J. Ultra-pH-Responsive and Tumor-Penetrating Nanoplatform for Targeted siRNA Delivery with Robust Anti-Cancer Efficacy. *Angew. Chem. Int. Ed.* **2016**, *55*, 7091-7094.

(4) Guo, J. S.; Li, J. J.; Wang, Z. H.; Liu, Y.; Yue, Y. X.; Li, H. B.; Zhao, X. H.; Sun, Y. J.; Ding, Y. H.; Ding, F.; et al. Dual Hypoxia-Responsive Supramolecular Complex for Cancer Target Therapy. *Nat. Commun.* **2023**, *14*, 5634.

(5) Wang, B.; Van Herck, S.; Chen, Y.; Bai, X.; Zhong, Z.; Deswarte, K.; Lambrecht, B. N.; Sanders, N. N.; Lienenklaus, S.; Scheeren, H. W.; et al. Potent and Prolonged Innate Immune Activation by Enzyme-Responsive Imidazoquinoline TLR7/8 Agonist Prodrug Vesicles. *J. Am. Chem. Soc.* **2020**, *142*, 12133-12139.

(6) Zhang, W.; Ji, T. J.; Li, Y.; Zheng, Y. Q.; Mehta, M.; Zhao, C.; Liu, A. D.; Kohane, D. S. Light-Triggered Release of Conventional Local Anesthetics from a Macromolecular Prodrug for on-Demand Local Anesthesia. *Nat. Commun.* **2020**, *11*, 2323.

(7) Tu, L.; Liao, Z. H.; Luo, Z.; Wu, Y. L.; Herrmann, A.; Huo, S. D. Ultrasound-Controlled Drug Release and Drug Activation for Cancer Therapy. *Exploration* **2021**, *1*, 20210023.

(8) Ding, C. D.; Chen, C. B.; Zeng, X. W.; Chen, H. Z.; Zhao, Y. L. Emerging Strategies in Stimuli-Responsive Prodrug Nanosystems for Cancer Therapy. *Acs Nano* **2022**, *16*, 13513-13553.

(9) Read, G. H.; Bailleul, J.; Vlashi, E.; Kesarwala, A. H. Metabolic Response to Radiation Therapy in Cancer. *Mol. Carcinog.* **2022**, *61*, 200-224.

(10) Zhang, L.; Wu, X. J.; Xu, T.; Luo, C.; Qian, J.; Lu, Y. C. Chemotherapy Plus Radiotherapy Versus Radiotherapy Alone in Patients with Anaplastic Glioma: a Systematic Review and Meta-Analysis. *J. Cancer Res. Clin. Oncol.* **2013**, *139*, 719-726.

(11) Shi, Y.; Guo, Z.; Fu, Q.; Shen, X.; Zhang, Z.; Sun, W.; Wang, J.; Sun, J.; Zhang, Z.; Liu, T.; et al. Localized Nuclear Reaction Breaks Boron Drug Capsules Loaded with Immune Adjuvants for Cancer Immunotherapy. *Nat. Commun.* **2023**, *14*, 1884.

(12) Cao, W.; Gu, Y.; Meineck, M.; Xu, H. The Combination of Chemotherapy and Radiotherapy Towards more Efficient Drug Delivery. *Chem. Asian J.* **2014**, *9*, 48-57.

(13) Kamkaew, A.; Chen, F.; Zhan, Y.; Majewski, R. L.; Cai, W. Scintillating Nanoparticles as Energy Mediators for Enhanced Photodynamic Therapy. *ACS Nano* **2016**, *10*, 3918-3935.

(14) Sun, W.; Chu, C.; Li, S.; Ma, X.; Liu, P.; Chen, S.; Chen, H. Nanosensitizer-Mediated Unique Dynamic Therapy Tactics for Effective Inhibition of Deep Tumors. *Adv. Drug Deliv. Rev.* **2023**, *192*, 114643.

(15) Zhang, X.; Lan, B.; Wang, S.; Gao, P.; Liu, T.; Rong, J.; Xiao, F.; Wei, L.; Lu, H.; Pang, C.; et al. Low-Dose X-ray Excited Photodynamic Therapy Based on $NaLuF_4:Tb^{3+}$-Rose Bengal Nanocomposite. *Bioconjug. Chem.* **2019**, *30*, 2191-2200.

(16) Cao, Y.; Si, J.; Zheng, M.; Zhou, Q.; Ge, Z. X-Ray-Responsive Prodrugs and Polymeric Nanocarriers for Multimodal Cancer Therapy. *Chem. Commun.* **2023**, *59*, 8323-8331.

(17) Liu, H.; Zhao, J.; Xue, Y.; Zhang, J.; Bai, H.; Pan, S.; Peng, B.; Li, L.; Voelcker, N. H. X-Ray-Induced Drug Release for Cancer Therapy. *Angew. Chem. Int. Ed.* **2023**, *62*, e202306100.

(18) Richter, H. W. Radiation Chemistry: Principles and Applications. In *Photochemistry and Radiation Chemistry*, Advances in Chemistry, 1998; pp 5-33.

(19) Radiation Chemistry from Basics to Applications in Chapter 1: An Overview of the Radiation Chemistry of liquids.

(20) O'Neill, P.; Wardman, P. Radiation Chemistry Comes Before Radiation Biology. *Int. J. Radiat. Biol.* **2009**, *85*, 9-25.

(21) Wardman, P. The Importance of Radiation Chemistry to Radiation and Free Radical Biology (The 2008 Silvanus Thompson Memorial Lecture). *Brit. J. Radiol.* **2009**, *82*, 89-104.

(22) Buxton, G. V.; Radiation chemistry of the liquid state. In Radiation Chemistry of the Liquid State: (1) Water and Homogeneous Aqueous Solutions. In: Farhataziz, Rodgers MAJ, eds. *Radiation Chemistry Principles and Applications*., VCH Publishers, New York, NY, 1987.

(23) LaVerne, J. A. Hydrated Electron Yields in the Heavy Ion Radiolysis of Water. *J. Phys. Chem. A* **2005**, *109*, 9393-9401.

(24) LaVerne, J. Radiation chemical effects of heavy ions, in *Charged particle and photon interactions with matter*, Eds.: Mozumder, A. and Hatano, Y, M. Dekker, New York: 2004.

(25) Farhataziz; Rodgers, M. A. J. *Radiation Chemistry: Principles and Applications*; VCH Publishers, New York, NY, 1987.

(26) Spinks, J. W. T.; Woods, R. J. An Introduction to Radiation Chemistry; John Wiley and Sons Inc, 1990.

(27) Elliot, A. J.; Bartels, D. M. The reaction set, rate constants and g-values for the simulation of the radiolysis of light water over the range 20 deg to 350 deg C based on information available in 2008. **2008**.

(28) Wu, H. Y.; Fan, C. W.; Fang, C.; Huang, L. B.; Li, Y.; Zhou, Z. G. Preoperative Short-Course Radiotherapy Followed by Consolidation Chemotherapy for Treatment with Locally Advanced Rectal Cancer: a Meta-Analysis. *Radiat. Oncol.* **2022**, *17*, 14.

(29) Bernier, J. Alteration of Radiotherapy Fractionation and Concurrent Chemotherapy: a New Frontier in Head and Neck Oncology? *Nat. Clin. Pract. Oncol.* **2005**, *2*, 305-314.

(30) De Ruysscher, D.; Niedermann, G.; Burnet, N. G.; Siva, S.; Lee, A. W. M.; Hegi-Johnson, F. Radiotherapy Toxicity. *Nat. Rev. Dis. Primers* **2019**, *5*, 13.

(31) Wardman, P. Initiating Redox Reactions by Ionizing Radiation: A Versatile, Selective and Quantitative Tool. *Redox Biochemistry and Chemistry* **2023**, *5-6*.

(32) Buxton, G. Chapter 1 An overview of the radiation chemistry of liquids. In *Radiation Chemistry*, EDP Sciences, 2008; 3-16.

(33) Buxton, G. V.; Greenstock, C. L.; Helman, W. P.; Ross, A. B. Critical Review of Rate Constants for Reactions of Hydrated Electrons, Hydrogen Atoms and Hydroxyl Radicals ($\cdot OH/\cdot O^-$) in Aqueous Solution. *J. Phys. Chem. Ref. Data* **1988**, *17*, 513-886.

(34) Daily, R.; Minakata, D. Reactivities of Hydrated Electrons with Organic Compounds in Aqueous-Phase Advanced Reduction Processes. *Environ. Sci.: Water Res. Technol.* **2022**, *8*, 543-574.

(35) Daily, R.; Minakata, D. Development of a Group Contribution Method to Predict the Aqueous-Phase Reactivities of Hydrated Electrons with Organic Compounds. *J. Adv. Chem. Eng.* **2023**, *15*, 100493.

(36) Hart, E. J.; Gordon, S.; Thomas, J. K. Rate Constants of Hydrated Electron Reactions with Organic Compounds. *J. Phys. Chem.* **1964**, *68*, 1271-1274.

(37) Cadet, J.; Angelov, D.; Wagner, J. R. Hydroxyl Radical is Predominantly Involved in Oxidatively Generated Base Damage to Cellular DNA Exposed to Ionizing Radiation. *Int. J. Radiat. Biol.* **2022**, 1-7.

(38) Coussens, L. M.; Werb, Z. Inflammation and Cancer. *Nature* **2002**, *420*, 860-867.

(39) Winterbourn, C. C. Reconciling the Chemistry and Biology of Reactive Oxygen Species. *Nat. Chem. Biol.* **2008**, *4*, 278-286.

(40) Dong, C.; Zhou, Q.; Xiang, J.; Liu, F.; Zhou, Z.; Shen, Y. Self-Assembly of Oxidation-Responsive Polyethylene Glycol-Paclitaxel Prodrug for Cancer Chemotherapy. *J. Control. Release* **2020**, *321*, 529-539.

(41) Skarbek, C.; Serra, S.; Maslah, H.; Rascol, E.; Labruère, R. Arylboronate Prodrugs of Doxorubicin as Promising Chemotherapy for Pancreatic Cancer. *Bioorg. Chem.* **2019**, *91*, 103158.

(42) Anderson, A. R.; Hart, E. J. Molecular Product and Free Radical Yields in the Decomposition of Water by Protons, Deuterons, and Helium Ions. *Radiat. Res.* **1961**, *14*, 689-704.

(43) Pastina, B.; LaVerne, J. A. Hydrogen Peroxide Production in the Radiolysis of Water with Heavy Ions. *J. Phys. Chem. A* **1999**, *103*, 1592-1597.

(44) Wardman, P. Approaches to Modeling Chemical Reaction Pathways in Radiobiology. *Int. J. Radiat. Biol.* **2022**, *98*, 1399-1413.

(45) Michaels, H. B.; Hunt, J. W. A Model for Radiation Damage in Cells by Direct Effect and by Indirect Effect: a Radiation Chemistry Approach. *Radiat. Res.* **1978**, *74*, 23-34.

(46) Hwang, C.; Sinskey, A. J.; Lodish, H. F. Oxidized Redox State of Glutathione in the Endoplasmic Reticulum. *Science* **1992**, *257*, 1496-1502.

(47) Lee, M. H.; Yang, Z.; Lim, C. W.; Lee, Y. H.; Dongbang, S.; Kang, C.; Kim, J. S. Disulfide-Cleavage-Triggered Chemosensors and Their Biological Applications. *Chem. Rev.* **2013**, *113*, 5071-5109.

(48) Hassan, S. S. M.; Rechnitz, G. A. Determination of Glutathione and Glutathione Reductase with a Silver Sulfide Membrane Electrode. *Anal. Chem.* **1982**, *54*, 1972-1976.

(49) Fu, X.; Cate, S. A.; Dominguez, M.; Osborn, W.; Ozpolat, T.; Konkle, B. A.; Chen, J.; Lopez, J. A. Cysteine Disulfides (Cys-ss-X) as Sensitive Plasma Biomarkers of Oxidative Stress. *Sci. Rep.* **2019**, *9*, 115.

(50) Kleinman, W. A.; Richie, J. P. Status of Glutathione and Other Thiols and Disulfides in Human Plasma. *Biochem. Pharmacol.* **2000**, *60*, 19-29.

(51) McKeown, S. R. Defining Normoxia, Physoxia and Hypoxia in Tumours-Implications for Treatment Response. *Brit. J. Radiol.* **2014**, *87*, 20130676.

(52) Koobotse, M. O.; Schmidt, D.; Holly, J. M. P.; Perks, C. M. Glucose Concentration in Cell Culture Medium Influences the BRCA1-Mediated Regulation of the Lipogenic Action of IGF-I in Breast Cancer Cells. *Int. J. Mol. Sci.* **2020**, *21*, 8674.

(53) Shibamoto, Y.; Zhou, L.; Hatta, H.; Mori, M.; Nishimoto, S. In Vivo Evaluation of a Novel Antitumor Prodrug, 1-(2′-Oxopropyl)-5-Fluorouracil (OFU001), which Releases 5-Fluorouracil upon Hypoxic Irradiation. *Int. J. Radiat. Oncol. Biol. Phys.* **2001**, *49*, 407-413.

(54) Tanabe, K.; Sugiura, M.; Ito, T.; Nishimoto, S. Synthesis and One-Electron Reduction Characteristics of Radiation-Activated Prodrugs Possessing Two 5-Fluorodeoxyuridine Units. *Bioorg. Med. Chem.* **2012**, *20*, 5164-5168.

(55) Peng, H. J.; Cheng, Y. F.; Dai, C. F.; King, A. L.; Predmore, B. L.; Lefer, D. J.; Wang, B. H. A Fluorescent Probe for Fast and Quantitative Detection of Hydrogen Sulfide in Blood. *Angew. Chem. Int. Ed.* **2011**, *50*, 9672-9675.

(56) Tanabe, K.; Ishizaki, J.; Ando, Y.; Ito, T.; Nishimoto, S. Reductive Activation of 5-Fluorodeoxyuridine Prodrug Possessing Azide Methyl Group by Hypoxic X-Irradiation. *Bioorg. Med. Chem. Lett.* **2012**, *22*, 1682-1685.

(57) Geng, J.; Zhang, Y.; Gao, Q.; Neumann, K.; Dong, H.; Porter, H.; Potter, M.; Ren, H.; Argyle, D.; Bradley, M. Switching on Prodrugs Using Radiotherapy. *Nat. Chem.* **2021**, *13*, 805-810.

(58) Wilson, W. R.; Hay, M. P. Targeting Hypoxia in Cancer Therapy. *Nat. Rev. Cancer* **2011**, *11*, 393-410.

(59) Ding, Z.; Guo, Z.; Zheng, Y.; Wang, Z.; Fu, Q.; Liu, Z. Radiotherapy Reduces N-Oxides for Prodrug Activation in Tumors. *J. Am. Chem. Soc.* **2022**, *144*, 9458-9464.

(60) Kriste, A. G.; Tercel, M.; Anderson, R. F.; Ferry, D. M.; Wilson, W. R. Pathways of Reductive Fragmentation of Heterocyclic Nitroarylmethyl Quaternary Ammonium Prodrugs of Mechlorethamine. *Radiat. Res.* **2002**, *158*, 753-762.

(61) Guo, Z.; Hong, H.; Zheng, Y.; Wang, Z.; Ding, Z.; Fu, Q.; Liu, Z. Radiotherapy-Induced Cleavage of Quaternary Ammonium Groups Activates Prodrugs in Tumors. *Angew. Chem. Int. Ed.* **2022**, *61*, e202205014.

(62) Fu, Q.; Gu, Z.; Shen, S.; Bai, Y.; Wang, X.; Xu, M.; Sun, P.; Chen, J.; Li, D.; Liu, Z. Radiotherapy Activates Picolinium Prodrugs in Tumours. *Nat. Chem.* **2024**, *16*, 1348-1356.

(63) Akisawa, K.; Makanai, H.; Nishihara, T.; Tanabe, K. Hypoxic X-irradiation as a Trigger for Reduction of Metal Ion and Azide-Alkyne Cycloaddition on Oligodeoxynucleotides. *Tetrahedron Lett.* **2022**, *92*.

(64) Cao, W.; Wang, J.; Liang, Y.; Wu, S.; Deng, R.; Zhu, H. Radiotherapy Mediated Catalytic Prodrug Therapy with Higher Radiochemical Conversion than Hydrated Electrons. *ChemRxiv*, **2024**.

(65) Fu, Q.; Zhang, S.; Shen, S.; Gu, Z.; Chen, J.; Song, D.; Sun, P.; Wang, C.; Guo, Z.; Xiao, Y.; et al. Radiotherapy-Triggered Reduction of Platinum-Based Chemotherapeutic Prodrugs in Tumours. *Nat. Biomed. Eng.* **2024**.

(66) Fu, Q.; Li, H.; Duan, D.; Wang, C.; Shen, S.; Ma, H.; Liu, Z. External-Radiation-Induced Local Hydroxylation Enables Remote Release of Functional Molecules in Tumors. *Angew. Chem. Int. Ed.* **2020**, *59*, 21546-21552.

(67) Ma, N.; Li, Y.; Xu, H.; Wang, Z.; Zhang, X. Dual redox responsive assemblies formed from diselenide block copolymers. *J. Am. Chem. Soc.* **2010**, *132*, 442-443.

(68) Li, T.; Pan, S.; Gao, S.; Xiang, W.; Sun, C.; Cao, W.; Xu, H. Diselenide-Pemetrexed Assemblies for Combined Cancer Immuno-, Radio-, and Chemotherapies. *Angew. Chem. Int. Ed.* **2020**, *59*, 2700-2704.

(69) Li, T.; Pan, S.; Zhuang, H.; Gao, S.; Xu, H. Selenium-Containing Carrier-Free Assemblies with Aggregation-Induced Emission Property Combine Cancer Radiotherapy with Chemotherapy. *ACS Appl. Bio. Mater.* **2020**, *3*, 1283-1292.

(70) Gao, S. Q.; Li, T. Y.; Guo, Y.; Sun, C. X.; Xianyu, B. R.; Xu, H. P. Selenium-Containing Nanoparticles Combine the NK Cells Mediated Immunotherapy with Radiotherapy and Chemotherapy. *Adv. Mater.* **2020**, *32*, e1907568.

(71) Li, T. Y.; Pan, S. J.; Gao, S. Q.; Xiang, W. T.; Sun, C. X.; Cao, W.; Xu, H. P. Diselenide-Pemetrexed Assemblies for Combined Cancer Immuno-, Radio-, and Chemotherapies. *Angew. Chem. Int. Ed.* **2020**, *59*, 2700-2704.

(72) Ma, N.; Xu, H.; An, L.; Li, J.; Sun, Z.; Zhang, X. Radiation-Sensitive Diselenide Block Co-Polymer Micellar Aggregates: Toward the Combination of Radiotherapy and Chemotherapy. *Langmuir* **2011**, *27*, 5874-5878.

(73) Cao, W.; Zhang, X.; Miao, X.; Yang, Z.; Xu, H. Gamma-Ray-Responsive Supramolecular Hydrogel Based on a Diselenide-Containing Polymer and a Peptide. *Angew. Chem. Int. Ed.* **2013**, *52*, 6233-6237.

(74) Dai, Y. H.; Guan, J.; Zhang, S. H.; Pan, S. J.; Xianyu, B. R.; Ge, Z. X.; Si, J. Y.; He, C. W.; Xu, H. P. Tellurium-Containing Polymers: Recent Developments and Trends. *Prog. Polym. Sci.* **2023**, *141*, 101678.

(75) Cao, W.; Gu, Y.; Li, T.; Xu, H. Ultra-Sensitive ROS-Responsive Tellurium-Containing Polymers. *Chem. Commun.* **2015**, *51*, 7069-7071.

(76) Tanabe, K.; Kuraseko, E.; Yamamoto, Y.; Nishimoto, S. One-electron reductive template directed ligation of oligodeoxynucleotides possessing a disulfide bond. *J. Am. Chem. Soc.* **2008**, *130*, 6302-6303.

(77) Tanabe, K.; Matsumoto, E.; Ito, T.; Nishimoto, S. Radiolytic Cyclization of Stem-and-Loop Structured Oligodeoxynucleotide with Neighboring Arrangement of Alpha, Omega-bis-disulfides. *Org. Biomol. Chem.* **2010**, *8*, 4837-4842.

(78) Tanabe, K.; Asada, T.; Ito, T.; Nishimoto, S. Radiolytic Reduction Characteristics of Drug-Encapsulating DNA Aggregates Possessing Disulfide Bond. *Bioconjug. Chem.* **2012**, *23*, 1909-1914.

Organochlorides Mediate Oxidation Reactions Induced by Low Dose Ionizing Radiation

3

Abstract

The controlled release of drugs using local ionizing radiation presents a promising approach for targeted cancer treatment, particularly when applied in concurrent radio-chemotherapy. In these approaches, radiation-generated reactive species often play an important role. However, the reactive species that can be used to trigger release have low yield and lack selectivity. Here, we demonstrate the generation of highly oxidative species when aqueous solutions containing low concentrations of organochlorides (such as chloroform) are irradiated with ionizing radiation at therapeutically relevant doses. These reactive species were identified as peroxyl radicals, which formed in a reaction cascade between organochlorides and aqueous electrons. We employed stilbene-based probes to investigate the oxidation process, showing double bond oxidation and cleavage. To translate this reactivity into a radiation-sensitive material, we have synthesized a micelle forming amphiphilic block copolymer that has stilbene as the linker between two blocks. Upon exposure to ionizing radiation, the oxidation of stilbene led to the cleavage of the polymer, which induces the dissociation of the block-copolymer micelles and the release of loaded drugs.

Availability and Contributions

This chapter is adapted from an article published as: Liu, J.; Brevé, T. G.; Xu, B.; Hagedoorn, P.-L.; Denkova, A. G.; Eelkema, R. *CCS Chem.* **2024**, *6*, 1712-1720.

J.L., A.D. and R.E. developed the project idea. J.L. conducted most of the experiments, designed all the figures and schemes and wrote the first draft. T.B. observed the first oxidation. B.X. helped the radiation experiments. A.D. and R.E. supervised the project, secured funding and corrected manuscript.

Introduction

Over the last few decades, smart materials that exhibit responses to various stimuli have found wide application in drug delivery systems.[1,2] In the area of cancer treatment, stimuli-responsive self-assemblies composed of amphiphilic block copolymers are used to encapsulate hydrophobic anti-tumor drugs to transport them in the bloodstream, which helps to address the challenge of poor solubility and also mitigates the toxic effects of the drugs.[3,4] Several biodegradable polymer building blocks, including poly(ε-caprolactone) (PCL), poly(lactide-co-glycolide) (PLGA)[5], and polyethylene glycol (PEG), have been approved by the FDA (U. S. Food and Drug Administration) for clinical application.[6] These polymers can be modified such that they exhibit changes in physical or chemical properties upon exposure to stimuli from external sources (*e.g.*, light[7], ultrasound[8], magnetic field[9]) or from cancerous tissues (*e.g.*, pH[10], reactive oxygen species[11,12], temperature[9], biomarkers[13]). These changes can include alterations in their aggregation state or bond cleavage, which in turn facilitate controlled drug release in tumor cells.

Among the various stimuli of interest, ionizing radiation is a promising external stimulus owing to its capability of precise and deep tissue penetration.[14-17] Combined chemo-radiation therapy has been demonstrated to exhibit improved therapeutic efficacy in the treatment of cancer.[18-21] In biological systems, the exposure to ionizing radiation initiates a cascade of reactions which result in the generation of reactive species including aqueous electrons, hydroxyl radicals, hydrogen radicals, and hydrogen peroxide. These species have been shown to trigger reactions that lead to bond cleavage and subsequent release of drugs. For example, the oxidative cleavage of diselenide bonds by hydroxyl radicals results in the disassembly of diselenide-based nanoparticles, facilitating the release of encapsulated drugs.[22-24] Radiation-responsive groups have been applied in prodrug therapy,[25-28] wherein an anti-tumor drug is protected and can be selectively activated upon reacting with hydroxyl radicals or aqueous electrons. The applied radiation dose should be within the clinically relevant window, which depends on the specific type of radiotherapy. For instance, in external beam radiotherapy, patients typically receive a dose fraction of 1.8-2 Gy over 6-7 weeks, accumulating to a total dose of 60-70 Gy[29-31], while in radioembolization higher doses (80-100 Gy) are applied.[32] In radionuclide therapy, localized doses as high as 100 Gy can be achieved.[33] Despite the success in applying

radiation-responsive functional groups, the studies of smart materials that exhibit response to ionizing radiation, especially clinically relevant doses, is still limited due to the poor sensitivity and selectivity when it is used to trigger reactions.

Herein, we present the discovery of an ionizing radiation induced oxidation reaction that is greatly amplified in the presence of low concentrations of aliphatic organochlorides. This amplification effect is attributed to the generation of aliphatic peroxyl radicals, which arise from the reaction between the organochlorides and radiation-generated aqueous electrons (**Figure 3.1**). Stilbene serves as a suitable probe for monitoring the oxidation process, as it undergoes oxidation specifically at its double bond motif, resulting in a measurable decrease in UV-vis light absorption. Subsequently, we have developed a stilbene-linked amphiphilic block copolymer (**PSP**) that allows for radiation-induced release of a chemotherapeutic drug.

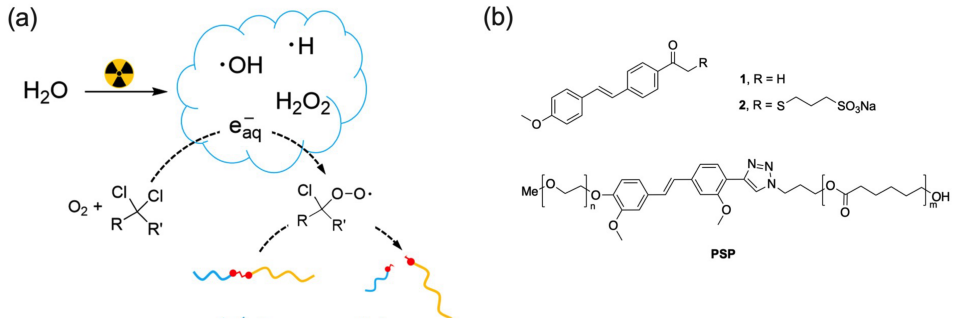

Figure 3.1. Oxidative cleavage of stilbene by radiation in water containing organochloride. (a) proposed sequence of events; (b) Chemical structure of compound **1**, **2** and block co-polymer **PSP**.

Results and Discussion

We found that the absorbance of a chloroform solution of the trans-stilbene derivative **1** decreased after exposure to γ-rays from a ^{60}Co source (**Figure 3.2a**). The *vic*-diol as well as 4-acetylbenzaldehyde and 4-anisaldehyde were identified as products indicating oxidation and oxidative cleavage of the ethene moiety in compound **1** (**Figures S3.3-S3.5**). Given that the concentration of compound **1** is 50 μM in chloroform, it is unlikely that compound **1** undergoes direct radiation-induced oxidation reactions. Rather, it is more plausible that

interaction of chloroform, the solvent, with ionizing radiation generates reactive species that subsequently oxidize compound **1**. Previous research by Wilhelm et al. reported the formation of Cl_2 and CCl_3OOH during γ-irradiation of O_2-saturated chloroform.[34] Given this precedent and the products identified from the reaction of **1**, we propose that compound **1** is oxidized by a peroxide species generated during radiolysis of chloroform.

To investigate the influence of the solvent on the radiolysis of stilbene, compound **1** was dissolved in various solvents and subsequently exposed to γ-radiation. We employed the relative UV-Vis light absorption to evaluate the extent of decomposition (**Figure 3.2b**). The relative absorption is calculated from the absorption of compound **1** at 350 nm post-irradiation divided by its initial absorption. Interestingly, oxidation occurs in all tested chlorinated organic solvents, whereas in non-chlorinated solvents, the molecule remains intact after irradiation. We therefore concluded that the carbon-chlorine bond plays a crucial role in the oxidation of stilbene during radiolysis. Furthermore, the extent of decomposition varies depending on the solvent used. Chloroform and methyl trichloroacetate, where a carbon atom is bonded to three chlorine atoms, showed the largest effect. In 1,2-dichloroethane and dichloromethane, where a carbon atom is bonded to fewer than three chlorine atoms, a lower degree of oxidation is observed. In contrast, for chlorinated aromatic solvents such as 1,2-dichlorobenzene and 1,2,4-trichlorobenzene, compound **1** exhibits the lowest degree of oxidation among all chlorine-based solvents. According to previous research conducted by Packer et al.[36], the reactivity of alkyl peroxyl radicals increases when the α-carbon is bonded with chlorine, with further enhancement observed upon multiple chlorine substitutions. These trends align with our observations.

To test if this organochloride-mediated radiolysis of stilbene could take place in water, we synthesized compound **2** (**Figure 3.1b**), in which a sulfonate group was introduced to increase solubility in water. Upon irradiation by γ-rays (75 Gy) in water, the concentration of compound **2** decreased from 90 µM to 56 ± 0.2 µM, indicating its oxidation (**Figure S3.6**). Only diol (compound **S11** in **Scheme S3.2** and **Figure S3.7c**) was identified as the product of radiolysis under these conditions. When 0.1 vol% chloroform was added in the solution (the maximum solubility of chloroform in water at 20 °C is 0.54 vol% according to the IUPAC-NIST database), a greater decrease was observed (from 90 µM to 28.1 ± 1.0

μM) after exposure to the same dose of radiation. This indicates the involvement of additional reactive species derived from the radiolysis of chloroform. The corresponding aldehyde (compound **S12** and *p*-anisaldehyde) and diol (compound **S11**) were found in MS, suggesting a further oxidating process compared to pure water.

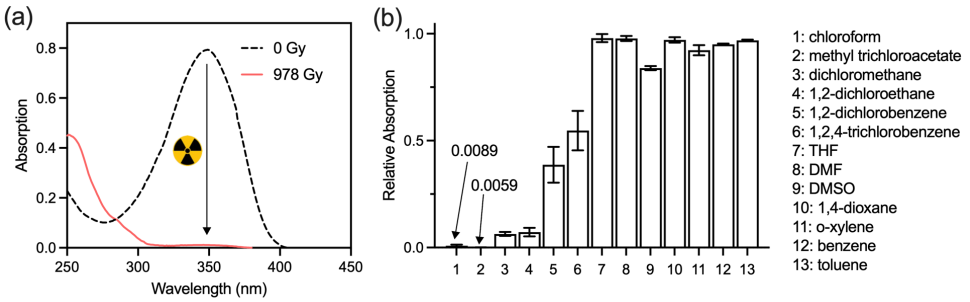

Figure 3.2. (a) UV-vis absorption of compound **1** before and after 978 Gy of γ-irradiation in chloroform. (b) Relative absorption of compound **1** after 978 Gy of γ-irradiation in different solvents. The γ-rays are delivered by the ^{60}Co source, absorption is relative to the unirradiated solution. Error bars represent experimental uncertainties of three samples.

Inspired by the ionizing radiation-induced oxidative cleavage of stilbene, we aimed to design a radiation-responsive nanocarrier capable of dissociating upon exposure to radiation. For this purpose, we have synthesized an amphiphilic block co-polymer, poly(ε-caprolactone)-stilbene-poly(ethylene glycol) (denoted as **PSP)**, using a stilbene derivative as the linker connecting the hydrophilic and hydrophobic blocks (**Figure 3.1, b**). We chose PCL and PEG as the polymer blocks since they are widely employed materials for nanocarriers in biomedical settings.

To verify the radiation-induced cleavage of **PSP**, we prepared micelles and irradiated the solutions with γ-rays over a dose range of 0 to 8 Gy, using phosphate buffered saline (PBS, pH 7.4) or PBS/chloroform (0.1 vol% chloroform in PBS, pH 7.4) as the solvent. We employed X-rays (240 keV) as an alternative irradiation source. We used fractionated radiation of 2 Gy per fraction, since these conditions are close to clinical application. The micelle solution exhibits an absorption peak at 350 nm, corresponding to the absorption of the stilbene moiety in **PSP** (**Figure S3.9**). **Figure 3.3 (a)** shows a significant decrease of absorption after 4 Gy of irradiation in PBS/chloroform. The gradual decrease indicates a

dose-dependent oxidation of stilbene. However, irradiation with the same dose in PBS leads to a much less pronounced decrease in absorption and no change in the peak shape (**Figure S3.9**), indicating no oxidation in the absence of chloroform. The energy of the irradiation source does not significantly influence the efficiency of the oxidation process, as evidenced by the similar slopes of absorption decrease observed for X-rays and γ-rays. This phenomenon should be universal to chemical reactions triggered by species formed when exposed to radiation of the same type, since the yield of the species, known as G-values (molecules produced per 100 eV absorbed energy), remains consistent regardless of the energy level of the radiation source.

We varied the concentration of chloroform in PBS to investigate the effect of the molar ratio of chloroform-to-stilbene on the oxidation process. The extent of the decrease in absorption correlates with the chloroform-to-stilbene ratio (**Figure 3.3b**). At the molar ratio of 500:1, the absorption decreases from 1.0 to 0.60, whereas at molar ratios ranging from 10:1 to 0.5:1, the absorption does not decrease. The dependence indicates that the oxidation is not catalytic in nature but rather requires an excess amount of chloroform.

We lyophilized the micelle solutions after irradiation and measured the molecular weight of the polymers using gel permeation chromatography (GPC) to verify the oxidative cleavage of **PSP**. As shown in **Figure 3.3c**, **PSP** has a retention time of 8.19 min, correspond to a molecular weight of 9.3 kDa. Following the exposure to 15 Gy of γ-irradiation in the presence of chloroform, a shoulder peak appears at a retention time of 8.44 min, which is the same retention time as the PCL-block. Higher exposure dose of 30 Gy increases the intensity of the PCL peak, further supporting the conclusion that the oxidative cleavage by radiation is dose dependent.

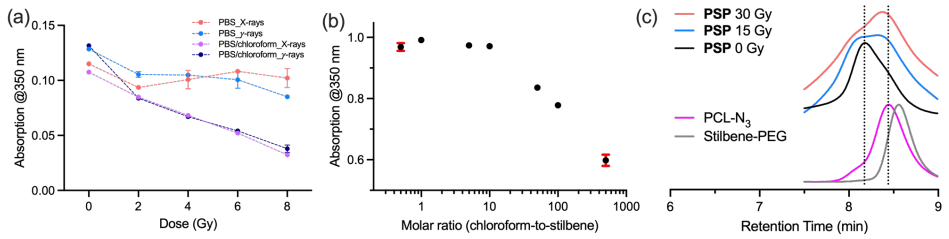

Figure 3.3. (a) Decrease of the absorption of **PSP** micelle solutions (0.05 mg/mL) at 350 nm against radiation dose; (b) decrease of absorption after 75 Gy of irradiation in solutions with varied chloroform-to-stilbene ratio (for some data, error bars are smaller than data markers); (c) GPC retention time of PCL-block, PEG-block, **PSP** before and after γ-irradiation in water/0.1 vol% chloroform solution. The γ-rays are delivered by the ^{60}Co source. We used 240 keV X-rays. Error bars represent experimental uncertainties of three samples.

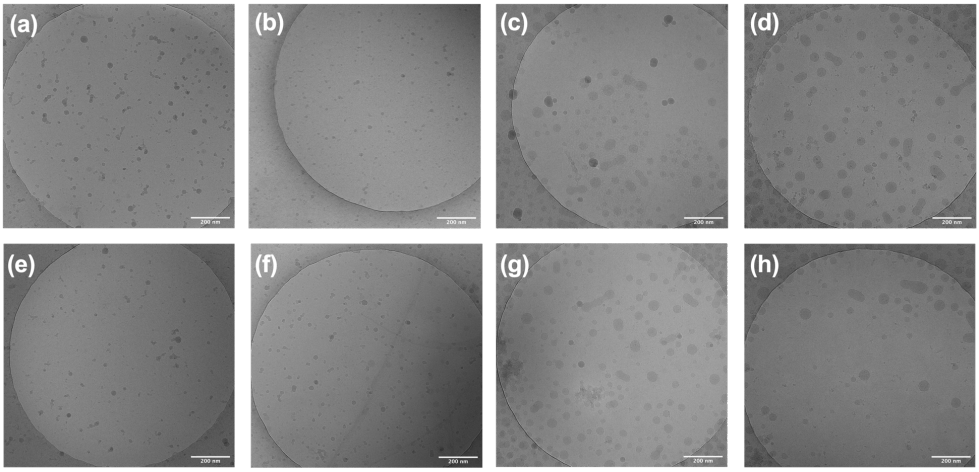

Figure 3.4. Cryo-EM images of PSP micelles and PSP encapsulating doxorubicin (a) PSP micelle solution in water, 0 Gy; (b) PSP micelle solution in water/chloroform, 0 Gy; (c) PSP-Dox micelle solution in water, 0 Gy; (d) PSP-Dox micelle solution in water/chloroform, 0 Gy; (e) PSP micelle solution in water, 15 Gy; (f) PSP micelle solution in water/chloroform, 15 Gy; (g) PSP-Dox micelle solution in water, 15 Gy; (h) PSP-Dox micelle solution in water/chloroform, 15 Gy.

Cryo-EM images were used to investigate the morphological changes of the micelles after irradiation in water or water/0.1 vol% chloroform solution. As shown in **Figure 3.4**, the non-irradiated samples exhibit predominantly spherical particles, with a minor presence of worm-like structures. Particle analysis of the non-irradiated micelles showed an average core diameter of 16.3 ± 4.9 nm in water and 14.7 ± 3.0 nm in water/chloroform (**Figure S3.10**). Upon exposure to 15 Gy of γ-radiation, the micelles maintained their spherical

morphology, with an average core diameter of 16.1 ± 3.6 nm in water and 14.4 ± 4.1 nm in water/chloroform. The size distribution of the micelles before and after irradiation in water or in water/chloroform exhibited minimal variation, indicating that the structure of the micelles was preserved. The hydrodynamic diameter (D_h) of PSP, determined by dynamic light scattering (DLS), exhibited no size distribution shift after irradiation in water and water/chloroform (**Figure S3.10 a, d**).

The oxidation pathway of stilbene varies depending on the solvent, as the irradiated medium generating reactive species is different. In chloroform, the oxidizing agents generated through the radiolysis of chloroform include Cl_2 and CCl_3OOH.[34] However, in aqueous solutions, the majority of ionizing radiation energy is absorbed by water molecules, leading to the generation of primary species such as aqueous electrons (e_{aq}^-), hydroxyl radicals (OH•) and hydrogen radicals (H•) [equation. (1)]. Experimental studies using pulse radiolysis[36-40] have confirmed that in the presence of chloroform, the primary reaction of chloroform involves reduction by e_{aq}^- because of the high electron affinity, resulting in the formation of chloride ions and the carbon-centered radical •$CHCl_2$ [equation. (2)]. In the presence of trace amount of oxygen, the •$CHCl_2$ reacts with oxygen at a diffusion-controlled rate, leading to the formation of peroxyl radicals [equation. (3)] that are able to oxidize stilbene.

$$H_2O \xrightarrow{\gamma\text{-rays}} \cdot H + \cdot OH + e_{aq}^- \quad (1)$$

$$CHCl_3 + e_{aq}^- \longrightarrow \cdot CHCl_2 + Cl^- \quad (2)$$

$$\cdot CHCl_2 + O_2 \longrightarrow Cl_2HCOO\cdot \quad (3)$$

We conducted scavenger experiments to investigate the underlying mechanism of radiation-induced stilbene oxidation in water/0.1 vol% chloroform solution. Micelle solutions were irradiated in PBS (pH 7.4) containing 0.1 vol% chloroform and scavengers. Irradiation of the micelle solution in a PBS buffer yields negligible absorption reduction (96.0% remaining), whereas the addition of 0.1 vol% chloroform results in a notable reduction to 38.9% (**Figure 3.5a**). The presence of 10 mM tert-butanol (•OH scavenger) leads to no significant difference in absorption reduction compared to that of the chloroform experiment ($P = 0.17$), suggesting that scavenging of the hydroxyl radical does not impede

the reaction. Scavenging of the peroxyl radical by 10 mM ascorbic acid or of aqueous electrons by 100 mM $NaNO_3$ shows much less absorption reduction than the chloroform experiment, which means the peroxyl radical and aqueous electrons must play a role in the reaction. Removal of oxygen via nitrogen purging results in an absorption reduction to 73% of the original value, suggesting the participation of oxygen in the oxidation. Additional EPR experiments using spin traps showed the formation of hydrated electrons under γ-irradiation of PBS, and their efficient removal in the presence of chloroform (See **Figure S3.11**). These findings provide further confirmation that the oxidation of stilbene is associated to aqueous electron and peroxyl radical formation during the radiolysis of aqueous solutions containing chlorinated compound.

We investigated whether chlorinated organic molecules, apart from chloroform, can induce oxidation of stilbene under irradiation. Micelle solutions containing various chlorinated molecules at equal concentration (12 mM, equal to that of 0.1 vol% chloroform in PBS) were irradiated with the same dose of γ-rays, and the degree of oxidation was evaluated based on the reduction in absorption. Note that all used organochlorides are added at concentrations below their solubility limit in water, i.e. in all cases homogenous solutions were used. As illustrated in **Figure 3.5b**, all multi-chlorinated organic additives exhibit oxidizing capabilities, whereas the monochlorinated 2-chloroethanol shows no significant difference in reduction compared to that observed in PBS alone. This suggests that the peroxyl radical formed from 2-chloroethanol (**R1**, **Scheme 3.1**) lacks sufficient reactivity to react with stilbene. In contrast, **R2**, formed from 2,2,2-trichloroethanol, shows the highest reactivity among all tested molecules, resulting in an absorption decrease of 80%. This can be attributed to the electron-withdrawing effect of the chlorine and hydroxyl groups, which render the corresponding peroxyl radical more reactive. The same trend is observed in experiments involving chloroform and dichloromethane. At the pH of these experiments, trichloroacetic acid and the so formed peroxyl radicals are ionized. The carboxylate ion group exhibits a deactivating effect, as previously reported by Packer and coworkers[36], so the degree of oxidation in trichloroacetic acid is lower compared to that in the chloroform experiment.

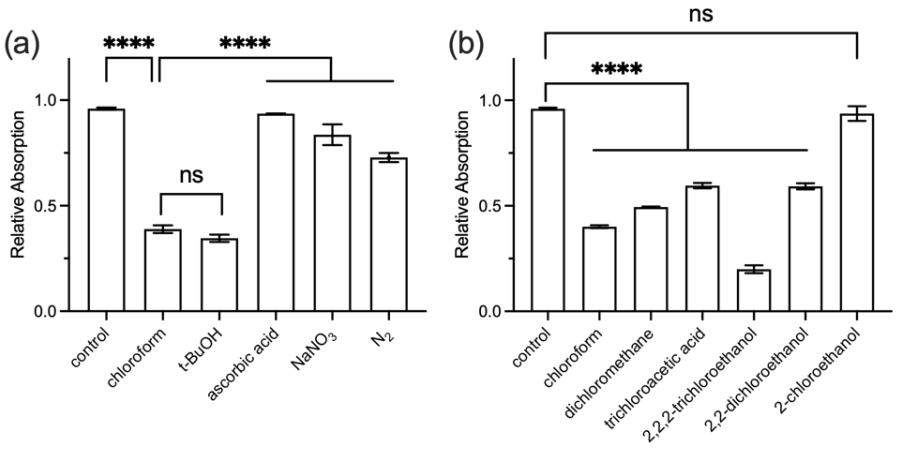

Figure 3.5. (a) The relative absorption of micelles solutions with scavengers after 75 Gy of γ-irradiation. Control, 0.5 mg/mL **PSP** in 10 mM PBS (pH 7.4); chloroform, 0.1 vol% chloroform was added to the control solution. Scavengers were added to the 0.1 vol% chloroform solution: *t*-BuOH, 10 mM; ascorbic acid, 10 mM; $NaNO_3$, 100 mM. N_2, solution was degassed and backfilled with N_2 before adding chloroform. (n = 3, one-way ANOVA t-test, *P*-values >0.05 show as "ns", *P*-values <0.0001 are indicated with four asterisks). (b) The relative absorption of micelles solutions after 75 Gy of γ-irradiation contain 12 mM organochlorides. Control, 0.5 mg/mL PSP in 10 mM PBS (pH 7.4). Organochlorides were added to the control solution respectively.

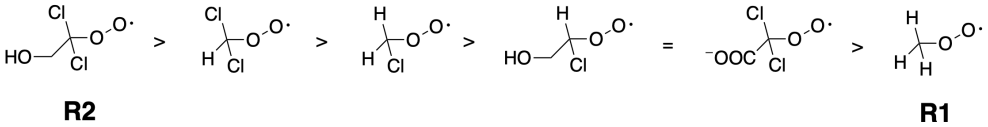

Scheme 3.1. Relative reactivity towards stilbene.

To test the drug release property of **PSP** micelles under irradiation, we used doxorubicin (Dox) as a model drug. The Dox loading efficiency in the micelles was 0.23-0.25 mg/mg (Dox/**PSP**). PSP-Dox micelles showed significantly larger core diameter than PSP micelles (36.2 ± 10.7 nm in water and 43.9 ± 10.1 nm in water/chloroform, **Figure 3.4 c, d**). The D_h of Dox-loaded micelles was 97.8 ± 1.0 nm, while that of unloaded micelles was 38.2 ± 0.2 nm (**Figure S3.13**, **Table S3.3**). The relatively larger diameter of **PSP-Dox** compares to **PSP** alone is attributed to the high Dox loading in the hydrophobic core of the micelles. Upon exposure to 15 Gy of γ-irradiation in water/chloroform, PSP-Dox showed lower number of large micelles (40-55 nm) and relatively more small micelles (15-30 nm) (**Figure 3.4 d, h** and **Figure S3.10 k, l**). In contrast, PSP-Dox micelles in water exhibited

no significant change of morphology when irradiated by γ-rays (**Figure 3.4 c, g** and **Figure S3.10 h, i**). The Dox release ratio after irradiation was determined, representing the releasing Dox from the micelles divided by the total Dox after irradiation. As shown in **Figure 3.6**, both groups exhibited a Dox release of approximately 30% at 0 Gy, indicating a passive release of Dox during the preparation of the micelle solutions. After 8 Gy of irradiation, there was no significant difference in Dox release between the PBS and PBS/chloroform group. However, an increase in radiation dose to 15 Gy, resulted in a higher release of Dox in the in PBS/chloroform group, i.e. a release of 74.4%, while in the PBS group 45.7% released from the micelles. Increasing the exposure dose to 30 Gy showed the same trend as observed in the 15 Gy case.

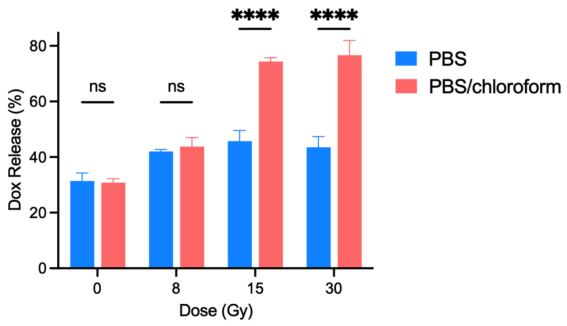

Figure 3.6. The release profiles of Dox from **PSP** micelles solutions irradiated in PBS and PBS/chloroform solution (n = 3, two-way ANOVA t-test, *P*-values < 0.0001 are indicated with four asterisks).

Conclusions

We show that the presence of low concentration organochloride compounds can have a profound effect on the oxidizing capabilities of reactive species generated in the radiolysis of water. Using clinical dose gamma-rays or X-rays, we observed oxidative cleavage of stilbene derivatives in buffered aqueous solutions containing 0.1 vol% chloroform or other multi-chloro compounds. Mechanistic studies revealed that the reactive species responsible for the oxidation reaction were peroxyl radicals generated through the reaction between

aqueous electrons and chlorinated molecules. Irradiation of micelles, composed of an amphiphilic block copolymer with stilbene serving as the linkage between the two building blocks, in a water/0.1 vol% chloroform solution, resulted in the breakage of polymer chains. This, in turn, led to the disruption of the micelles and the subsequent release of the cargo encapsulated within them. This study offers valuable insights into the molecular design of radiation-sensitive materials intended for use in controlled drug delivery applications, in particular for combined chemotherapy and radiotherapy. As the application of small molecular organochlorides in clinical settings poses biocompatibility concerns, we are currently investigating avenues to reduce organochloride toxicity.

References

(1) Cao, Z. Q.; Wang, G. J. Multi-Stimuli-Responsive Polymer Materials: Particles, Films, and Bulk Gels. *Chem. Rec.* **2016**, *16*, 1398-1435.

(2) Criado-Gonzalez, M.; Mecerreyes, D. Thioether-Based ROS Responsive Polymers for Biomedical Applications. *J. Mater. Chem. B* **2022**, *10*, 7206-7221.

(3) Ge, Z.; Liu, S. Functional Block Copolymer Assemblies Responsive to Tumor and Intracellular Microenvironments for Site-Specific Drug Delivery and Enhanced Imaging Performance. *Chem. Soc. Rev.* **2013**, *42*, 7289-7325.

(4) Lv, S.; Wu, Y.; Cai, K.; He, H.; Li, Y.; Lan, M.; Chen, X.; Cheng, J.; Yin, L. High Drug Loading and Sub-Quantitative Loading Efficiency of Polymeric Micelles Driven by Donor-Receptor Coordination Interactions. *J. Am. Chem. Soc.* **2018**, *140*, 1235-1238.

(5) Bawa, K. K.; Oh, J. K. Stimulus-Responsive Degradable Polylactide-Based Block Copolymer Nanoassemblies for Controlled/Enhanced Drug Delivery. *Mol. Pharm.* **2017**, *14*, 2460-2474.

(6) Bobo, D.; Robinson, K. J.; Islam, J.; Thurecht, K. J.; Corrie, S. R. Nanoparticle-Based Medicines: A Review of FDA-Approved Materials and Clinical Trials to Date. *Pharm. Res.* **2016**, *33*, 2373-2387.

(7) Men, Y.; Breve, T. G.; Liu, H.; Denkova, A. G.; Eelkema, R. Photo Cleavable Thioacetal Block Copolymers for Controlled Release. *Polym. Chem.* **2021**, *12*, 3612-3618.

(8) Wei, P.; Cornel, E. J.; Du, J. Ultrasound-Responsive Polymer-based Drug Delivery Systems. *Drug Deliv. Transl. Res.* **2021**, *11*, 1323-1339.

(9) Zou, H.; Yuan, W. Temperature- and Redox-responsive Magnetic Complex Micelles for Controlled Drug Release. *J. Mater. Chem. B* **2015**, *3*, 260-269.

(10) Mao, J.; Li, Y.; Wu, T.; Yuan, C.; Zeng, B.; Xu, Y.; Dai, L. A Simple Dual-pH Responsive Prodrug-Based Polymeric Micelles for Drug Delivery. *ACS Appl. Mater. Interfaces* **2016**, *8*, 17109-17117.

(11) Piergentili, I.; Bouwmans, P. R.; Reinalda, L.; Lewis, R. W.; Klemm, B.; Liu, H.; de Kruijff, R. M.; Denkova, A. G.; Eelkema, R. Thioanisole Ester based Logic Gate Cascade to Control ROS-Triggered Micellar Degradation. *Polym. Chem.* **2022**, *13*, 2383-2390.

(12) Sun, C.; Liang, Y.; Hao, N.; Xu, L.; Cheng, F.; Su, T.; Cao, J.; Gao, W.; Pu, Y.; He, B. A ROS-Responsive Polymeric Micelle with a pi-Conjugated Thioketal Moiety for Enhanced Drug Loading and Efficient Drug Delivery. *Org. Biomol. Chem.* **2017**, *15*, 9176-9185.

(13) Ding, Y.; Kang, Y.; Zhang, X. Enzyme-Responsive Polymer Assemblies Constructed through Covalent Synthesis and Supramolecular Strategy. *Chem. Commun.* **2015**, *51*, 996-1003.

(14) Liu, H.; Laan, A. C.; Plomp, J.; Parnell, S. R.; Men, Y.; Dalgliesh, R. M.; Eelkema, R.; Denkova, A. G. Ionizing Radiation-Induced Release from Poly(ε-caprolactone-b-ethylene glycol) Micelles. *ACS Appl. Polym. Mater.* **2020**, *3*, 968-975.

(15) Starkewolf, Z. B.; Miyachi, L.; Wong, J.; Guo, T. X-ray Triggered Release of Doxorubicin from Nanoparticle Drug Carriers for Cancer Therapy. *Chem. Commun.* **2013**, *49*, 2545-2547.

(16) Zhang, L.; Zhang, S.; Xu, J.; Li, Y.; He, J.; Yang, Y.; Huynh, T.; Ni, P.; Duan, G.; Yang, Z.; et al. Low-Dose X-ray-Responsive Diselenide Nanocarriers for Effective Delivery of Anticancer Agents. *ACS Appl. Mater. Interfaces* **2020**, *12*, 43398-43407.

(17) Zhou, Z.; Chan, A.; Wang, Z.; Huang, X.; Yu, G.; Jacobson, O.; Wang, S.; Liu, Y.; Shan, L.; Dai, Y.; et al. Synchronous Chemoradiation Nanovesicles by X-Ray Triggered Cascade of Drug Release. *Angew. Chem. Int. Ed.* **2018**, *57*, 8463-8467.

(18) Denkova, A. G.; Liu, H.; Men, Y.; Eelkema, R. Enhanced Cancer Therapy by Combining Radiation and Chemical Effects Mediated by Nanocarriers. *Adv. Ther.* **2020**, *3*.

(19) Li, H.; Luo, Q.; Zhang, H.; Ma, X.; Gu, Z.; Gong, Q.; Luo, K. Nanomedicine Embraces Cancer Radio-Immunotherapy: Mechanism, Design, Recent Advances, and Clinical Translation. *Chem. Soc. Rev.* **2023**, *52*, 47-96.

(20) Pan, Y.; Tang, W.; Fan, W.; Zhang, J.; Chen, X. Development of Nanotechnology-Mediated Precision Radiotherapy for Anti-Metastasis and Radioprotection. *Chem. Soc. Rev.* **2022**, *51*, 9759-9830.

(21) Son, S.; Kim, J.; Kim, J.; Kim, B.; Lee, J.; Kim, Y.; Li, M.; Kang, H.; Kim, J. S. Cancer Therapeutics Based on Diverse Energy Sources. *Chem. Soc. Rev.* **2022**, *51*, 8201-8215.

(22) Cao, W.; Zhang, X.; Miao, X.; Yang, Z.; Xu, H. Gamma-Ray-Responsive Supramolecular Hydrogel Based on a Diselenide-Containing Polymer and a Peptide. *Angew. Chem. Int. Ed.* **2013**, *52*, 6233-6237.

(23) Li, T.; Pan, S.; Zhuang, H.; Gao, S.; Xu, H. Selenium-Containing Carrier-Free Assemblies with Aggregation-Induced Emission Property Combine Cancer Radiotherapy with Chemotherapy. *ACS Appl. Bio. Mater.* **2020**, *3*, 1283-1292.

(24) Ma, N.; Xu, H.; An, L.; Li, J.; Sun, Z.; Zhang, X. Radiation-Sensitive Diselenide Block co-Polymer Micellar Aggregates: Toward the Combination of Radiotherapy and Chemotherapy. *Langmuir* **2011**, *27*, 5874-5878.

(25) Ding, Z.; Guo, Z.; Zheng, Y.; Wang, Z.; Fu, Q.; Liu, Z. Radiotherapy Reduces N-Oxides for Prodrug Activation in Tumors. *J. Am. Chem. Soc.* **2022**, *144*, 9458-9464.

(26) Fu, Q.; Li, H.; Duan, D.; Wang, C.; Shen, S.; Ma, H.; Liu, Z. External-Radiation-Induced Local Hydroxylation Enables Remote Release of Functional Molecules in Tumors. *Angew. Chem. Int. Ed.* **2020**, *59*, 21546-21552.

(27) Geng, J.; Zhang, Y.; Gao, Q.; Neumann, K.; Dong, H.; Porter, H.; Potter, M.; Ren, H.; Argyle, D.; Bradley, M. Switching on Prodrugs Using Radiotherapy. *Nat. Chem.* **2021**, *13*, 805-810.

(28) Guo, Z.; Hong, H.; Zheng, Y.; Wang, Z.; Ding, Z.; Fu, Q.; Liu, Z. Radiotherapy-Induced Cleavage of Quaternary Ammonium Groups Activates Prodrugs in Tumors. *Angew. Chem. Int. Ed.* **2022**, *61*, e202205014.

(29) Manikantan, K.; Khode, S.; Sayed, S. I.; Roe, J.; Nutting, C. M.; Rhys-Evans, P.; Harrington, K. J.; Kazi, R. Dysphagia in head and neck cancer. *Cancer Treat. Rev.* **2009**, *35*, 724-732.

(30) Curran, W. J., Jr.; Paulus, R.; Langer, C. J.; Komaki, R.; Lee, J. S.; Hauser, S.; Movsas, B.; Wasserman, T.; Rosenthal, S. A.; Gore, E.; et al. Sequential vs. concurrent chemoradiation for stage III non-small cell lung cancer: randomized phase III trial RTOG 9410. *J. Natl. Cancer Inst.* **2011**, *103*, 1452-1460.

(31) De Ruysscher, D.; Niedermann, G.; Burnet, N. G.; Siva, S.; Lee, A. W. M.; Hegi-Johnson, F. Radiotherapy toxicity. *Nat. Rev. Dis. Primers* **2019**, *5*, 13.

(32) Ridouani, F.; Soliman, M. M.; England, R. W.; Hsu, M.; Moskowitz, C. S.; Doustaly, R.; Sofocleous, C. T.; Boas, F. E.; Yarmohammadi, H.; Deipolyi, A. R. Relationship of radiation dose to efficacy of radioembolization of liver metastasis from breast cancer. *Eur. J. Radiol.* **2021**, *136*, 109539.

(33) Lawhn-Heath, C.; Hope, T. A.; Martinez, J.; Fung, E. K.; Shin, J.; Seo, Y.; Flavell, R. R. Dosimetry in radionuclide therapy: the clinical role of measuring radiation dose. *Lancet Oncol.* **2022**, *23*, e75-e87.

(34) Schulte, J. W.; Suttle, J. F.; Wilhelm, R. Chemical Effects Produced in Chloroform by γ-Rays. *J. Am. Chem. Soc.* **1953**, *75*, 2222-2227.

(35) Packer, J. E.; Willson, R. L.; Bahnemann, D.; Asmus, K. D. Electron-Transfer Reactions of Halogenated Aliphatic Peroxyl Radicals-Measurement of Absolute Rate Constants by Pulse-Radiolysis. *J. Chem. Soc., Perkin Trans.* **1980**, (2), 296-299.

(36) Abadie, M. J. M. Radiolysis of Liquid Chloroform in an Oxygen Free Atmosphere. *Radiat. Phys. Chem.* **1982**, *19*, 63-71.

(37) Getoff, N. Decomposition of Biological Resistant Pollutants in Water by Irradiation. *Radiat. Phys. Chem.* **1990**, *35*, 432-439.

(38) Rajesh, P.; LaVerne, J. A.; Pimblott, S. M. High Dose Radiolysis of Aqueous Solutions of Chloromethanes: Importance in the Storage of Radioactive Organic Wastes. *J. Nucl. Mater.* **2007**, *361*, 10-17.

(39) Taghipour, F.; Evans, G. J. Radiolytic Dechlorination of Chlorinated Organics. *Radiat. Phys. Chem.* **1997**, *49*, 257-264.

(40) Weber, L. W.; Boll, M.; Stampfl, A. Hepatotoxicity and Mechanism of Action of Haloalkanes: Carbon Tetrachloride as a Toxicological Model. *Crit. Rev. Toxicol.* **2003**, *33*, 105-136.

Supporting Information

General methods

All compounds were purchased from commercial suppliers (Sigma Aldrich, Tokyo Chemical Industry and abcr Gute Chemie) and used without further purification unless otherwise specified. Compound **S3** was synthesized according to previous work from our group.[1] Detailed synthesis procedures of compound **1**, **2** and polymer **PSP** are presented in the supporting information. Reactions were monitored by thin-layer chromatography (TLC) on a silica gel plate and visualized by UV light (254 nm) or stained using a $KMnO_4/OH^-$ solution. Flash column chromatography was carried out on a 30 cm column loaded with 230-400 mesh silica gel. ^{1}H-NMR spectra were recorded on an Agilent-400 MR DD2 (399.67 MHz) at 298 K. UV-Vis spectroscopic measurements were performed on an Analytik Jena Specord spectrometer. Milli-Q water was obtained by purification of demineralized water with a Milli-Q IQ 7000 machine equipped with a Millipak 0.22 µM filter. HPLC-MS was performed on a LTQ XL spectrometer that was connected with a Shimadzu setup with D2 detector and Discovery C18 reverse phase column. Water/MeCN with 0.1% (v/v) formic acid was used as the mobile phase at a flow rate of 0.2 mL/min. The average molecular weight and dispersity (Đ, M_w/M_n) of the synthesized polymers were determined using a Shimadzu GPC system, which was equipped with a Shimadzu RID-10A refractive index detector and a Shimadzu SPD-20A UV-vis detector. Two columns, a PL gel guard column (MIXED-C, 5 µm) with dimensions of 50 mm x 7.5 mm, and an Agilent PLGel (MIXED-C, 5 µm) column with dimensions of 300 mm x 7.5 mm were used. The GPC system provided an effective molar mass range of 200 to 2 x 10^6 g/mol. The eluent used was DMF LiBr (25 mM), and the flow rate was set to 1.0 mL/min. The measurements were conducted at a temperature of 50 °C. The GPC was calibrated with low dispersity PEG standards (Sigma Aldrich) from 200 to 200,000 g/mol. Dynamic light scattering (DLS) was performed on a Zetasizer Pro equipped with laser operating at 633 nm. The irradiations with γ-rays were performed using a Nordion 220 ^{60}Co gamma cell. The dose rate at the experimental date was around 460 Gy/h which is calculated based on the decay law and the half-life of ^{60}Co. The delivered dose was calculated by the dose rate at the date of the experiments multiplied by the exposure time. Radiation was given in one fraction unless otherwise specified. The X-ray irradiation was carried out using an X-ray source (Philips

MCN 321 variable-energy X-ray tube) performed in a working voltage of 240 keV and a current of 10 mA. The dose rate of the X-ray source was determined using the method as described in literature.[2]

Synthesis

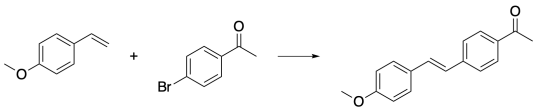

S1 **S2** **1**

3.56 g **S1** (17.9 mmol, 1.2 eq.), 2 g **S2**, (14.9 mmol, 1 eq.), 9 mL N,N-Dicyclohexylmethylamine (44.7 mmol, 3 eq.) and 100 mL 1,4-dioxane were added to a 100 mL round bottom flask. After degassing thoroughly, $Pd_2(dba)_3$ (171 mg, 0.30 mmol, 2 mol%) and bis(tri-tert-butylphosphine)palladium (76 mg, 0.15 mmol, 1 mol%) were added. The mixture was stirred at 100 ºC overnight under Ar. The solvent was removed under reduced pressure. The crude product was purified using flash column chromatography eluted with PE: DCM = 1:1 (v/v). The product was collected as a white power, yield 2.53 g, 67.3%. ^{1}H-NMR (399.67 MHz, $CDCl_3$, ppm) $\boldsymbol{\delta}$ = 7.93 (d, J = 8.24 Hz, 2H), 7.54 (d, J = 8.28 Hz, 2H), 7.47 (d, J = 8.64, 2H), 7.17 (d, J = 16.32 Hz, 1H), 6.98 (d, J = 16.32 Hz, 1H), 6.91 (d, J = 8.64 Hz, 2H), 3.83 (s, 3H), 2.59 (s, 3H). Spectroscopic data corresponds to data reported in the literature.[3]

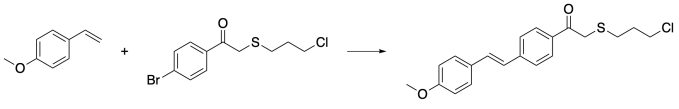

S1 **S3** **S4**

S4 was synthesized using the same procedure as compound **1**. **S4** was obtained as a yellow powder, yield 48.5%. ^{1}H-NMR (399.67 MHz, $CDCl_3$, ppm) $\boldsymbol{\delta}$ = 7.94 (d, J = 8.44 Hz, 2H), 7.56 (d, J = 8.36 Hz, 2H), 7.48 (d, J = 8.68, 2H), 7.49 (d, J = 16.32 Hz, 1H), 6.99 (d, J = 16.32 Hz, 1H), 6.91 (d, J = 8.76, 2H), 3.83 (s, 3H), 3.79 (s, 2H), 3.62 (t, J = 7.00 Hz, 2H), 2.73 (t, J = 7.00 Hz, 2H), 2.10 - 2.03 (m, 2H). ^{13}C-NMR (99.91 MHz, $CDCl_3$, ppm) $\boldsymbol{\delta}$ = 193.73, 159.91, 142.81, 133.43, 131.34, 129.40, 129.32, 128.19, 126.28, 125.15, 114.26, 55.34, 43.28, 36.97, 31.52, 29.29. MS (ESI+) *m/z* found $[M+H]^+$: 361.06, calcd.: 361.10.

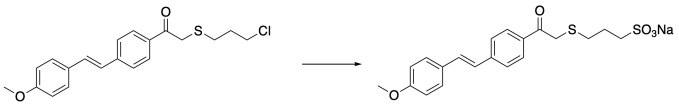

S4 **2**

Compound **S4** (200 mg, 0.55 mmol, 1 eq.) was dissolved in 4 mL methanol. Na_2SO_3 (138.6 mg, 1.1 mmol, 2 eq.) and benzyltriethylammonium bromide (7.5 mg, 5 mol%) in 5 mL water was added to the mixture and the solution was allowed to reflux overnight. The crude reaction was diluted with 5 mL water and washed with Et_2O. The aqueous phase was collected and lyophilized to get compound **2** as yellow powder, yield 70 mg, 29.7%. ^{1}H-NMR (399.67 MHz, $CDCl_3$, ppm) $\boldsymbol{\delta}$ = 7.95 (d, J = 8.36 Hz, 2H), 7.67 (d, J = 8.32 Hz, 2H), 7.58 (d, J = 8.64, 2H), 7.38 (d, J = 16.44 Hz, 1H), 7.16 (d, J = 15.68 Hz, 1H), 6.95 (d, J = 8.64, 2H), 3.92 (s, 2H), 3.76 (s, 3H), 2.55 (t, J = 7.32 Hz, 2H), 2.44 (t, J = 7.36 Hz, 2H), 1.82 - 1.75 (m, 2H). ^{13}C-NMR (99.91 MHz, d_6-DMSO, ppm) $\boldsymbol{\delta}$ = 194.63, 159.92, 142.75, 133.99, 131.54, 129.71, 129.65, 128.76, 126.62, 125.43, 114.71, 55.65, 37.38, 37.09, 31.18, 25.41. MS (ESI-) *m/z* found $[M-Na]^-$: 405.18, calc.: 405.08.

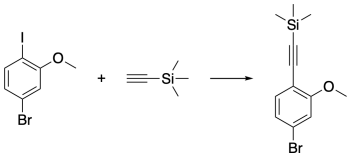

S5

To a 100 mL Schlenk flask was added 4-bromo-1-iodo-2-methoxybenzene (2 g, 6.39 mmol, 1 eq.), THF (20 mL) and triethylamine (2.9 mL, 3 eq.). The mixture was cooled to 0 ºC with an ice bath and degassed using a vacuum-nitrogen cycle. $Pd(PPh_3)_2Cl_2$ (49.3 mg, 0.01 eq.) and CuI (26 mg, 0.02 eq.) were added and the solution was degassed another 10 times. Ethynyltrimethylsilane (1 mL, 1.1 eq.) was slowly injected. The mixture was allowed to return to room temperature and stirred overnight. After completion of the reaction, detected by TLC, the mixture was diluted with DCM, washed with 1M HCl and brine, dried over $MgSO_4$ and concentrated under reduced pressure. The crude product was purified using flash column chromatography (PE: DCM=5:1 (v/v)). The product was collected as a white power, yield 1.58 g, 87.4%. ^{1}H-NMR (399.67 MHz, $CDCl_3$, ppm) $\boldsymbol{\delta}$ = 7.26 (d, J = 8.2 Hz,

1H), 7.02 (d, *J* = 8.2 Hz, 2H), 6.97 (s,1H), 3.84 (s, 3H), 0.24 (s, 9H). Spectroscopic data corresponds to data reported in the literature.[4]

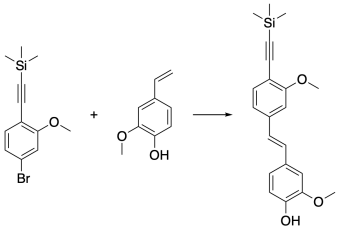

S5 **S6**

Compound **S5** (1g, 3.53 mmol, 1eq.), 2-methoxy-4-vinylphenol (0.58 g, 3.88 mmol, 1.1eq.) and N,N-dicyclohexylmethylamine (5 mL) were dissolved in 30 mL dioxane in a 100 mL Schlenk flask. The mixture was carefully degassed with N_2, followed by addition of $Pd(PPh_3)_4$ (203 mg, 0.05 eq.) and $[(t\text{-}Bu)_3P]_2Pd$ (90 mg, 0.02 eq.). The mixture was degassed again with N_2 and stirred at 100 ºC for 24 h. After completion of reaction detected by TLC, the mixture was diluted with DCM, washed with 1M HCl and brine, dried over $MgSO_4$ and concentrated under reduced pressure. The crude product was purified on a silica gel column eluted with PE: EA from 10:1 to 5:1. The pure product was collected as yellow power, yield 0.35 g, 28.2%. ^{1}H-NMR (399.67 MHz, $CDCl_3$, ppm) $\boldsymbol{\delta}$ = 7.39 (d, *J* = 7.9 Hz, 1H), 7.05 - 7.00 (m, 4H), 6.93 - 6.86 (m, 3H), 3.95 (s, 3H), 3.91 (s, 3H), 0.25 (s, 9H). ^{13}C-NMR (99.91 MHz, $CDCl_3$, ppm) $\boldsymbol{\delta}$ = 160.49, 146.72, 145.89, 139.45, 134.26, 129.78, 129.59, 125.97, 120.72, 118.55, 114.61, 111.11, 108.27, 108.15, 101.46, 99.16, 55.90, 55.83, 0.095. MS (ESI+) *m/z* found $[M]^+$: 352.24, calcd.: 352.15.

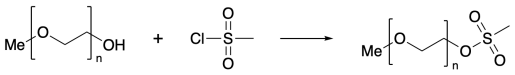

Me-PEG-Ms

Methyl PEG-5000 (5 g, 1 mmol) was dissolved in anhydrous DCM (10 mL) and the solution was cooled to 0 ºC with an ice bath. Triethylamine (232.7 mg, 2.3 mmol) was added followed by slow injection of methanesulfonyl chloride (MsCl, 389.4 mg, 3.4 mmol). The solution was allowed to return to room temperature and stirred overnight. The solution was diluted with DCM (0.12 g PEG/mL), washed with 1M HCl and brine, dried over $MgSO_4$ and concentrated under reduced pressure. The crude product was dissolved in DCM

and precipitated using 10 times (v/v) of Et_2O. The precipitate was cooled to 4 ºC overnight, filtered, dried under vacuum at room temperature overnight. The product was collected as a white power, yield 4.7 g. ^{1}H-NMR (399.67 MHz, $CDCl_3$, ppm) $\boldsymbol{\delta}$ = 3.62 (s, 528H), 3.36 (s, 3H), 3.06 (s, 3H). $M_{n,NMR}$ = 5.8 kDa. $M_{n,GPC}$ = 4.4 kDa, $Đ$ = 1.11.

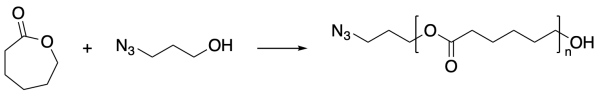

PCL-N_3

ε-Caprolactone (5 mL, 43.8 mmol) and 3-azido-1-propanol (22 mg, 0.21 mmol) were added to a 100 mL Schlenk flask followed by carefully degassing with N_2. 4 drops of $Sn(Oct)_2$ were injected. The solution was immersed in an oil bath which had been pre-heated to 130 ºC, and subsequently stirred for 45 minutes. After polymerization, the mixture was poured into Et_2O to precipitate PCL-N_3. The product was kept in refrigerator overnight and filtered. The white power was dried in vacuum oven at 40 ºC overnight, yield 2.3 g. ^{1}H-NMR (399.67 MHz, $CDCl_3$, ppm) $\boldsymbol{\delta}$ = 4.14 (t, J = 6.12 Hz, 2H), 4.05 - 4.02 (m, 247H), 3.63 (t, J = 6.52 Hz, 2H), 3.37 (t, J = 6.52 Hz, 2H), 2.30 - 2.27 (m, 247H), 1.92 - 1.86 (m, 2H), 1.66 - 1.59 (m, 494H), 1.40 - 1.32 (m, 247H). $M_{n,NMR}$ = 14.1 kDa. $M_{n,GPC}$ = 5.6 kDa, $Đ$ = 1.24.

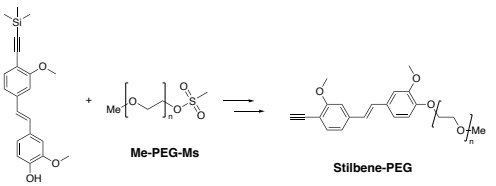

S6 **Me-PEG-Ms** **Stilbene-PEG**

S6 (105 mg, 0.3 mmol, 5 eq.), Me-PEG-Ms (300 mg, 0.06 mmol, 1 eq.) and 2 mL DMF were added to a 10 mL Schlenk flask. The mixture was stirred for 10 min and degassed with N_2. K_2CO_3 (50 mg, 0.36 mmol, 6 eq.) was added and the mixture was stirred at 50 ºC for 24 h. The solution was poured into Et_2O to precipitate the product. The product was filtered and dried in vacuum overnight. To remove the TMS group, the polymer was dissolved in 10 mL methanol with K_2CO_3 (6 eq.). The mixture was allowed to stir for 6 h and filtered, the solvent was removed under reduced pressure. The product was obtained by dissolving in 5 mL DCM and precipitating with Et_2O. The mixture was kept in the

refrigerator overnight and subsequently filtered. The light-yellow power was collected and dried in a vacuum oven at 40 ºC overnight, yield 210 mg. ^{1}H-NMR (399.67 MHz, $CDCl_3$, ppm) $\boldsymbol{\delta}$ = 7.42 (d, J = 8.48Hz, 1H), 7.04 - 6.88 (m, 7H), 3.95 (s, 3H), 3.90 (s, 3H), 3.63 (s, 464H), 3.36 (s, 3H). $M_{n,NMR}$ = 5.1 kDa. $M_{n,GPC}$ = 4.5 kDa, $Đ$ = 1.11.

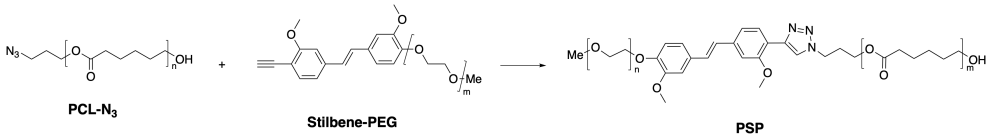

Stilbene-PEG (208 mg, 0.036 mmol, 1eq.) and PCL-N_3 (507 mg, 1eq.) were dissolved in 1 mL DMF. After degassing with N_2, CuI (18.4 mg, 3 eq.) and DIPEA (13.9 mg, 3 eq.) were added and the solution was heated to 40 ºC and stirred for two days. The solution was diluted with 10 mL DCM and poured to 100 mL cold Et_2O. The yellow precipitate was kept in refrigerator overnight, filtered and redissolved in 35 mL THF, followed by slowly dropping 35 mL demineralized water over 1 h. The suspension was dialyzed (MWCO = 1.4 kDa) for 3 days (3 * 1 L) to remove the unreacted Stilbene-PEG and centrifuged to remove the unreacted PCL-N_3 (precipitate). The supernatant was collected and lyophilized to obtain **PSP** as yellow fluffy powder, yield 280 mg, 40.2%. ^{1}H-NMR (399.67 MHz, $CDCl_3$, ppm) $\boldsymbol{\delta}$ = 7.36 - 7.35 (m, 1H), 7.06 - 6.88 (m, 8H), 4.05 - 4.02 (m, 217H), 3.93 - 3.90 (m, 6H), 3.62 (s, 433H), 2.30 - 2.62 (m, 217H), 1.69 - 1.59 (m, 434H), 1.39 - 1.32 (m, 217H). $M_{n,NMR}$ = 17.1 kDa. $M_{n,GPC}$ = 9.3 kDa, $Đ$ = 1.30.

Irradiation experiments of compound 1 in chloroform

Compound **1** was dissolved in chloroform to a final concentration of 50 μM. During transportation, the vials containing the solution were shielded with aluminum foil to minimize exposure to external light. The irradiation experiment was conducted using a GC-220 gamma cell, with the dose rate determined based on the decay law and the half-life of ^{60}Co. The vials were carefully positioned at the center of the machine and subjected to irradiation for a specific duration. Fractionated radiation was delivered to the solution with 20 Gy of each fraction. UV-vis absorption spectra of the solution were acquired both before and after irradiation to monitor any changes.

For NMR analysis of the reaction mixture, the concentration of compound **1** was 2.5 mM, and the sample received 3 kGy delivered by γ-rays. After irradiation, the solvent was evaporated under reduced pressure, and the resulting residue was re-dissolved in deuterated chloroform ($CDCl_3$) prior to measurement.

Upon irradiation with UV light, *trans*-stilbene isomerizes to *cis* conformation, which can be monitored by the decrease of the molar extinction coefficient. Since the energy threshold of the γ-rays (1.17 and 1.33 MeV) is high enough to create Cerenkov radiation in the solution, we were curious if the Cerenkov radiation can cause the isomerization of the stilbene. As shown in **Figure S3.2b**, after UV-irradiation, new peaks appear at around 6.5 ppm with a coupling constant of 15.6 Hz, indicating the formation of *cis*-product. However, no *cis*-product is formed after γ-irradiation. Several products have been identified from ^{1}H-NMR spectroscopy and mass spectrometry. Besides 4-acetylbenzaldehyde and *p*-anisaldehyde (**Figure S3.3**), the other product was purified by column chromatography and analyzed by ^{1}H NMR spectroscopy and mass spectrometry. The NMR spectrum shows two groups of peaks, and the MS is found at $[M+H]^+$ 269.16 (**Figure S3.4, S3.5**). It can be concluded that the purified molecules are compound **S9** and **S10**, which are formed from compound **S7** during the purification process (**Scheme S3.1**).

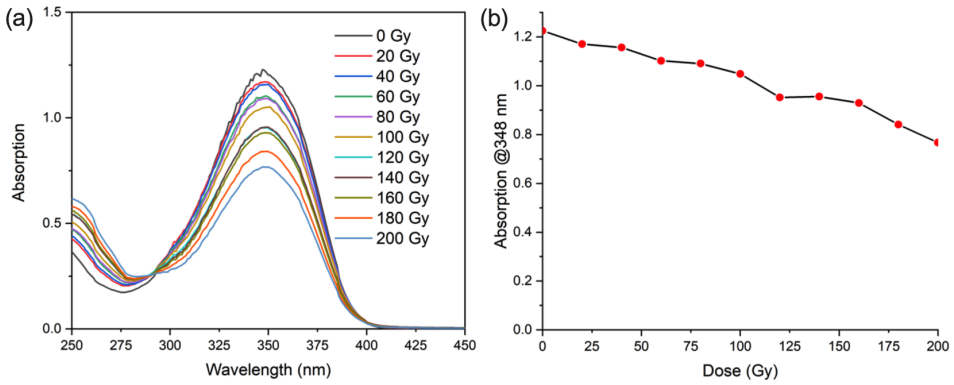

Figure S3.1. (a) UV-vis absorbance of compound **1** after γ-irradiation in chloroform. (b) The absorption of compound **1** @350 nm against radiation dose.

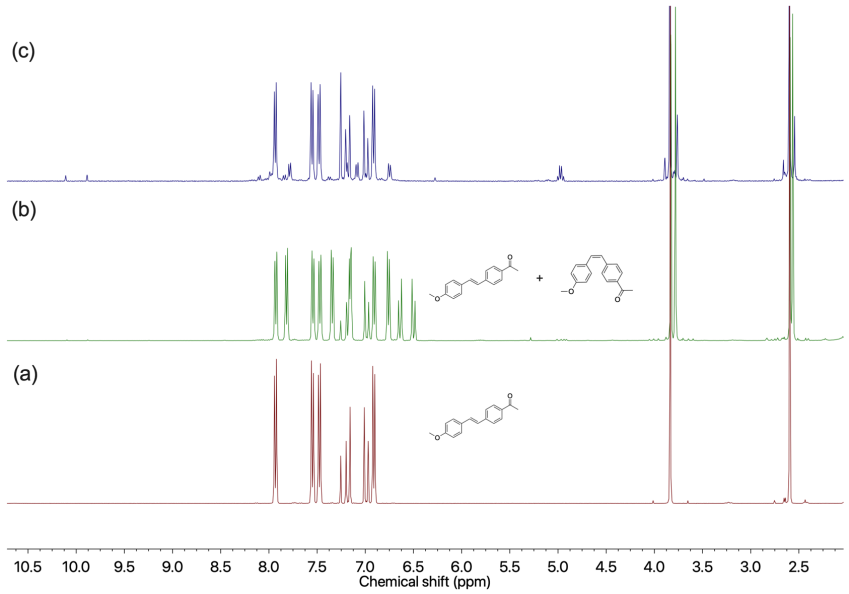

Figure S3.2. ^{1}H NMR comparison of (a) compound **1** in *d*-chloroform, (b) crude reacting mixture after 375 nm UV irradiation and (c) after 3 kGy of γ-irradiation.

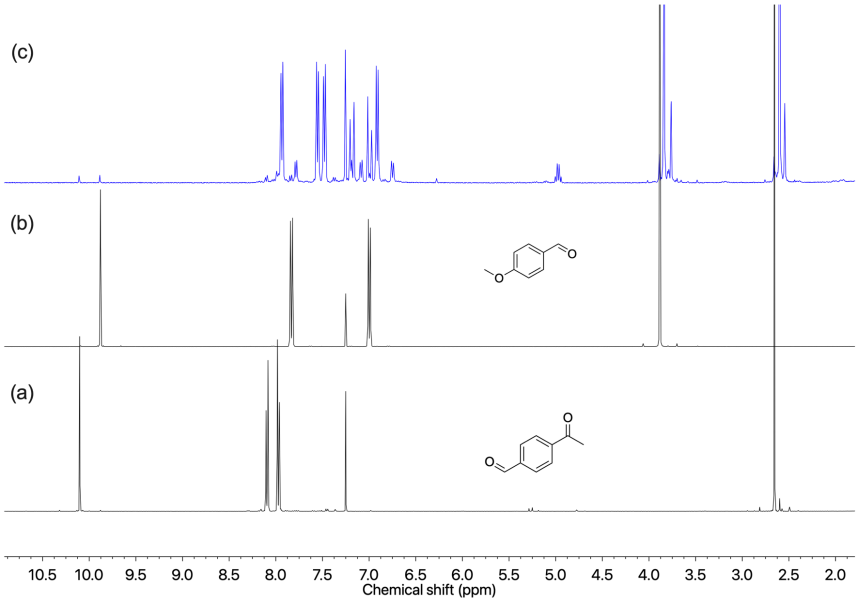

Figure S3.3. ^{1}H NMR comparison of (a) 4-acetylbenzaldehyde, (b) *p*-anisaldehyde and (c) crude reacting mixture of compound 1 after 3 kGy of γ-irradiation.

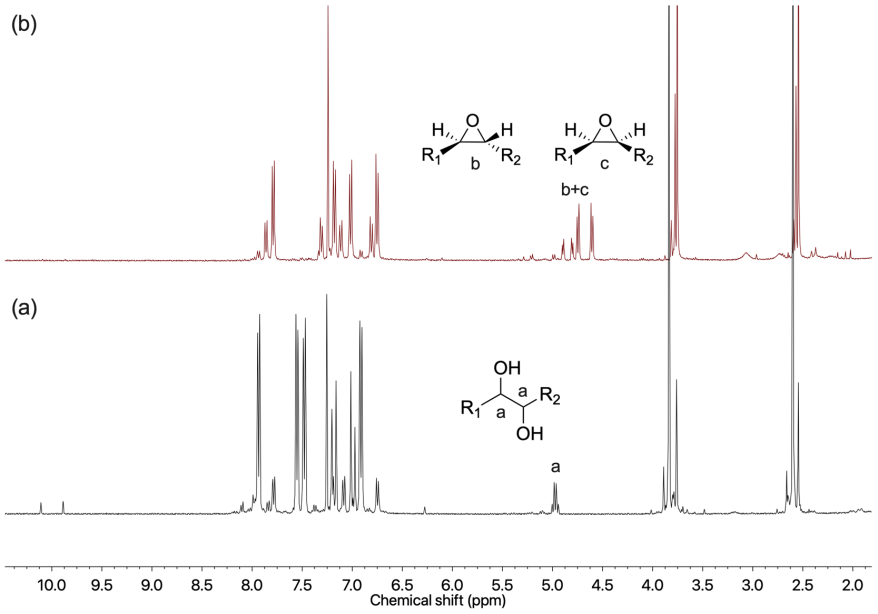

Figure S3.4. [1]H NMR comparison of (a) crude reacting mixture of compound **1** after 3 kGy of γ-radiation and (b) the separated main product.

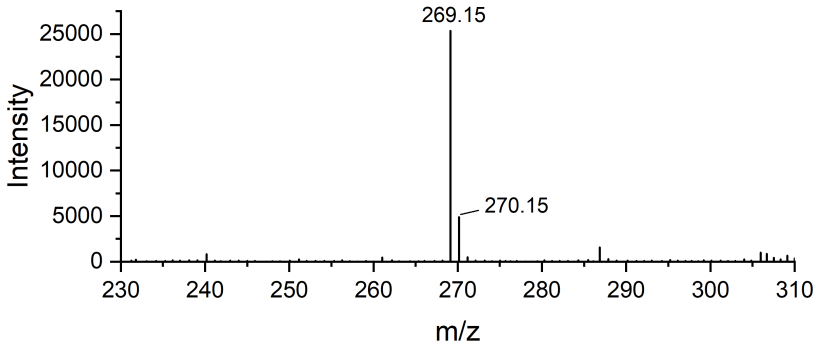

Figure S3.5. Mass spectrum of the separated main product.

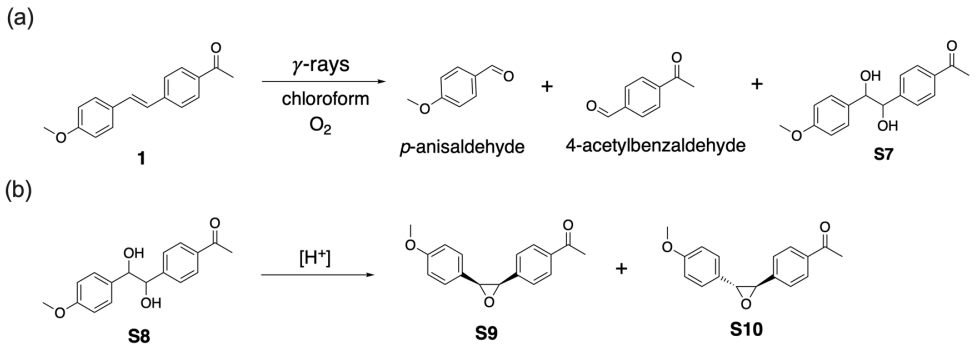

Scheme S3.1. (a) The proposed reacting scheme of compound **1** irradiated in chloroform. (b) Formation of epoxide **S9** and **S10** in acidic condition.

Irradiation experiments of compound 1 in various solvents

Compound **1** was dissolved in solvents including chloroform, methyl trichloroacetate, dichloromethane, 1,2-dichloroethane, 1,2-dichlorobenzene, 1,2,4-trichlorobenzene, THF, DMF, DMSO, 1,4-dioxane, *o*-xylene, benzene and toluene. Compound **1** showed good solubility to all the aforementioned solvents. For each experiment, 2 mL of a 2 mM solution of compound **1** was divided equally over four vials, three of which were exposed to 978 Gy of γ-rays, while the remaining sample served as the non-irradiated control. After irradiation, samples were diluted 100 times with chloroform and UV spectra were measured. The relative absorption was then determined by the absorption of irradiated samples divided by that of the non-irradiated sample.

Irradiation experiments of compound 2

Compound **2** was dissolved in Milli-Q water at a concentration of 90 μM using sonication to ensure complete dissolution. In the case of the water/chloroform solution (0.1 vol%), 1 μL of chloroform was added to 1 mL of water (the maximum solubility of chloroform in water is 0.54 vol% at 20 ºC). The resulting mixture was sonicated until a clear solution was obtained. The prepared samples were then exposed to γ-rays with a dose of 75 Gy. UV-vis spectra were recorded both before and after irradiation to monitor any changes of absorption. For LC-MS analysis, 1 mM compound **2** in Milli-Q water containing 0.1% v/v chloroform was irradiated reaching 450 Gy. The solution was filtered with a 0.45 μm filter. An aliquot of 2 μL was injected and eluted using a gradient from 15% MeCN/water to 95%

MeCN/water over a duration of 20 minutes. Mass spectra were recorded in negative mode (ESI^-) to analyze the negatively charged ions.

The concentration-absorption calibration curve of compound **2** was made with the concentration varying from 10 to 100 µM. After irradiation in water, the concentration of compound **2** is 56.2 ± 0.4 µM, while after irradiation in water/chloroform, the concentration of compound **2** is 28.1 ± 1.0 µM.

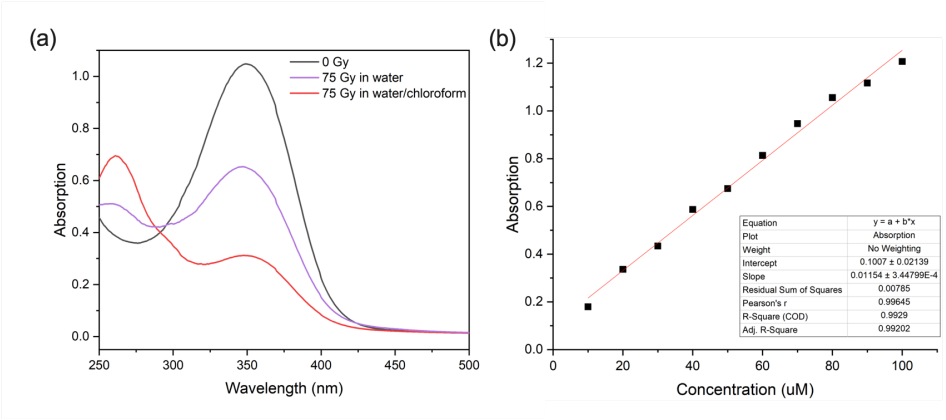

Figure S3.6. (a) UV-vis absorption spectra of compound **2** before and after 75 Gy of γ-radiation in water and water/0.1 vol% chloroform. (b) The calibration curve for absorption-concentration of compound 2 in water.

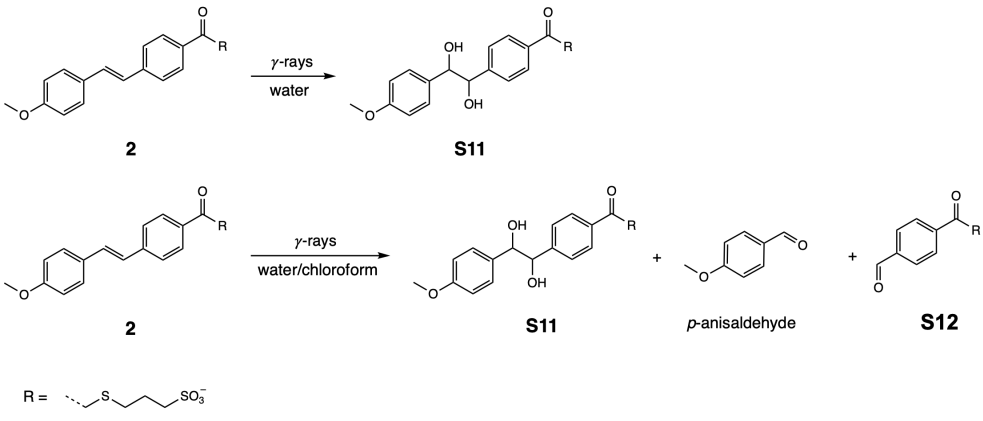

Scheme S3.2. The proposed reacting scheme of compound **2** in water and water/chloroform.

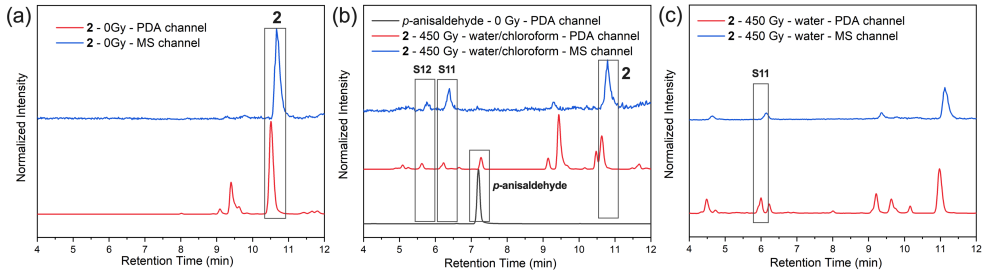

Figure S3.7. LC-MS spectra of compound **2** (a) before irradiation; (b) irradiated by γ-rays (450 Gy) in water/chloroform and (c) irradiated by γ-rays (450 Gy) in water. LC spectra of *p*-anisaldehyde is shown in (b) as comparison.

Table S3.1. MS determination of compound **2**, **S11** and **S12**.

compound	Calculated [M^-]	Found [M^-]
2	405.08	405.18
S11	439.09	439.16
S12	301.02	301.06

GPC data of polymers

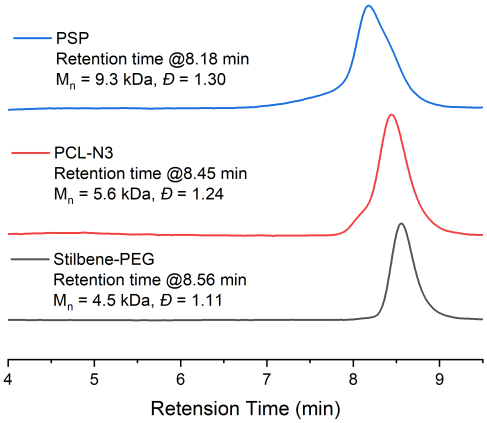

Figure S3.8. Molecular weight and dispersity (*Đ*) of **PSP**, PCL-N_3 and Stilbene-PEG measured by GPC.

Micelle preparation

The micelles were prepared by a solvent switching method. Briefly, 10 mg of polymer was dissolved in 0.5 mL THF. The solution was sonicated for 30 min followed by slowly adding 0.5 mL Milli-Q water over 1 h. The obtained transparent solution was dialyzed against Milli-Q water for 12 h with the water being refreshed every 2 h.

Irradiation of micelle solutions

The PBS/chloroform solution was prepared using the same method as preparing the water/chloroform solution. The micelle solutions were diluted to a concentration of 0.05 mg/mL (above the critical micelle concentration) using 10 mM PBS buffer (pH 7.4) or PBS/chloroform. Gamma irradiation was performed in a GC-220 gamma cell. The X-ray irradiation was carried out using an X-ray source (Philips MCN 321 variable-energy X-ray tube) performed in a working voltage of 240 keV and a current of 10 mA. The dose rate of the X-ray source was determined using the method as described in literature.[3] Fractionated radiation was delivered to the solution in fractions of 2 Gy each.

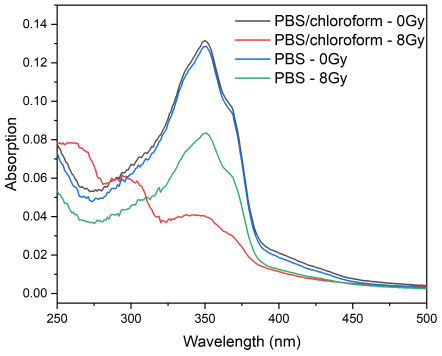

Figure S3.9. UV-vis absorption spectra of **PSP** micelles solution before and after exposure to 8 Gy of γ-irradiation.

Preparation of micelle solutions with different chloroform-to-stilbene ratio

Micelles solutions with different chloroform-to-stilbene ratio were prepared by diluting micelles stock solution from 10 mg/mL to 0.4 mg/mL (stilbene concentration, 25 μM) using PBS/chloroform solution. The concentration of chloroform ranges from 12 mM to 12

μM to obtain molar ratios (chloroform-to-stilbene) from 480:1 to 0.48:1. Samples were irradiated in a GC-220 gamma cell, depositing a total dose of 75 Gy, after which their UV-vis absorption spectra were measured.

Preparation of micelle solutions for GPC

Micelles were diluted to 0.05 mg/mL in water/chloroform (0.1 vol%) solution and irradiated in GC-220 gamma cell, delivering a dose of 15 and 30 Gy. The resulting solutions were lyophilized and subjected to GPC measurement.

Preparation of cyro-EM and DLS measurements

Micelle solutions were diluted to a **PSP** concentration of 0.05 mg/mL using Milli-Q water or water/chloroform and irradiated with γ-rays to reach 15 Gy of dose. After irradiation, the solutions were concentrated to 10 mg/mL using an Amicon Ultra-4 centrifugal filter (molecular weight cut-off: 13 kDa). The non-irradiated sample was treated in the same procedure as irradiated samples.

The hydrodynamic diameter (D_h) of micelles PSP and PSP-Dox were measured by DLS. Micelle solutions (0.5 mL) with a polymer concentration of 0.1 mg/mL were measured at 25 ºC. For each sample, measurement was carried out three times.

Cryo-EM images were acquired using the following procedure: 3 μL of the solution was applied onto a Quantifoil 1.2/1.3 200 mesh Cu grid. The grid was blotted for 5 seconds with filter paper to create a thin layer, and then rapidly immersed in liquid ethane (Leica EM GP version 16222032) for vitrification. Subsequently, the grid was inserted into a cryo-holder (Gatan model 626) and transferred to the JEOL JEM 3200-FSC TEM. Three images were captured for each sample to perform statistical analysis of the micelle diameters. The cryo-EM images were manually analyzed using ImageJ.

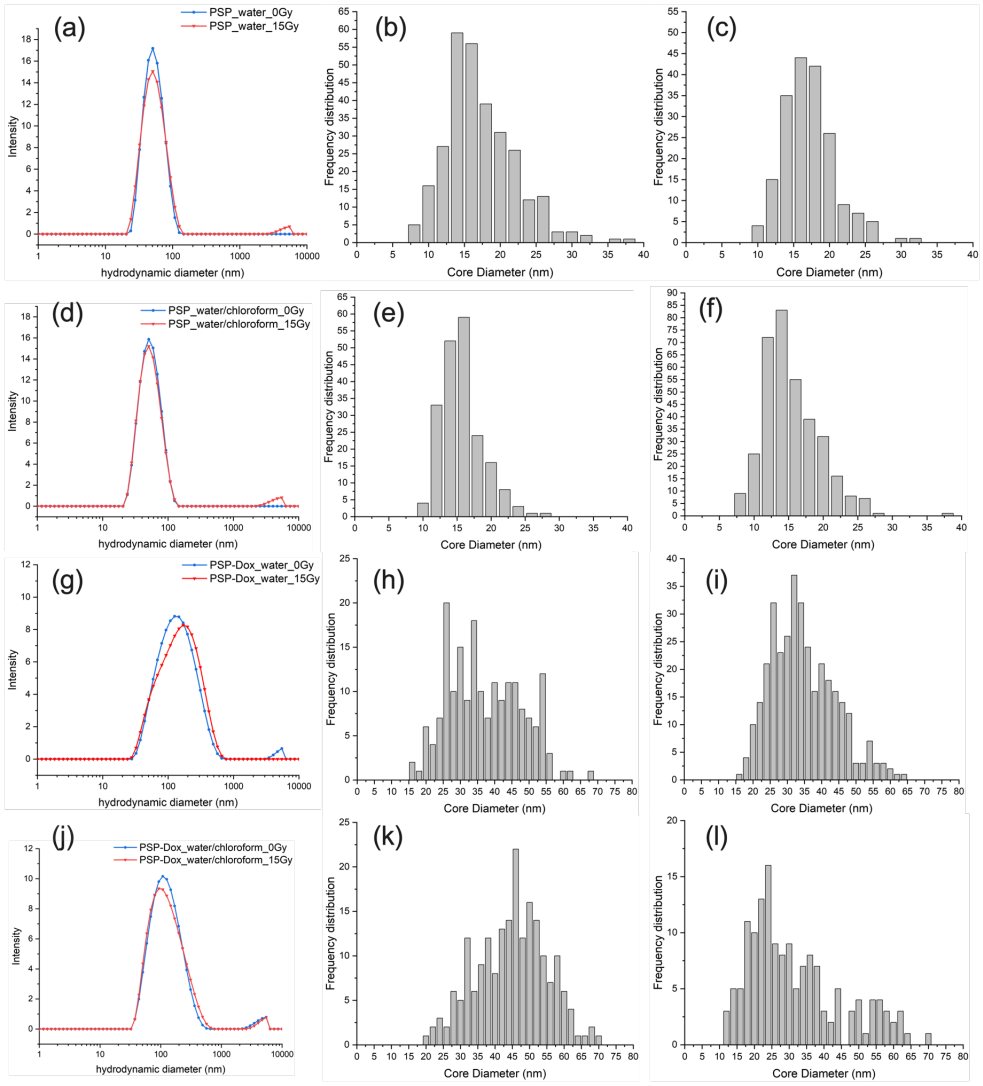

Figure S3.10. Size distribution before and after irradiation measured by DLS (a) PSP micelles in water, (d) PSP micelles in water/chloroform, (g) PSP-Dox micelles in water, (j) PSP-Dox in water/chloroform, and frequency distribution based on TEM images analysis of PSP in water (b) 0 Gy, (c) 15 Gy; PSP in water/chloroform (e) 0 Gy, (f) 15 Gy; PSP-Dox in water (h) 0 Gy, (i) 15 Gy; PSP-Dox in water/chloroform (k) 0 Gy, (l) 15 Gy.

Preparation of scavenger solutions

Phosphate buffered saline (PBS) at pH 7.4 was prepared by diluting 10×PBS stock solution (Invitrogen by Thermo Fisher Scientific) 10 times, and the pH was measured using a pH meter (HAMILTON, Mettler Toledo). PBS/chloroform/10 mM *t*-BuOH was prepared by adding 1.89 μL *t*-BuOH to 2 mL PBS/chloroform solution; PBS/chloroform/10 mM ascorbic acid was prepared by dissolving 4.2 mg ascorbic acid in 2 mL PBS/chloroform solution, a 1 M NaOH solution was used to adjust the pH; PBS/chloroform/100 mM $NaNO_3$ was prepared by dissolving 16.7 mg $NaNO_3$ in 2 mL PBS/chloroform solution. 2 mL micelle solution ([polymer] = 0.5 mg/mL) with scavenger was prepared by adding 0.1 mL micelle stock solution (10 mg/mL) to 1.9 mL desired scavenger solution. To prepare an N_2 saturated solution, micelle solutions and chloroform were bubbled with N_2 in a glove box for 10 minutes, then 0.1% v/v chloroform was added to the micelle solution. For each experiment, the micelle solution was divided into four vials. Three of them were exposed to 75 Gy of γ-rays, while the remaining sample served as the non-irradiated control. The relative absorption was calculated using the same method as described above.

Electron paramagnetic resonance (EPR) measurement

The spin trap PBN (α-phenyl N-tertiary-butyl nitrone) was dissolved in two separate solutions, PBS (pH 7.4) and PBS (pH 7.4) solution containing 0.5 vol% chloroform. The solutions were irradiated with γ-rays to reach a dose of 830 Gy. The EPR spectra were recorded approximately 30 minutes post-irradiation.

EPR spectroscopy was conducted using a Bruker EMXplus 9.5 spectrometer under controlled experimental conditions, microwave frequency of 9.79 GHz, microwave power of 20 mW, modulation frequency of 100 kHz, and modulation amplitude of 1.0 Gauss. All measurements were carried out at room temperature.

As reported by Gardy et al.,[5] trapping of aqueous electrons forms nitroxide **a**, while trapping of hydroxyl radical forms nitroxide **b**. As shown in **Figure S3.11**, the intensity of nitroxide **a** in PBS/chloroform solution is much lower than that in PBS solution, indicating the scavenging of aqueous electrons by chloroform.

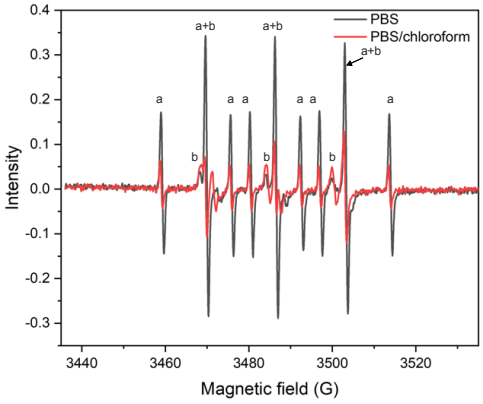

Figure S3.11. EPR signal of 25 mM PBN in PBS (pH 7.4) and PBS/0.5 vol% chloroform after exposure to 830 Gy of γ-rays.

a **b**

Scheme S3.3. Chemical structure of spin adducts **a** and **b**.

Table S3.2. Coupling constants of **a** and **b** in Gauss

	α^N	α^H	α^N *	α^H *
a	16.6	10.4	16.8	10.9
b	15.7	2.7	15.6	2.7

*Data from literature[5]

Radiolysis in water with other chlorinated molecules

Micelle solutions with other chlorinated molecules were prepared using the same method. 0.1 mL micelle stock solution (10 mg/mL) was added to 1.9 mL PBS (pH 7.4) containing 12 mM of chlorinated molecules. Samples were divided into 4 vials and three of them were irradiated while the remaining one served as the non-irradiated sample. The relative absorption was obtained using the same method as described above.

Preparation of dox-loaded micelles (PSP-Dox)

To achieve a higher loading efficiency, the drug-loaded micelles were prepared by the nanoprecipitation method. Typically, 5 mg of **PSP** and 5 mg of Dox-HCl were dissolved in 0.5 mL DMF. Dox-HCl was neutralized by adding 1.6 μL of triethylamine to the mixture, followed by sonication for 10 minutes. The solution was dropped into 1 mL of Milli-Q water over 1 h. The resulting solution was transferred to a dialysis bag (Spectrum Laboratories, Inc., molecular weight cut-off 3.5 kDa) and dialyzed against demineralized water for 12 h with the water refreshed every 2 h. The removal of DMF and triethylamine were verified by ^{1}H-NMR. The solution after dialyzing was centrifuged at 6000 rpm for 5 min and the supernatant was collected. The concentration of Dox was calculated by UV absorbance at 500 nm with a calibration line plotted as **Figure S3.12**. The drug loading (DL) efficiency is calculated by the equation:

$$DL(w/w) = \frac{m(loaded\ Dox)}{m(polymer)}$$

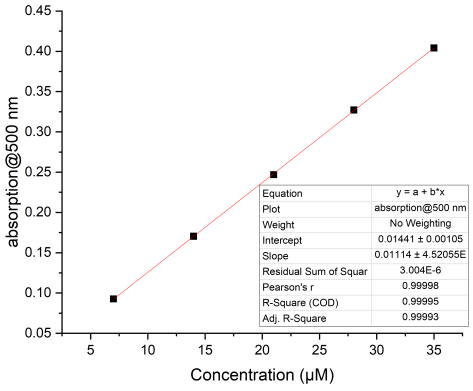

Figure S3.12. Calibration curve of Dox-HCl in Milli-Q water.

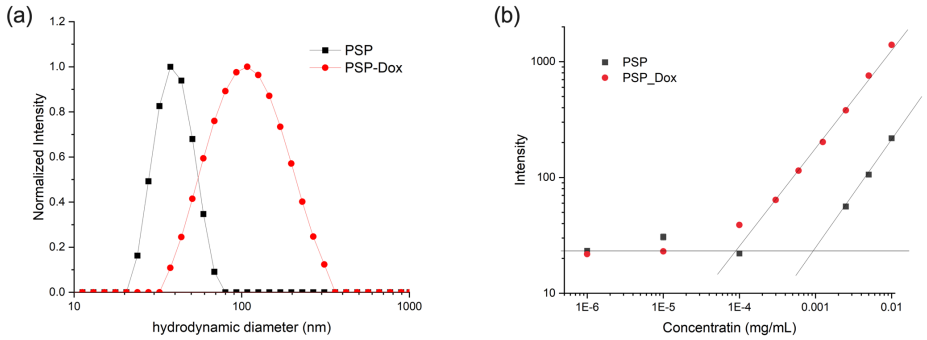

Figure S3.13. (a) Intensity plot measured by DLS of PSP and PSP-Dox micelles; (b) The light scattering intensities plotted against the concentration of **PSP** and **PSP-Dox** micelle solutions, respectively.

Critical Micellar Concentration (CMC)

The CMC of **PSP** and **PSP-Dox** in aqueous solution was determined using a method based on DLS[6]. Micelle solutions of **PSP** and **PSP-Dox** were prepared within the concentration range from 1.0×10^{-6} to 1.0×10^{-2} mg/mL. The intensity values of scattered light against concentration are shown in **Figure S3.13**. At concentrations below CMC, the intensity of the scattered light shows approximately constant values equal to that of deionized water, while at concentrations higher than CMC, the intensity shows linear increase since the concentration of micelle increases. The CMC values are determined by drawing the intersection line of the best fit through the data points, which is 9.0×10^{-4} mg/mL for **PSP** and 9.0×10^{-5} mg/mL for **PSP-Dox**, respectively.

Table S3.3. Summary of the obtained micelle parameters as obtained by DLS.

	Hydrodynamic diameter D_h (nm)	CMC (mg/mL)
PSP	38.2 ± 0.2	9.0×10^{-4}
PSP-Dox	97.8 ± 1.0	9.0×10^{-5}

Drug release experiment

The obtained **PSP-Dox** micelle solutions were diluted to a polymer concentration of 0.05 mg/mL (above the CMC of **PSP-Dox**) using PBS (pH 7.4) or PBS/chloroform and were

exposed to γ-radiation. The UV-vis absorption of the irradiated samples was measured after irradiation. The released Dox was removed by using an Amicon Ultra-4 centrifugal filter with a molecular weight cut-off of 10 kDa. The centrifugation was performed at 10,000 rpm for 20 minutes. The remaining solutions were measured again with UV-vis absorbance to determine the concentration of Dox. The retention ratio was calculated by dividing the remaining mass of Dox by the initial amount before separation.

$$Dox\ release\ (\%) = \frac{n(Dox\ after\ seperation)}{n(Dox\ before\ seperation)}$$

References

(1) Breve, T. G.; Filius, M.; Weerdenburg, S.; van der Griend, S. J.; Groeneveld, T. P.; Denkova, A. G.; Eelkema, R. Light-Sensitive Phenacyl Crosslinked Dextran Hydrogels for Controlled Delivery. *Chem. Eur. J.* **2022**, *28*, e202103523.

(2) Yao, T.; Luthjens, L. H.; Gasparini, A.; Warman, J. M. A Study of Four Radiochromic Films Currently Used for (2D) Radiation Dosimetry. Radiat. Phys. Chem. **2017**, 133, 37-44.

(3) Hung, C.-H.; Zheng, W.-Y.; Lee, H. M. Palladium Complexes with Phenoxy- and Amidate-Functionalized N-Heterocyclic Carbene Ligands Based on 3-Phenylimidazo[1,5-a]pyridine: Synthesis and Catalytic Application in Mizoroki–Heck Coupling Reactions with Ortho-Substituted Aryl Chlorides. Organometallics **2021**, 40, 702-713.

(4) Ganesh, V.; Odachowski, M.; Aggarwal, V. K. Alkynyl Moiety for Triggering 1,2-Metallate Shifts: Enantiospecific sp2-sp3 Coupling of Boronic Esters with p-Arylacetylenes. Angew. Chem. Int. Ed. **2017**, 56, 9752-9756.

(5) Sargent, F. P.; Gardy, E. M. Spin Trapping of Radicals Formed during Radiolysis of Aqueous-Solutions - Direct Electron-Spin Resonance Observations. Can. J. Chem. **1976**, 54, 275-279.

(6) Topel, Ö.; Çakır, B. A.; Budama, L.; Hoda, N. Determination of Critical Micelle Concentration of Polybutadiene-Block-Poly(ethyleneoxide) Diblock Copolymer by Fluorescence Spectroscopy and Dynamic Light Scattering. J. Mol. Liq. **2013**, 177, 40-43.

Polymeric Organochloride Mediated Oxidation of Thioethers Initiated by Ionizing Radiation

4

Abstract

Irradiating aqueous solutions containing organochlorides generates peroxyl radicals because of their reactions with aqueous electrons and dissolved oxygen. These radicals can oxidize thioethers to sulfoxides. However, the application of small molecular organochlorides in anti-cancer therapy is limited since they can induce liver damage. In this chapter we show that organochlorides bound to a polymer chain behave similar to small molecular organochlorides, when the polymer was fully dissolved in aqueous solution. The oxidation was significantly inhibited if the polymeric organochloride self-assembled in micelles. We hypothesize that aqueous electrons are scavenged by dissolved oxygen before they could diffuse into the hydrophobic core containing the organochloride groups. Nevertheless, our work shows that using polymeric organochlorides can be an alternative to small organochlorides provided that they are easily accessible to aqueous electrons.

Availability and Contributions

This chapter is based on an article currently in preparation for submission, in collaboration with Irene Piergentili, Bing Xu, Antonia G. Denkova and Rienk Eelkema.

J.L., A.D. and R.E. developed the project idea. J.L. conducted most of the experiments, designed all the figures and schemes and wrote the first draft. I.P. provided the polymer P1. B.X. helped the radiation experiments. A.D. and R.E. supervised the project, secured funding and corrected manuscript.

Introduction

Radiotherapy and chemotherapy are two primary cancer treatments used in clinical practice.[1-6] Radiotherapy uses ionizing radiation to damage cancerous cells, while chemotherapy employs anti-tumor drugs to kill cells or inhibit their proliferation.[7,8] However, both ionizing radiation and anti-tumor drugs can also harm healthy tissues during treatment. The effectiveness of these therapies is determined by the balance between tumor damage and systemic toxicity to normal tissues. Ionizing radiation-induced drug release presents a promising strategy to reduce side effects when combining radiotherapy with chemotherapy.[9-11] As water is the most abundant matter in tissues, radiation mostly deposits its energy to water causing water radiolysis.[12] The drug release process is then mediated by reactive species generated from water radiolysis. An example of such systems are polymeric nano-carriers encapsulating drugs to minimize systemic toxicity which upon exposure to ionizing radiation can degrade, releasing the drug precisely at the site of radiation.[13,14] This approach profits from the precise spatial control of radiotherapy to ensure targeted drug release exclusively at the tumor site. Several chemical reactions have been explored to achieve effective radiation-induced drug release. For example, Ma et al.[15] demonstrated that a diselenide bond could be cleaved under ionizing radiation, facilitated by hydroxyl radicals generated from water radiolysis. They developed polymeric aggregates with doxorubicin encapsulated in the hydrophobic core. Upon exposure to 5 Gy of X-rays, the aggregates slightly swelled and released approximately 40% of the encapsulated drug. Similarly, Tanabe et al.[16] used DNA amphiphiles linked by a disulfide bond between the hydrophilic and hydrophobic blocks. Irradiation under hypoxic conditions results in reductive species such as aqueous electrons and hydrogen radicals that could trigger a chain reaction of disulfide exchange, enabling micelle degradation and drug release. However, most of these polymers have not been applied *in vivo* due to the high radiation doses required to achieve sufficient drug release. Therefore, more efficient reactions must be developed to make radiation-induced drug release viable for clinical applications.

Organic compounds containing thioethers exhibit distinctive properties after oxidation. The thioether group itself is hydrophobic, whereas its oxidation products, sulfoxides and sulfones, are hydrophilic. Exploiting this property, Napoli et al.[17] developed an ABA-type

block copolymer, using poly(propylenesulfide) as the hydrophobic block. Oxidation of the thioether group switched the hydrophobic block into a hydrophilic one, leading to vesicle disassembly. For aromatic thioethers, an intriguing property is the change in electronic effects upon oxidation.[18] While the thioether group is electron-donating, its oxidized forms, sulfoxide and sulfone, are electron-withdrawing groups. Phenol acetate esters with electron-withdrawing substituents on the aromatic ring are more labile towards hydrolysis than those with electron-donating groups. Our research group applied this principle to design H_2O_2-responsive amphiphilic block copolymers (see **Figure 4.1**).[19] Poly(4-(methylthio)phenyl acrylate) functions as the hydrophobic block. Upon H_2O_2 addition, MTPA undergoes oxidation followed by hydrolysis, converting the hydrophobic core into hydrophilic polyacrylate polyanion, which led to micelle disassembly. However, the oxidation of thioethers by H_2O_2 is slow, requiring several days to weeks to respond to cellular H_2O_2 concentrations (50-100 μM). While enzymatic and organic catalysts have been developed to accelerate this process, controlling catalyst concentration within cells poses challenges.[20,21] Thus, more efficient oxidants are needed to make this approach viable in biological systems.

In chapter 3, we demonstrated the oxidative cleavage of a stilbene derivative, induced by ionizing radiation. The presence of 0.1 vol% of an organochloride such as chloroform or trichloroethanol in aqueous solutions significantly enhances the oxidation product yield. We hypothesized that the aqueous electrons generated from water radiolysis can react rapidly with the organochloride to form a carbon-centered radical and a chloride anion. In the presence of oxygen, the carbon-centered radical reacts with molecular oxygen and forms a strong oxidant, i.e. peroxyl radical. In this chapter, we show that a thioether, dissolved in aqueous solutions with organochlorides, can be oxidized to a sulfoxide when it is exposed to ionizing radiation. We use this reaction to trigger the hydrophilicity switch of a reactive oxygen species (ROS)-responsive micelle (**Figure 4.1**). Although oxidation and hydrolysis are observed, the amount of polyacrylate anion is not enough to induce micelle disassembly after exposure to 600 Gy gamma-radiation. We copolymerized organochloride and 4-(methylthio)phenyl acrylate (MTPA) to reduce the potential toxicity of small molecule organochlorides.[22] However, we find that when the organochloride is incorporated in the hydrophobic block, the reaction of organochloride and aqueous

electrons is inhibited, leading to reduced yields of the oxidation products. We anticipated that the hydrophilic nature of the hydrated electron prevents it from entering the micelle, leading to reduced reactivity. To test this hypothesis, we synthesized a random-copolymer **rP2** using MTPA, organochloride-acrylate and *N*,*N*-dimethylacrylamide as monomers. **rP2** is fully soluble and does not form micelles in aqueous solution. **rP2** solutions show higher yields of oxidized product after irradiation than its micelle forming analogs. These findings show that the organochloride covalently bond to a polymer can work similar to small molecular organochlorides, which paves the way to the future application of organochloride mediated oxidation induced by ionizing radiation.

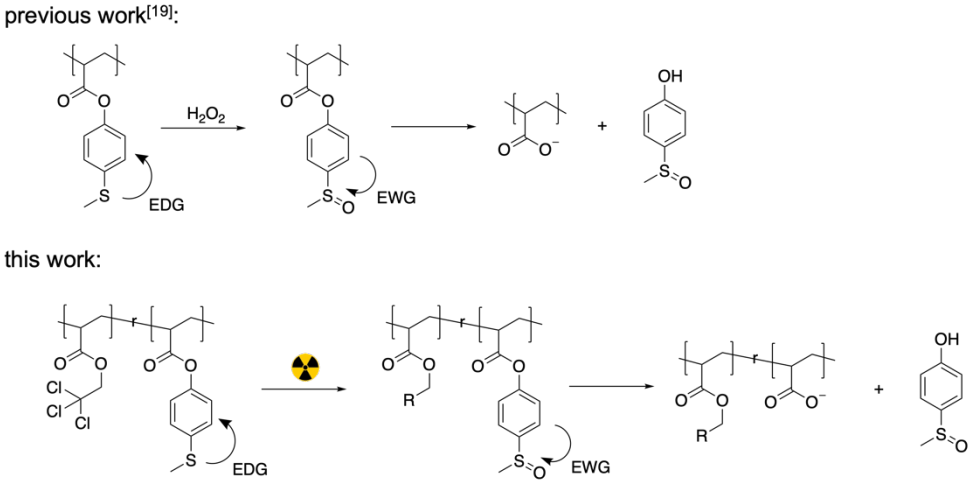

Figure 4.1. Schematic illustration of radiation-induced hydrophilicity switch, enabled by the oxidation from an electron donating (EDG) thioether to electron withdrawing (EWG) sulfoxide.

Results and Discussion

To test the reaction of thioethers under irradiation in water or in water with organochloride, we chose 4-(methylthio)phenol (compound **1**) as the model thioether and 2,2,2-trichloroethan-1-ol (TCE) as the model organochloride. Proton nuclear magnetic resonance spectroscopy (^{1}H NMR) was employed to quantify the oxidation. After exposure to gamma-radiation (60 Gy) in water, the spectrum of the solution of compound **1** (50 μM) remained the same as it was before irradiation (**Figure 4.2b**). Although water radiolysis generates

hydrogen peroxide which can oxidize the thioether, we could not detect any oxidation products after irradiation. This is likely caused by the low concentration of H_2O_2 after 60 Gy (ca. 4.2 μM) and the slow reaction kinetics of thioether oxidation. However, when 0.1 vol% TCE was present during the irradiation, a new methyl peak appeared at 2.73 ppm, corresponding to the formation of sulfoxide compound 2.[19] This indicates that the peroxyl radical generated from the water/TCE system can oxidize the thioether.

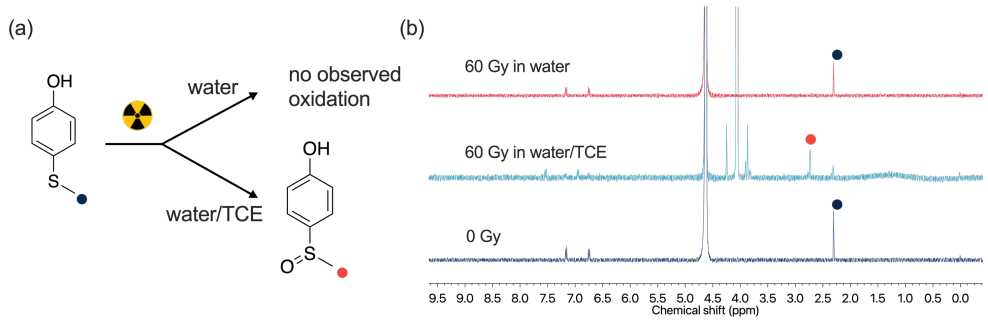

Figure 4.2. (a) Schematic illustration of the reactions of compound **1** under irradiation in water and water/TCE; (b) ^{1}H NMR spectrum of compound **1** before and after irradiation (spectra were taken within 3 hours after irradiation).

Having confirmed the oxidation of a small molecule thioether, we then investigated if the oxidation occurs when the thioether group is grafted to a polymer chain. We synthesized an amphiphilic block co-polymer (**P1**, **Figure 4.3a**) which incorporates 4-(methylthio)phenol acrylate (MTPA) as the hydrophobic monomer and *N*,*N*-dimethylacrylamide (DMA) as the hydrophilic monomer. The molecular weight of **P1** is 16.9 kDa determined by ^{1}H NMR. In deuterated phosphate buffer (*d*-PB, 100 mM, pD 7.4), **P1** self-assembles to form micelle with a hydrodynamic diameter (D_h) of 56 nm (**Figure S4.1a**) measured by dynamic light scattering (DLS). After exposure to 600 Gy of gamma-radiation, micelle solutions (polymer concentration, 1.0 mg/mL) demonstrated a gradual release of 4-(methylsulfinyl)phenol (MSP), as evidenced by the measured increase of peak intensity at chemical shift of 7.67-7.65 ppm and 7.07-7.05 ppm (**Figure 4.3b**). Using sodium trimethylsilylpropanesulfonate (DSS) as internal standard of ^{1}H NMR spectrum, we determined the concentration of released sulfoxide (**Figure 4.3c**). Irradiation (600 Gy) in *d*-PB resulted in 0.84 ± 0.71 μM MSP released after 1 hour of post-irradiation incubation, while the release increased to

14.25 ± 0.68 μM after incubation at 37 °C for 4 days. The same dose of radiation in *d*-PB/TCE resulted in 4.88 ± 0.24 μM MSP released after 3 hours of incubation and increased to 32.49 ± 2.80 μM after 4 days. The MSP release in *d*-PB is attributed to the oxidation by hydrogen peroxide generated from water radiolysis. In the presence of 0.1 vol% of TCE a more oxidizing species was generated, resulting in increased sulfoxide release. The micelle solution was incubated at 20 °C from day 4 to day 7, and the rate of sulfoxide release decreased. The D_h was measured following the radiation (**Figure 4.3d**). Although irradiation of micelles leads to MSP release, the D_h of the micelles remains unchanged in both *d*-PB or *d*-PB/TCE. These results are attributed to the low ratio of thioether oxidation versus unreacted thioether. For instance, 1.0 mg/mL **P1** contains approximately 1.1 mM thioether monomer. However, after exposure to 600 Gy of gamma-radiation in *d*-PB/TCE and 3 days of incubation, only 27.28 μM sulfoxide was released. By this calculation, only 2.8% of hydrophobic poly-4-(methylthio)phenol acrylate converted to hydrophilic polyacrylic acid, which might be insufficient to trigger micelle disassembly.

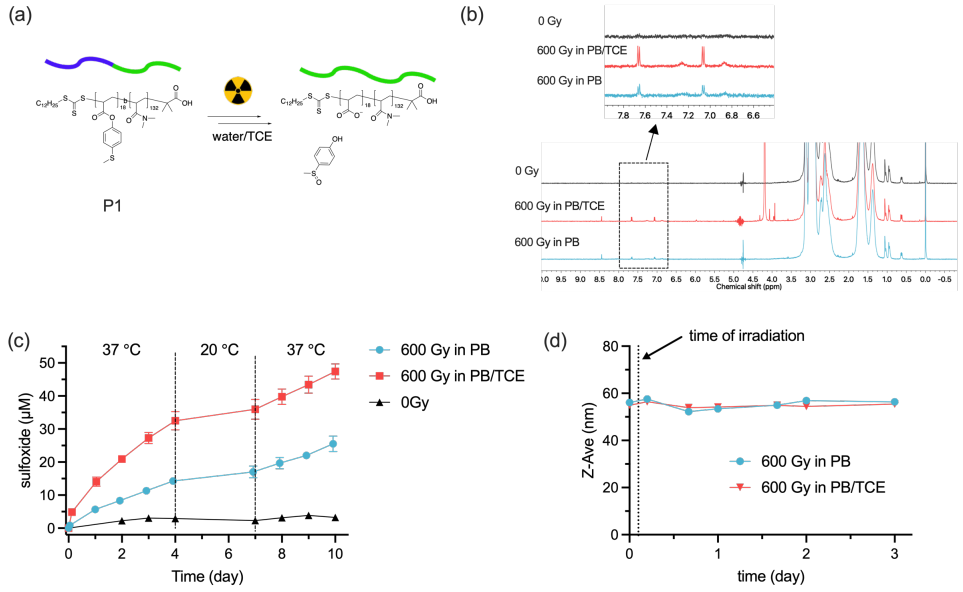

Figure 4.3. (a) Chemical structure of **P1** and radiation-induced oxidation and hydrolysis; (b) ^{1}H NMR of **P1** micelle solutions after exposure to 600 Gy of gamma-rays (spectra were taken after 4 days of incubation at 37 °C); (c) Time evolution of sulfoxide formation after irradiation, quantified by the integration of the 1H-NMR doublet at 7.06 ppm; (d) Z-average size of **P1** micelles after 600 Gy of gamma-rays measured by DLS.

Although **P1** micelles seem not to disassemble after exposure to radiation in *d*-PB/TCE, we wanted to investigate the behavior of these micelles when organochloride is covalently bound to the hydrophobic block. To investigate this, we synthesized block copolymers **P2** and **P3**, where the organochloride and MTPA are randomly co-polymerized in the hydrophobic block (**Figure 4.4a**). **P2** incorporates 2,2,2-trichloroethyl acrylate as the organochloride, while **P3** incorporates 4,4,4-trichlorobutyl acrylate. In *d*-PB (100 mM, pD 7.4), **P2** and **P3** self-assemble into micelles with D_h of 52 and 41 nm, respectively (**Figure S4.1b**, **c**). Following exposure to 600 Gy of gamma radiation in *d*-PB, **P2** and **P3** demonstrated similar sulfoxide release profiles, with approximately 5 µM of MSA detected after 4 days of incubation at 37 °C. Addition of 0.1 vol% TCE to the **P2** and **P3** micelle solutions before irradiation significantly enhanced MSP release (**Figure 4.4b**). These results suggest that observed oxidation in absence of TCE is related to H_2O_2 formation, and that the covalent modification of the hydrophobic block with chlorinated side chains does not lead to increased oxidation. The D_h of **P2** and **P3** micelles remained unchanged after 4 days of incubation irrespective of the presence of additional TCE (**Figure 4.4c**), indicating that no micelle dis-assembly occurred following radiation exposure.

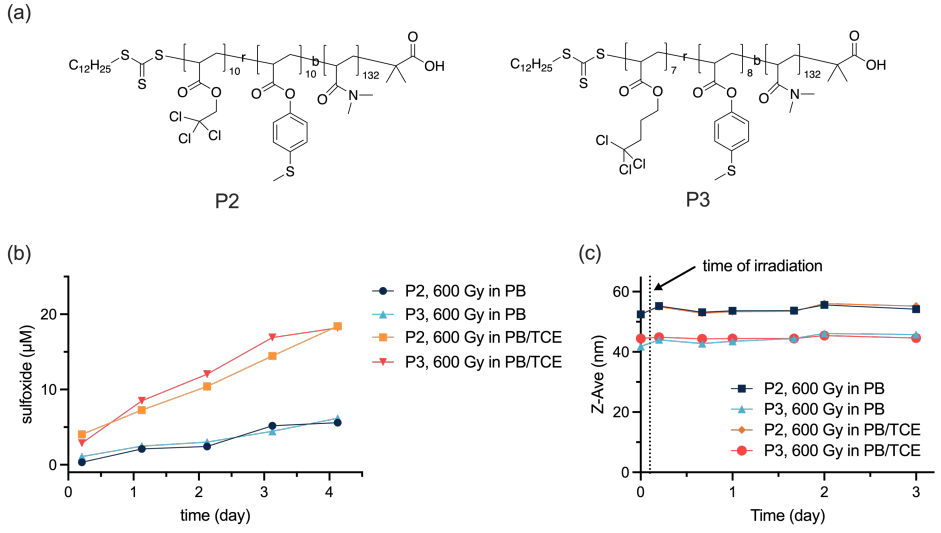

Figure 4.4. (a) Chemical structure of **P2** and **P3**; (b) time evolution of sulfoxide release after radiation; (c) time evolution of Z-average size of **P2** and **P3** micelles after irradiation.

Apparently, organochloride groups located in the hydrophobic core of the micelles cannot enhance the radiation-induced thioether oxidation. We hypothesize that the penetration of aqueous electrons into the hydrophobic core of the micelles is inhibited, and these electrons will be scavenged by dissolved molecular oxygen before reacting with the organochloride groups. To investigate this hypothesis, we synthesized a copolymer (**rP2**) where DMA, MTPA and 2,2,2-trichloroethyl acrylate are randomly copolymerized (**Figure 4.5a**). Because of absence of blocks and the high ratio of hydrophilic DMA repeating unit, **rP2** has good solubility in *d*-PB (100 mM, pD 7.4). The appearance of peaks of the polymer aromatic groups in the ^{1}H NMR spectrum (7.40-7.10 ppm, **Figure 4.5e**) indicates that the hydrophobic units are solvated. As shown in **Figure 4.5b**, a broad peak "*a*" (7.84 ppm) and two sharp doublet peaks "*b*, *c*" (7.65 and 7.06 ppm, respectively) were observed after addition of 600 mM hydrogen peroxide. Peak "*a*" can be assigned to the poly(4-(methylsulfinyl)phenol acrylate) while peak "*b*" and "*c*" can be assigned to MSP. After exposure of **rP2** (2 mg/mL in *d*-PB) to 600 Gy gamma-radiation following incubation at 37 °C for 5 hours, peak "*a*" was observed. After incubation for 4 days, poly(4-(methylsulfinyl)phenol acrylate) slowly hydrolyzed to release MSP. The concentration of poly(4-(methylsulfinyl)phenol acrylate) repeating unit was 115 μM after gamma-irradiation (600 Gy) and 5 hours of incubation (**Figure 4.5d**), calculated from integration of peak "a". After 4 days of incubation, the MSP was calculated to be 13 μM, which is more than two times higher than that of **P2** and **P3** under the same conditions. The oxidation of **rP2** and the high yield of poly(4-(methylsulfinyl)phenol acrylate) prove that the organochloride groups that are covalently bound to the polymer chains are able to enhance the oxidation of the thioether.

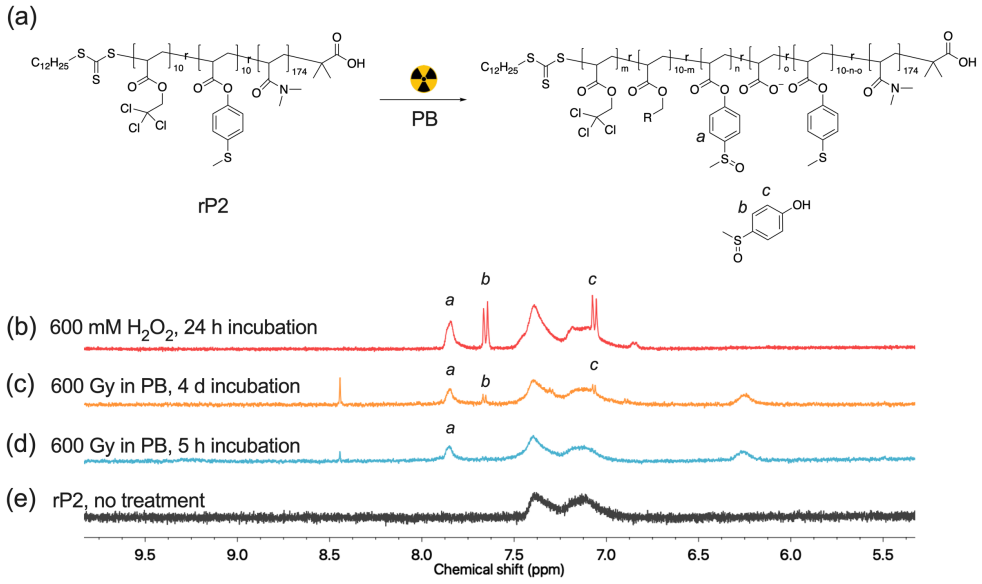

Figure 4.5. (a) Reaction scheme of **rP2** solution when exposed to gamma-radiation; (b) ^{1}H NMR spectrum of **rP2** after exposure to 600 Gy gamma-radiation or adding 600 mM H_2O_2.

Conclusions

We show that the reactive oxygen species generated from irradiated aqueous solutions containing organochloride can oxidize thioether compounds to form sulfoxides. The oxidation also works if the thioether in covalently bound to an amphiphilic block copolymer. In aqueous solution containing organochloride, the peroxyl radical formed in the bulk solvent can diffuse into the hydrophobic core and oxidize the core component. However, the oxidation yield is severely reduced if the organochloride is covalently bound to the hydrophobic block on the inside of polymer surfactant micelles, since aqueous electrons formed in bulk solution are too hydrophilic to enter into the core of micelles and instead will be scavenged by oxygen. Nevertheless, provided that the organochloride groups bound to a polymer are not shielded in the hydrophobic core, they can react with aqueous electrons and form peroxyl radical that can oxidize thioether groups, which paves the way for further application of radiation-induced organochloride mediated oxidation.

References

(1) Denkova, A. G.; Liu, H. H.; Men, Y. J.; Eelkema, R. Enhanced Cancer Therapy by Combining Radiation and Chemical Effects Mediated by Nanocarriers. *Adv. Therap.* **2020**, *3*, 1900177.

(2) Begg, A. C.; Stewart, F. A.; Vens, C. Strategies to Improve Radiotherapy with Targeted Drugs. *Nat. Rev. Cancer* **2011**, *11*, 239-253.

(3) Bernier, J. Alteration of Radiotherapy Fractionation and Concurrent Chemotherapy: a New Frontier in Head and Neck Oncology? *Nat. Clin. Pract. Oncol.* **2005**, *2*, 305-314.

(4) Cao, W.; Gu, Y.; Meineck, M.; Xu, H. The Combination of Chemotherapy and Radiotherapy Towards more Efficient Drug Delivery. *Chem. Asian J.* **2014**, *9*, 48-57.

(5) Read, G. H.; Bailleul, J.; Vlashi, E.; Kesarwala, A. H. Metabolic Response to Radiation Therapy in Cancer. *Mol. Carcinog.* **2022**, *61*, 200-224.

(6) Zhou, Z.; Chan, A.; Wang, Z.; Huang, X.; Yu, G.; Jacobson, O.; Wang, S.; Liu, Y.; Shan, L.; Dai, Y.; et al. Synchronous Chemoradiation Nanovesicles by X-Ray Triggered Cascade of Drug Release. *Angew. Chem. Int. Ed.* **2018**, *57*, 8463-8467.

(7) Vaidya, J. S. Principles of Cancer Treatment by Radiotherapy. *Surgery (Oxf)* **2021**, *39*, 193-201.

(8) Makin, G. Principles of Chemotherapy. *Paediatr. Child Health* **2018**, *28*, 183-188.

(9) Cao, Y. F.; Si, J. L.; Zheng, M. J.; Zhou, Q. H.; Ge, Z. S. X-Ray-Responsive Prodrugs and Polymeric Nanocarriers for Multimodal Cancer Therapy. *Chem. Commun.* **2023**, *59*, 8323-8331.

(10) Liu, H.; Zhao, J.; Xue, Y. F.; Zhang, J. X.; Bai, H.; Pan, S. J.; Peng, B.; Li, L.; Voelcker, N. H. X-Ray-Induced Drug Release for Cancer Therapy. *Angew. Chem. Int. Ed.* **2023**, *62*, e202306100.

(11) Zhang, B. B.; Xue, R.; Lyu, J.; Gao, A.; Sun, C. Y. Tumor Acidity/Redox Hierarchical-Activable Nanoparticles for Precise Combination of X-Ray-Induced Photodynamic Therapy and Hypoxia-Activated Chemotherapy. *J. Mater. Chem. B* **2022**, *10*, 3849-3860.

(12) Wardman, P. Factors Important in the Use of Fluorescent or Luminescent Probes and Other Chemical Reagents to Measure Oxidative and Radical Stress. *Biomolecules* **2023**, *13*, 1041.

(13) Brevé, T. G.; Liu, H. H.; Denkova, A. G.; Eelkema, R. Gamma Radiation Induced Contraction of Alkyne Modified Polymer Hydrogels. *Macromol. Mater. Eng.* **2022**, *307*, 2100623.

(14) Liu, H.; Laan, A. C.; Plomp, J.; Parnell, S. R.; Men, Y.; Dalgliesh, R. M.; Eelkema, R.; Denkova, A. G. Ionizing Radiation-Induced Release from Poly(ε-caprolactone-*b*-ethylene glycol) Micelles. *ACS Appl. Polym. Mater.* **2021**, *3*, 968-975.

(15) Ma, N.; Xu, H. P.; An, L. P.; Li, J.; Sun, Z. W.; Zhang, X. Radiation-Sensitive Diselenide Block Co-polymer Micellar Aggregates: Toward the Combination of Radiotherapy and Chemotherapy. *Langmuir* **2011**, *27*, 5874-5878.

(16) Tanabe, K.; Asada, T.; Ito, T.; Nishimoto, S. Radiolytic Reduction Characteristics of Drug-Encapsulating DNA Aggregates Possessing Disulfide Bond. *Bioconjug. Chem.* **2012**, *23*, 1909-1914.

(17) Napoli, A.; Valentini, M.; Tirelli, N.; Müller, M.; Hubbell, J. A. Oxidation-Responsive Polymeric Vesicles. *Nat. Mater.* **2004**, *3*, 183-189.

(18) Sharko, A.; Spitzbarth, B.; Hermans, T. M.; Eelkema, R. Redox-Controlled Shunts in a Synthetic Chemical Reaction Cycle. *J. Am. Chem. Soc.* **2023**, *145*, 9672-9678.

(19) Piergentili, I.; Bouwmans, P. R.; Reinalda, L.; Lewis, R. W.; Klemm, B.; Liu, H. H.; de Kruijff, R. M.; Denkova, A. G.; Eelkema, R. Thioanisole Ester Based Logic Gate Cascade to Control ROS-Triggered Micellar Degradation. *Polym. Chem.* **2022**, *13*, 2383-2390.

(20) Piergentili, I.; Cai, M.; Klemm, B.; Xu, B.; Luo, S. Z.; Eelkema, R. Enhancing Trigger Sensitivity of Nanocarriers Through Organocatalytic Oxidant Activation. *Cell Rep. Phy. Sci.* **2023**, *4*, 101547.

(21) Piergentili, I.; Hilberath, T.; Klemm, B.; Hollmann, F.; Eelkema, R. Enhancing the ROS Sensitivity of a Responsive Supramolecular Hydrogel Using Peroxizyme Catalysis. *Biomacromolecules* **2023**, *24*, 3184-3192.

(22) Weber, L. W. D.; Boll, M.; Stampfl, A. Hepatotoxicity and Mechanism of Action of Haloalkanes: Carbon Tetrachloride as a Toxicological Model. *Crit. Rev. Toxicol.* **2003**, *33*, 105-136.

Supporting Information

General experimental methods

All compounds were purchased from commercial suppliers (Sigma Aldrich, Tokyo Chemical Industry and abcr Gute Chemie) and used without further purification unless otherwise specified. Reactions were monitored by thin-layer chromatography (TLC) on a silica gel plate and visualized by UV light (254 nm) or stained using a $KMnO_4/OH^-$ solution. Flash column chromatography was carried out on a 30 cm column loaded with 230-400 mesh silica gel. ^{1}H-NMR spectra of small molecules were recorded on an Agilent-400 MR DD2 (399.67 MHz) or a Bruker 600 MHz at 298 K. Dynamic light scattering (DLS) was performed on a Zetasizer Pro equipped with a laser operating at 633 nm. The irradiation with gamma-rays were performed using a Nordion 220 ^{60}Co gamma cell. The dose rate at the experimental date was around 0.1080 Gy/s which was calculated based on the decay law and the half-life of ^{60}Co. The delivered dose was calculated by the dose rate at the date of the experiments multiplied by the exposure time. Radiation was given in one fraction unless otherwise specified.

Synthesis

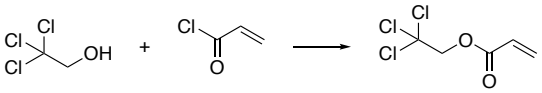

S1

Acryloyl chloride (2.2 g, 1 eq.), 1,1,1-trichloroethanol (4.1 g, 1.1 eq.) and DCM (30 mL). were added to a flame dried Schlenk flask. The mixture was degassed with N_2 and cooled to -20 °C using an ethanol/liquid nitrogen bath. Triethylamine (3.05 g, 1.2 eq) was added slowly. The mixture was allowed to return to room temperature and stirred for overnight. The reaction was quenched by adding 1 M HCl (100 mL). The organic phase was washed with brine 3 times and dried with $MgSO_4$. The solvent was evaporated under reduced pressure. The crude product was purified using flash column chromatography eluted with PE/DCM = 10/1. The product was collected as a colorless oil (yield 4.85 g, 86.9%). ^{1}H-NMR (399.67 MHz, $CDCl_3$, ppm) $\boldsymbol{\delta}$ = 6.56 (dd, J_1 = 1.16 Hz, J_2 = 17.32 Hz, 1H), 6.22 (dd, J_1 = 17.32 Hz, J_2 = 10.48 Hz, 1H), 5.99 (dd, J_1 = 1.12 Hz, J_2 = 10.48 Hz, 1H), 4.81 (s, 2H). ^{13}C NMR (99.91 MHz, $CDCl_3$, ppm) $\boldsymbol{\delta}$ = 164.30, 133.00, 127.03, 94.88, 74.03.

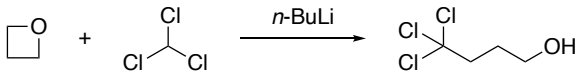

S2

Compound **S2** was synthesized using the method reported by Tsuji et al.[1] Anhydrous chloroform (1.32 mL, 1.2 eq.) and THF (20 mL) were added to a flame dried Schlenk flask. The mixture was degassed with nitrogen and cooled to -95 °C using an ethanol/liquid nitrogen bath. *n*-butyllithium (1.6 M in hexane, 10.3 mL, 1.2 eq) was then slowly added, followed by adding $BF_3 \cdot OEt_2$ (2.04 mL, 1.2 eq.) and oxetane (895 μL, 1 eq.). The mixture was returned to room temperature and stirred overnight. The reaction was quenched by 1 M HCl and washed with brine 3 times. The organic phase was collected, dried over $MgSO_4$ and purified using flash column chromatography eluted with PE/EA = 5/1, yield yellow oil 673 mg, 27.5%. ^{1}H-NMR (399.67 MHz, $CDCl_3$, ppm) $\boldsymbol{\delta}$ = 3.75 (t, J = 6.24 Hz, 2H), 2.81 (t, J = 8.12 Hz, 2H), 2.06-1.99 (m, 2H). ^{13}C NMR (99.91 MHz, $CDCl_3$, ppm) $\boldsymbol{\delta}$ = 99.90, 61.18, 51.94, 29.61.

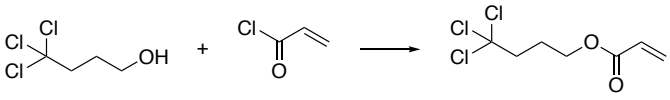

S3

Compound **S3** was synthesized using the same method as compound S1, and collected as colorless oil, yield 780 mg. ^{1}H-NMR (399.67 MHz, $CDCl_3$, ppm) $\boldsymbol{\delta}$ = 6.41 (d, J = 17.36 Hz, 1H), 6.12 (dd, J_1 = 17.36 Hz, J_2 = 10.40 Hz, 1H), 5.84 (d, J = 10.40 Hz, 1H), 4.25 (t, J = 6.28 Hz 2H), 2.78 (t, J = 7.84 Hz, 2H), 2.19-2.12 (m, 2H). ^{13}C NMR (99.91 MHz, $CDCl_3$, ppm) $\boldsymbol{\delta}$ = 165.95, 131.15, 128.08, 99.28, 62.67, 51.90, 25.99.

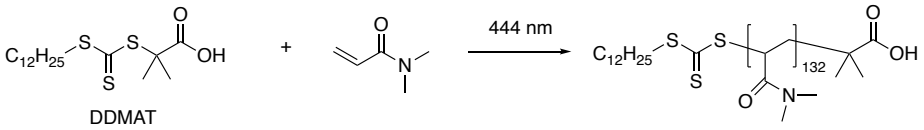

DDMAT (0.12 g, 1 eq.), basic alumina-filtered *N*,*N*-dimethylacrylamide (DMA, 6.90 g, 200 eq.) and 6.8 mL DMF were added in a 10 mL Schlenk flask. The solution was bubbled with nitrogen for 15 minutes and then sealed. ^{1}H NMR at t_0 was recorded. The reaction mixture

was stirred for 6 hours at room temperature in a LED light reactor giving blue light of 444 nm. ^{1}H NMR was taken to determine the conversion of DMA. The reaction mixture was diluted with DCM (50 mL) and precipitated three times in diethyl ether (500 mL), after which the product was dried in a vacuum oven at 40 °C for 3 days to obtain 7.32 g light yellow powder. The degree of polymerization was calculated to be on average 132 DMA repeating units.

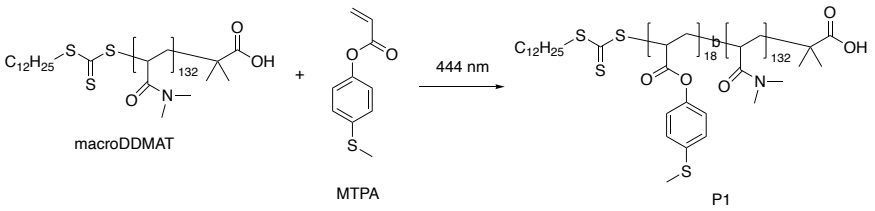

P1 was synthesized following an approach reported by our group.[2] The degree of polymerization for the MTPA was calculated to be on average 18 repeating units. $M_{n,NMR}$ = 16.9 kDa, $M_{n,GPC}$ = 9.9 kDa, $M_{w,GPC}$ = 10.6 kDa, dispersity index $Đ$ = 1.08.

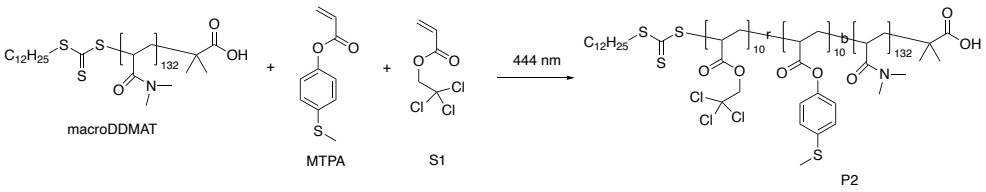

The used amount of chemicals in this synthesis is listed in **Table S4.1**. MacroDDMAT, MTPA and compound **S1** were dissolved in DMF, followed by bubbling with nitrogen for 15 minutes. ^{1}H NMR at t_0 was recorded. The resulting solution was stirred in a light reactor (444 nm) for the given time. ^{1}H NMR was taken to determine the conversion of MTPA and compound **S1**. After reaching the desired monomer conversion, the reaction mixture was diluted with DCM (50 mL) and precipitated three times in diethyl ether (500 mL). The product was filtrated and dried in a vacuum oven for 3 days (40 °C). **P2** was collected as light-yellow powder (0.78 g). The degree of polymerization for MTPA and **S1** are on average 10 repeating units. $M_{n,NMR}$ = 17.4 kDa, $M_{n,GPC}$ = 10.7 kDa, $M_{w,GPC}$ = 11.6 kDa, dispersity index $Đ$ = 1.08.

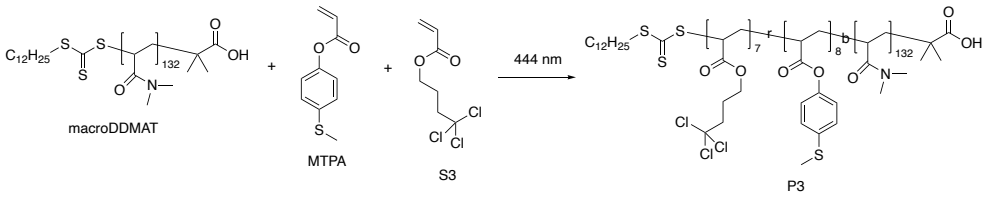

P3 was synthesized using the same method as **P2**. **P3** was collected as light-yellow powder, yield 1.10 g. The degree of polymerization for MTPA and **S3** are 8 and 7 repeating units, respectively. $M_{n,NMR}$ = 16.7 kDa, $M_{n,GPC}$ = 9.9 kDa, $M_{w,GPC}$ = 10.6 kDa, dispersity index $Đ$ = 1.07.

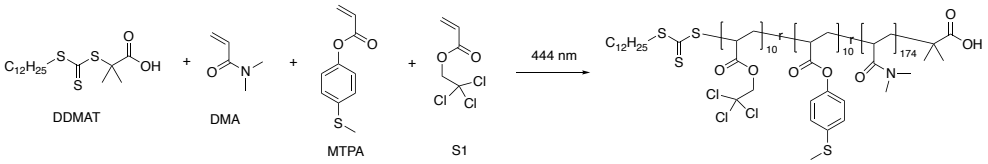

Specific amounts of DDMAT, DMA, MTPA, compound **S1** and DMF were added in a 10 mL Schlenk flask. The solution was bubbled with nitrogen for 15 minutes and sealed. ^{1}H NMR at t_0 was recorded. The reacting mixture was stirred for 16 hours at room temperature in a LED light reactor giving blue light of 444 nm. ^{1}H NMR was taken to determine the conversion of each monomer. The reacting mixture was diluted with DCM (50 mL) and precipitated in diethyl ether (500 mL) three times, after which the product was dried in a vacuum oven at 40 ℃ for 3 days to obtain 1.73 g light yellow powder. The degree of polymerization was calculated to be 174 DMA units, 10 **S1** units and 10 MTPA units. $M_{n,NMR}$ = 21.6 kDa, $M_{n,GPC}$ = 11.5 kDa, $M_{w,GPC}$ = 12.6 kDa, dispersity index $Đ$ = 1.09.

Table S4.1. P2, **P3** and **rP2** synthesis data.

	macro-DDMAT (g)	DDMAT (mg)	DMA (g)	MTPA (mg)	S1 (mg)	S3 (mg)	DMF (mL)	Reacting time (h)
P2	1.3	0	0	381	399	0	5	21
P3	1.3	0	0	381	0	498	5	11
rP2	0	34.8	2	197	206	0	2	16

Preparation of micelle solutions of P1, P2 and P3

The micelles were prepared by a solvent switching method. 2 mg of the polymer was dissolved in 0.1 mL THF. The solution was stirred for 10 min followed by slowly adding 1 mL *d*-PB. The obtained transparent solution was stirred in an open vial for 24 hours to evaporate THF. The solution was transferred to an NMR tube and was sent to ^{60}Co gamma irradiator.

Dynamic light scattering (DLS) measurements

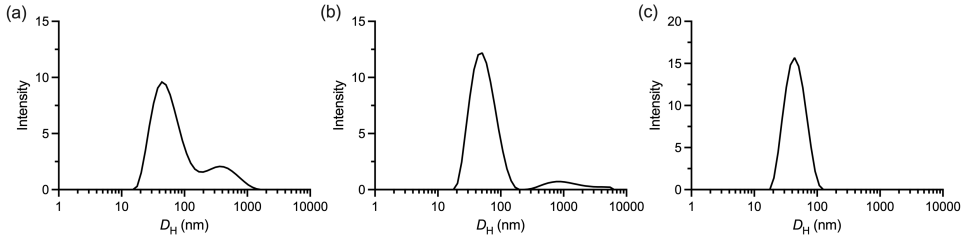

Figure S4.1. Hydrodynamic size distribution of (a) **P1** (1 mg/mL in 100 mM PB, pH 7.4), (b) **P2** (1 mg/mL in 100 mM PB, pH 7.4) and (c) **P3** (1 mg/mL in 100 mM PB, pH 7.4) micelles as measured by DLS.

References

(1) Imai, T.; Nishida, S.; Tsuji, T. Ring Opening Alkylation of Cyclic Ethers with α-Halogenoalkyllithiums in the Presence of Boron Trifluoride–Diethyl Ether. *J. Chem. Soc., Chem. Commun.* **1994**, 2353-2354.

(2) Piergentili, I.; Bouwmans, P. R.; Reinalda, L.; Lewis, R. W.; Klemm, B.; Liu, H. H.; de Kruijff, R. M.; Denkova, A. G.; Eelkema, R. Thioanisole Ester Based Logic Gate Cascade to Control ROS-Triggered Micellar Degradation. *Polym. Chem.* **2022**, *13*, 2383-2390.

Reaction Network Analysis of Organochloride Mediated Oxidation Induced by Ionizing Radiation

5

Abstract

The generation of organoperoxy radical by irradiating aqueous solutions of organochlorides depends on the concentration of organochloride, where low concentration results in low yield of peroxyl radical. The need of high concentration of organochloride limits the application in cancer therapy as most small molecule organochlorides show liver toxicity at elevated concentrations. To study if the oxidation is feasible at low concentration of organochloride, we proposed a reaction network where the effect of molecular oxygen is included. We hypothesized that oxygen competes with the organochloride to react with aqueous electrons, thereby causing a low yield of peroxyl radical at low organochloride concentrations. However, oxygen is necessary in the peroxyl radical formation pathway, which complicates straightforward prediction of reaction outcome. We developed a mathematic model to simulate the yield of peroxyl radical depending on organochloride and oxygen concentrations. The simulated results indicate that at low organochloride concentration, decreasing oxygen concentration leads to higher yield of peroxyl radical, with a peak at approximately 2% partial pressure of oxygen, and oxygen lower than 2% results in a sharp yield drop of peroxyl radical. Experiments using a thioether as reductant to quantify the peroxyl radical formation show good agreement with simulated data, verifying the proposed network. After irradiation in phosphate buffer saline/organochloride, a thioether caged dye showed a higher uncaging yield than the group without organochloride, demonstrating the viability of using thioether as a radiation sensitive group.

Availability and Contributions

This chapter is based on an article currently in preparation for submission, in collaboration with Bing Xu, Evgeny Uslamin, Evgeny Pidko, Antonia G. Denkova and Rienk Eelkema.

J.L., A.D. and R.E. developed the project idea. J.L. conducted most of the experiments, designed all the figures and schemes and wrote the first draft. B.X. helped the radiation experiments. E.U. and E.P. programmed the simulation participated in the mechanism discussion. A.D. and R.E. supervised the project, secured funding and corrected manuscript.

Introduction

Ionizing radiation induced chemical reactions have been intensively studied in recent years to design radiation sensitive materials for application in the combination of radiotherapy and chemotherapy.[1,2] In dilute aqueous solutions ([solute] < 0.1 M), e.g. biological systems, most of the energy deposited by ionizing radiation is absorbed by water molecules, and any subsequent chemical reactions are initiated by the products of water radiolysis.[3-5] The reactive species from water radiolysis include aqueous electrons, hydroxyl radicals and hydrogen peroxide, which can be used to react with especially designed radiation sensitive prodrugs and nanocarriers.[6-10] For example, Fu et al.[6] reported an antibody drug conjugate (ADC) where a fibroblast activation protein (FAP) targeted antibody and cytotoxin monomethyl auristatin E (MMAE) are linked by an *N*-alkyl-4-picolinium group. The picolinium can react efficiently with aqueous electrons, leading to cleavage of the carbamate group and release of MMAE. Tumour-bearing mice that received the ADC and radiotherapy showed efficient drug release at the irradiated site, indicating high precision local control of drug release. Although radiation induced drug release shows high potential for combination therapy, reported useful reactions are rare. One reason could be that the radiation-induced radical species are all highly reactive and short-lived, making it difficult to predict possible products and study reaction mechanisms.[11]

Kinetic models have been extensively used in predicting short-lived species (e.g. singlet oxygen[12], superoxide radical[13] and hydroxyl radical[14]) mediated advanced oxidation processes. Since these species react rapidly and unselectively with organic compounds, leading to their conversion to reactive intermediates which is difficult to measure.[14] Elementary reaction-based mathematical models that integrate the kinetics of each chemical reaction with reaction pathways, and the numerical solutions of their related ordinary differential equations (ODEs), can predict the time-dependent distribution of starting materials and reactive intermediates.[15-17] However, to precisely predict the yield of each species at a given time, the reaction rate of each elementary reaction should be known before calculating the numerical solution.[18]

In Chapter 3, we showed that reactive species generated by radiolysis of water can react with dissolved organochlorides, leading to the formation of potent oxidizing species. The

proposed mechanism is that an aqueous electron generated from water radiolysis reacts with an organochloride to form a chloride ion and a carbon-centered radical. The radical reacts with dissolved molecular oxygen to form a peroxyl radical, which is a strong oxidant. The results in Chapter 3 show that the oxidation depends on the concentration of organochloride: higher concentration of organochloride leads to more stilbene oxidation. We hypothesize that the molar ratio of dissolved oxygen to organochloride affects the yield of the peroxyl radical, since oxygen can compete with organochloride to react with aqueous electrons.[19]

In this chapter, we propose a reaction network which includes key reactions of the pathway of peroxyl radical formation. Based on the network, we have developed a kinetic model using coupled ODEs. By numerically solving this network of ODEs, we simulated the yield of peroxyl radical at different starting concentrations of oxygen and organochloride (**Scheme 5.1**). The simulation showed good agreement with the trend observed in Chapter 3. Moreover, the simulation suggested that, at a fixed concentration of organochloride, the yield of peroxyl radical increased with decreasing concentration of oxygen, with a peak at approximately 2% oxygen. The yield dropped to almost zero at 0% oxygen. The maximum yield was more pronounced at lower concentrations of organochloride. We then experimentally measured the concentrations of oxidizing product at selected concentrations of organochloride and oxygen. A thioether-based molecule, compound **1** (**Figure 5.1a**), was used as the scavenger to catch the peroxyl radical. The experimental results agreed with the predicted trend, with the yield of oxidizing product peaking at 2% oxygen. The agreement of simulated and experimental results further corroborated the proposed mechanism. Furthermore, we used compound **1** to cage the carboxylic acid moiety of a coumarin-based dye to test the viability of applying thioether-based cages in radiation-sensitive prodrugs. The uncaging of the dye by irradiation with gamma-rays in a PBS solution of organochloride showed a significantly enhanced uncaging compared to the experiment without organochloride, which means that compound **1** is a promising caging group. However, the uncaging efficiency was low, which was assigned to the water-insolubility of the caged dye.

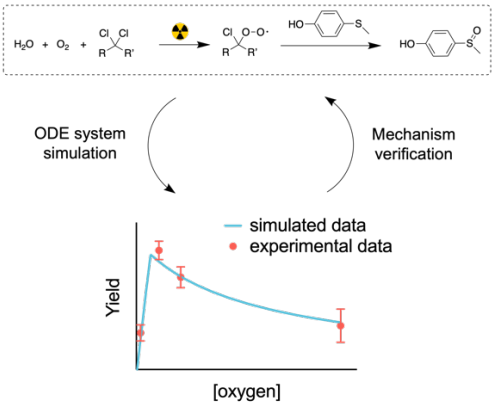

Scheme 5.1. The process of using a kinetic model to verify the mechanism of peroxyl radical formation.

Results and Discussion

To study the radiation-generated peroxyl radical in aqueous solution containing organochloride, we used 2,2,2-trichloroethan-1-ol (TCE) as the model organochloride since TCE is miscible with water and is the most efficient among organochlorides tested in Chapter 3. 4-(Methylthio)phenol (**1**, **Figure 5.1a**) was used as the reductant. Irradiation of compound **1** in deuterated water (D_2O)/TCE results in the formation of new peaks on proton nuclear magnetic resonance (^{1}H NMR) (**Figure S5.1b**), which can be assigned to 4-(methylsulfinyl)phenol **2**. In contrast, irradiation of compound **1** in D_2O (no TCE added) resulted in the same NMR spectrum as before irradiation (**Figure S5.1b**), indicating that compound **1** is not reactive to typical species formed by water radiolysis such as hydroxyl radical and hydrogen peroxide. Compound **1** (50 μM) in D_2O/12 mM TCE was exposed to increasing dose of gamma radiation. As shown in **Figure S5.2a**, the yield of compound **2** showed a linear increase with administered dose from 2 to 60 Gy, and the oxidation reached full conversion within 90 Gy of radiation (**Figure S5.2b**). The yield of compound **2** per received dose was 0.64 μM/Gy. It should be noted that the G-value (yield of species generated per received dose) of aqueous electrons is 0.28 μM/Gy. The higher yield of compound **2** suggests that the reaction of aqueous electrons and TCE can compete with the spur reactions thereby causing more aqueous electrons to be converted to peroxyl radicals. We then irradiated compound **1** (50μM) to reach 60 Gy in D_2O at various concentrations of

TCE and calculated the yield per received dose at different conditions. As shown in **Figure 5.1b**, the yield of compound **2** decreased when less TCE was applied, from 0.68 μM/Gy at 24 mM TCE to 0.054 μM/Gy at 60 μM of TCE. The phenomenon that the yield of oxidizing product depends on the concentration of organochloride was also observed in Chapter 3, where more chloroform resulted in more stilbene oxidation.

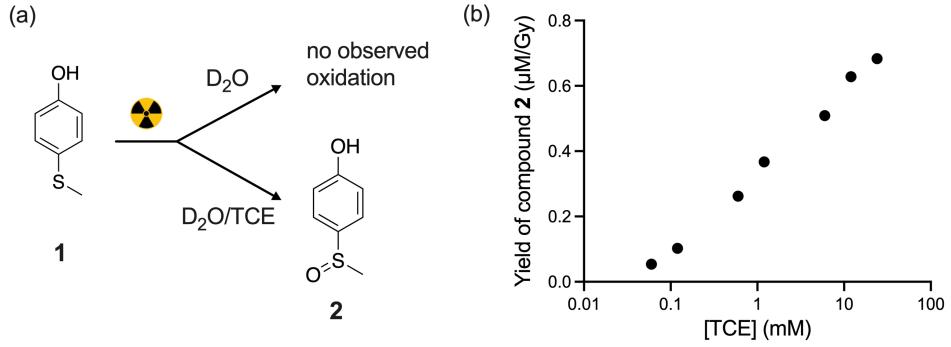

Figure 5.1. (a) Possible outcomes of the reaction of compound **1** under irradiation in D_2O and D_2O/TCE; (b) The yield of compound **2** (in μM/Gy) against TCE concentration.

The formation of the organochloride peroxyl radical intermediate (**M2** in **Scheme 5.2**) by irradiating an aqueous solution containing organochloride follows a series of reaction steps: radiolysis of water produces aqueous electrons which react with the organochloride to produce chloride ion and a carbon-centered radical. In aerated solutions, the carbon-centered radical reacts with molecular oxygen to produce the peroxyl radical. However, aqueous electrons can also react with dissolved molecular oxygen to form peroxyl radical anion that has been reported to be unreactive toward organochlorides.[19] In the previous experiments, the concentration of oxygen was constant and should be approximately 256 μM.[20] We hypothesized that the competition of aqueous electrons reacting with either molecular oxygen or the organochloride radical made the peroxyl radical generation rely on concentrations of organochloride and oxygen. Although higher oxygen concentration will inhibit the reaction of aqueous electrons with organochloride, oxygen is essential at the peroxyl radical generation pathway. So, the molar ratio of organochloride and oxygen is likely to exhibit an optimal value, which is difficult to predict without calculation.

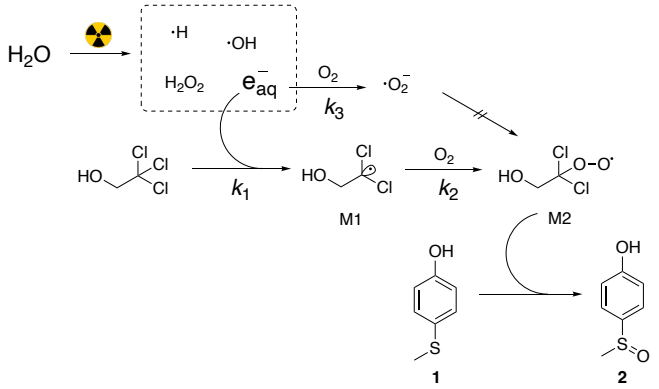

Scheme 5.2. Proposed reaction network of the oxidation of compound **1** by peroxyl radical generated from irradiating an aqueous solution containing organochloride and molecular oxygen.

To further corroborate the mechanism and to find the optimized ratio of organochloride to oxygen, we constructed a mathematic model to simulate the peroxyl radical generation pathway. The model is composed of coupled differential equations (equation **a** − **e**) which describe the reaction kinetics of species formation in the network. At room temperature, the reaction rate of aqueous electrons and oxygen (k_3) has been reported to be 1.9×10^{10} $M^{-1}s^{-1}$.[21] We used the reaction rate of chloroform and aqueous electrons (3.0×10^{10} $M^{-1}s^{-1}$)[21] as the value for k_1 since TCE has the same trichloro-group. For the rate of the carbon-centered radical and oxygen (k_2), we used 3.3×10^{9} $M^{-1}s^{-1}$ which is the rate of trichloromethyl radical and oxygen.[22,23] The approximated values of k_1 and k_2 may lead to an imprecise calculation of the final yield of **M2**, but using approximate values will allow prediction of trend in these reaction networks. The chemical reactions in the network occur at the end of physicochemical stage (ca. 10^{-12} sec) when aqueous electrons are in thermal equilibrium with the liquid. So, the producing rate of aqueous electron, as shown in the constant term of equation 4, is calculated from the dose rate (0.108 Gy s^{-1}) multiplying the G-value of aqueous electron (0.28×10^{-6} M Gy^{-1}). We set up the starting concentration of oxygen and TCE and the model calculated the numerical solution of [**M2**] at t = 555 sec, corresponding to the yield of **M2** after 60 Gy of irradiation. We plotted the yields of **M2** against different starting concentrations of TCE and oxygen in **Figure 5.2**. The oxygen content is expressed as both concentration (μM) and partial pressure (%) according to a linear relationship (256 μM = 21%). At a high concentration of oxygen, the yield of **M2** decreases with decreasing concentration of TCE, which is in line with the trend as shown in **Figure 5.1b**. At low

oxygen concentration (e.g. from 10 μM to 25 μM), the yield of **M2** slightly decreases when going from 500 μM to 50 μM TCE, followed by a sharp drop from 50 μM to 0 μM TCE. At very low oxygen concentration, the scavenging of aqueous electrons by oxygen becomes insignificant, resulting in a 90% of the maximum **M2** yield at low TCE concentration (e.g. 2% oxygen and 100 μM TCE). Oxygen concentration lower than 10 μM results in low yield of **M2** at any TCE concentration. It should be noted that the average physiological oxygen level in normal tissues is around 5% (61.0 μM) while that in cancerous tissues is around 2% (24.4 μM). Although some types of tumors are extremely hypoxic (lower than 0.5% oxygen where the formation of **M2** will be less than 2 μM at any [TCE]), the simulated results show that the organochloride mediated oxidation can occur in most tumors, with increased efficiency in hypoxic environments. To achieve a high yield of **M2**, TCE must be present in large excess. For example, the lowest limit of [TCE] to achieve 90% of the maximum yield is 46 μM. Moreover, by tuning the concentration of organochloride, healthy tissues with high oxygen concentrations can be less effected by the radiation induced oxidation. For instance, at 26 μM TCE, the yield of **M2** is 11.2 μM at 2% oxygen while the yield is 6.64 μM at 5% oxygen.

$$\frac{d[\mathrm{M2}]}{dt} = k_2[\mathrm{M1}][\mathrm{O_2}] \quad \text{(a)}$$

$$\frac{d[\mathrm{O_2}]}{dt} = -k_2[\mathrm{M1}][\mathrm{O_2}] - k_3\left[e_{aq}^-\right][\mathrm{O_2}] \quad \text{(b)}$$

$$\frac{d[\mathrm{M1}]}{dt} = k_1\left[e_{aq}^-\right][\mathrm{TCE}] - k_2[\mathrm{M1}][\mathrm{O_2}] \quad \text{(c)}$$

$$\frac{d\left[e_{aq}^-\right]}{dt} = -k_1\left[e_{aq}^-\right][\mathrm{TCE}] - k_3\left[e_{aq}^-\right][\mathrm{O_2}] + 0.108 \times 0.28 \times 10^{-6} \quad \text{(d)}$$

$$\frac{d[\mathrm{TCE}]}{dt} = -k_1\left[e_{aq}^-\right][\mathrm{TCE}] \quad \text{(e)}$$

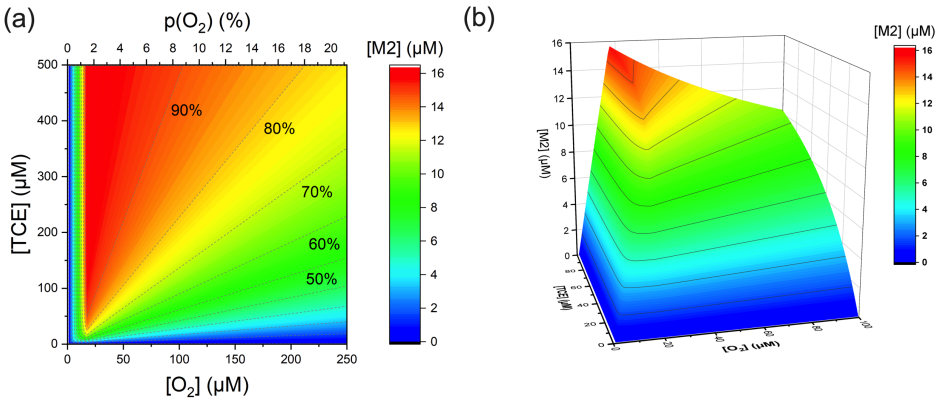

Figure 5.2. (a) The simulated yield of **M2** against different concentrations of TCE and oxygen. Dashed lines present the percentage of the maximum yield of **M2**. (b) 3D plot of the yield of **M2** at selected oxygen (0-100 μM) and TCE (0-100 μM) concentration.

We experimentally verified the model using compound **1** as the probe to react with **M2**. The concentration of compound **2** after 60 Gy of irradiation was measured by ^{1}H NMR spectroscopy. The signal-to-noise ratio of 1H NMR spectra at concentrations below 5 μM was too low to determine the conversion. As shown in **Figure 5.3a**, at 50 μM, 100 μM and 250 μM TCE, the yields of compound **2** increase when [oxygen] decreases from 256 μM to 27.4 μM and drop to the background value (approximately 3 μM) at 5.3 μM oxygen. At selected oxygen concentrations (27.4 μM, 54.2 μM and 256 μM), more TCE results in a higher yield of compound **2**. The observed trend is in line with the simulated trend (**Figure 5.3b** which is sliced from **Figure 5.2**), which indicates the proposed reaction network represent the mechanism of ROS formation.

We also see the limitations of the mathematic model and results from experiment. For example, as the model only includes the key reactions of the network, side reactions such as the radical recombination or deactivation of **M1** or **M2** are not considered, which could lead to a lower yield of compound **2**. Rate constants k_1 and k_2 can be measured by pulse radiolysis techniques or simulated using density functional theory (DFT) quantum mechanical calculations to precisely predict the yield. Besides, ^{1}H NMR is not sensitive enough to detect low concentrations of the probe, so the yields at 10 μM TCE are undetectable (**Figure 5.3a**). Also, regulating oxygen concentrations in aqueous solution is

challenging and that could cause large variation, especially at low TCE concentration. Still, the model describes general trends in line with experimental data and as such can be used to predict this system behavior.

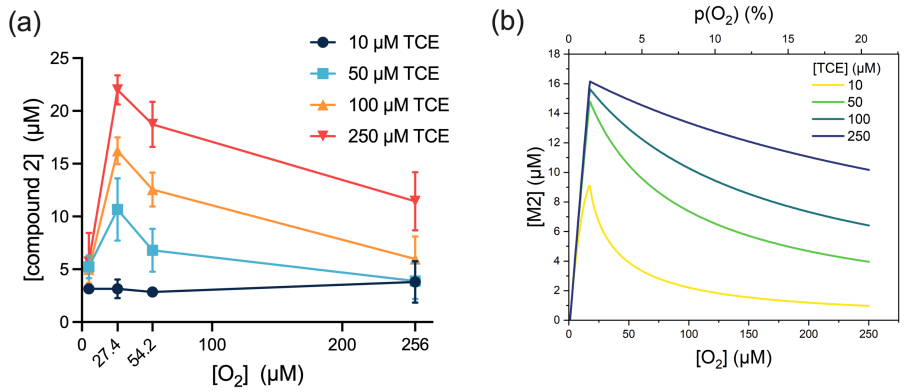

Figure 5.3. (a) Yield of compound **2** after irradiation with 60 Gy gamma-rays at selected concentration of TCE and oxygen; (b) simulated yield of **M2** at selected concentrations of TCE against various oxygen concentrations.

We then investigated the viability of using compound **1** as a caging group of radiation sensitive prodrugs. A coumarin derivative, 2-(7-Amino-2-oxo-2H-chromen-4-yl)acetic acid (AMC), was used as the probe (l_{max} = 350 nm). As shown in **Figure 5.4a**, the carboxylic acid group of AMC is caged as an ester bond with compound **1**, forming TE-AMC. Irradiation of TE-AMC with organochloride will generate TE-AMC sulfoxide, where the electron-withdrawing sulfoxide makes the phenol ester more reactive to hydrolysis.[24-26] Using high-performance liquid chromatography (HPLC), we calculated the conversion from TE-AMC to AMC after 60 Gy of gamma-irradiation and incubation at 37 °C for 35 minutes. TE-AMC has limited solubility in PBS so we added 10 vol% of DMSO in all the experiments. As shown in **Figure 5.4b**, after irradiating for 60 Gy in DMSO/PBS, the release profile of AMC shows no significant difference compared to that without radiation. In comparison, irradiation in the presence of TCE shows higher AMC conversion than the experiments without TCE (p = 0.0292). TE-AMC sulfoxide could only be detected after irradiation and 5 minutes incubation, after 15 minutes all sulfoxide ester had hydrolyzed (**Figure 5.4c**). Our results demonstrate that compound **1** can be used as the radiation

sensitive caging group in the presence of organochloride, although the hydrolysis of the ester before oxidation should be considered in the design of the prodrug.

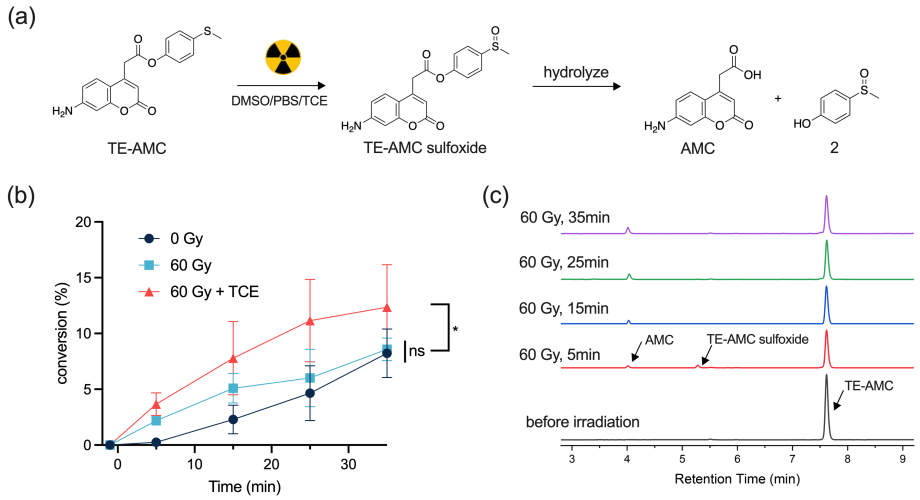

Figure 5.4. (a) Reaction scheme of radiation induced oxidation of TE-AMC and the subsequent hydrolysis reaction; (b) time evolution of the conversion from TE-AMC to AMC (10 µM in 10 vol% DMSO/PBS, 12 mM TCE was added in the organochloride group), the conversions were calculated from the peak areas of the HPLC chromatograms; (c) HPLC chromatograms at selected wavelength (340-360 nm) of TE-AMC after 60 Gy of gamma-irradiation in 10 vol% DMSO/PBS with 12 mM TCE. * indicates $p<0.05$.

Conclusions

For the previously developed radiation-induced oxidation mediated by organochlorides, we found that the yield of the organochloro peroxyl radical intermediate depends on the concentrations of organochloride and molecular oxygen. To investigate this dependency and determine the optimal ratio, we developed a reaction network and constructed a mathematical model that incorporates the key reactions within the network. We used the model to calculate the yields of peroxyl radical at various concentrations of oxygen and organochloride. Experimental detection of the peroxyl radical using a thioether as probe demonstrated similar yields and trends as the simulated results, corroborating the proposed network. A carboxylic acid-based dye was caged by the thioether to test the viability of using thioether as a radiation sensitive group. The oxidation of thioether by irradiating

aqueous solutions containing organochloride showed higher uncaging yields compared with the group without organochloride. The results indicate the thioether cage is a promising radiation sensitive group.

References

(1) Cao, Y. F.; Si, J. L.; Zheng, M. J.; Zhou, Q. H.; Ge, Z. S. X-Ray-Responsive Prodrugs and Polymeric Nanocarriers for Multimodal Cancer Therapy. *Chem. Commun.* **2023**, *59*, 8323-8331.

(2) Liu, H.; Zhao, J.; Xue, Y. F.; Zhang, J. X.; Bai, H.; Pan, S. J.; Peng, B.; Li, L.; Voelcker, N. H. X-Ray-Induced Drug Release for Cancer Therapy. *Angew. Chem. Int. Ed.* **2023**, *62*, e202306100.

(3) O'Neill, P.; Wardman, P. Radiation Chemistry Comes Before Radiation Biology. *Int. J. Radiat. Biol.* **2009**, *85*, 9-25.

(4) Wardman, P. The Importance of Radiation Chemistry to Radiation and Free Radical Biology (The 2008 Silvanus Thompson Memorial Lecture). *Brit. J. Radiol.* **2009**, *82*, 89-104.

(5) Wardman, P. Factors Important in the Use of Fluorescent or Luminescent Probes and Other Chemical Reagents to Measure Oxidative and Radical Stress. *Biomolecules* **2023**, *13*, 1041.

(6) Fu, Q. F.; Gu, Z.; Shen, S. Y.; Bai, Y. F.; Wang, X. L.; Xu, M. X.; Sun, P. W.; Chen, J. Y.; Li, D. X.; Liu, Z. B. Radiotherapy Activates Picolinium Prodrugs in Tumours. *Nat. Chem.* **2024**, *16*, 1348-1356.

(7) Fu, Q. F.; Zhang, S. R.; Shen, S. Y.; Gu, Z.; Chen, J. Y.; Song, D. F.; Sun, P. W.; Wang, C. H.; Guo, Z. B.; Xiao, Y. L.; et al. Radiotherapy-Triggered Reduction of Platinum-Based Chemotherapeutic Prodrugs in Tumours. *Nat. Biomed. Eng.* **2024**.

(8) Guo, Z. B.; Hong, H. Y.; Zheng, Y. D.; Wang, Z. Y.; Ding, Z. X.; Fu, Q. F.; Liu, Z. B. Radiotherapy-Induced Cleavage of Quaternary Ammonium Groups Activates Prodrugs in Tumors. *Angew. Chem. Int. Ed.* **2022**, *61*, e202205014.

(9) Ma, N.; Xu, H. P.; An, L. P.; Li, J.; Sun, Z. W.; Zhang, X. Radiation-Sensitive Diselenide Block Co-polymer Micellar Aggregates: Toward the Combination of Radiotherapy and Chemotherapy. *Langmuir* **2011**, *27*, 5874-5878.

(10) Tanabe, K.; Asada, T.; Ito, T.; Nishimoto, S. Radiolytic Reduction Characteristics of Drug-Encapsulating DNA Aggregates Possessing Disulfide Bond. *Bioconjug. Chem.* **2012**, *23*, 1909-1914.

(11) Ma, J. Y.; Minakata, D.; O'Shea, K.; Bai, L.; Dionysiou, D. D.; Spinney, R.; Xiao, R. Y.; Wei, Z. S. Determination and Environmental Implications of Aqueous-Phase Rate Constants in Radical Reactions. *Water Res.* **2021**, *190*, 116746.

(12) Barrios, B.; Mohrhardt, B.; Doskey, P.; Minakata, D. Mechanistic Insight into the Reactivities of Aqueous-Phase Singlet Oxygen with Organic Compounds. *Environ. Sci. Technol.* **2021**, *55*, 8054-8067.

(13) Bai, L.; Jiang, Y.; Xia, D. M.; Wei, Z. S.; Spinney, R.; Dionysiou, D. D.; Minakata, D.; Xiao, R. Y.; Xie, H. B.; Chai, L. Y. Mechanistic Understanding of Superoxide Radical-Mediated Degradation of Perfluorocarboxylic Acids. *Environ. Sci. Technol.* **2022**, *56*, 624-633.

(14) Kamath, D.; Mezyk, S. P.; Minakata, D. Elucidating the Elementary Reaction Pathways and Kinetics of Hydroxyl Radical-Induced Acetone Degradation in Aqueous Phase Advanced Oxidation Processes. *Environ. Sci. Technol.* **2018**, *52*, 7763-7774.

(15) Minakata, D. Development of an Elementary Reaction-Based Kinetic Model to Predict the Aqueous-Phase Fate of Organic Compounds Induced by Reactive Free Radicals. *Acc. Chem. Res.* **2024**, *57*, 1658-1669.

(16) Daily, R.; Minakata, D. Reactivities of Hydrated Electrons with Organic Compounds in Aqueous-Phase Advanced Reduction Processes. *Environ. Sci.: Water Res. Technol.* **2022**, *8*, 543-574.

(17) Daily, R.; Minakata, D. Development of a Group Contribution Method to Predict the Aqueous-Phase Reactivities of Hydrated Electrons with Organic Compounds. *J. Adv. Chem. Eng.* **2023**, *15*, 100493.

(18) Wardman, P. Approaches to Modeling Chemical Reaction Pathways in Radiobiology. *Int. J. Radiat. Biol.* **2022**, *98*, 1399-1413.

(19) Monig, J.; Krischer, K.; Asmus, K. D. One-Electron Reduction of Halothane and Formation of Halide Ions in Aqueous Solutions. *Chem. Biol. Interact.* **1983**, *45*, 43-52.

(20) Xing, W.; Yin, M.; Lv, Q.; Hu, Y.; Liu, C.; Zhang, J. Oxygen Solubility, Diffusion Coefficient, and Solution Viscosity. In *Rotating Electrode Methods and Oxygen Reduction Electrocatalysts*, Xing, W., Yin, G., Zhang, J. Eds.; Elsevier, 2014; pp 1-31.

(21) Buxton, G. V.; Greenstock, C. L.; Helman, W. P.; Ross, A. B. Critical Review of Rate Constants for Reactions of Hydrated Electrons, Hydrogen Atoms and Hydroxyl Radicals ($\cdot OH/\cdot O^-$) in Aqueous Solution. *J. Phys. Chem. Ref. Data* **1988**, *17*, 513-886.

(22) Lal, M.; Schoneich, C.; Monig, J.; Asmus, K. D. Rate Constants for the Reactions of Halogenated Organic Radicals. *Int. J. Radiat. Biol.* **1988**, *54*, 773-785.

(23) Neta, P.; Grodkowski, J.; Ross, A. B. Rate Constants for Reactions of Aliphatic Carbon-Centered Radicals in Aqueous Solution. *J. Phys. Chem. Ref. Data* **1996**, *25*, 709-1050.

(24) Piergentili, I.; Bouwmans, P. R.; Reinalda, L.; Lewis, R. W.; Klemm, B.; Liu, H. H.; de Kruijff, R. M.; Denkova, A. G.; Eelkema, R. Thioanisole Ester Based Logic Gate Cascade to Control ROS-Triggered Micellar Degradation. *Polym. Chem.* **2022**, *13*, 2383-2390.

(25) Piergentili, I.; Cai, M.; Klemm, B.; Xu, B.; Luo, S. Z.; Eelkema, R. Enhancing Trigger Sensitivity of Nanocarriers Through Organocatalytic Oxidant Activation. *Cell Rep. Phy. Sci.* **2023**, *4*, 101547.

(26) Piergentili, I.; Hilberath, T.; Klemm, B.; Hollmann, F.; Eelkema, R. Enhancing the ROS Sensitivity of a Responsive Supramolecular Hydrogel Using Peroxizyme Catalysis. *Biomacromolecules* **2023**, *24*, 3184-3192.

Supporting Information

General experimental methods

All compounds were purchased from commercial suppliers (Sigma Aldrich, Tokyo Chemical Industry and abcr Gute Chemie) and used without further purification unless otherwise specified. Reactions were monitored by thin-layer chromatography (TLC) on a silica gel plate and visualized by UV light (254 nm) or stained using a $KMnO_4/OH^-$ solution. Flash column chromatography was carried out on a 30 cm column loaded with 230 − 400 mesh silica gel. ^{1}H-NMR spectra were recorded on an Agilent-400 MR DD2 (399.67 MHz) at 298 K. Fluorescence spectra were recorded with Spex Fluorolog-3 equipped with a standard 90° setup. Milli-Q water was obtained by purification of demineralized water with a Milli-Q IQ 7000 machine equipped with a Millipak 0.22 μM filter. HPLC was performed on a Shimadzu setup with a D2 detector and Discovery C18 reverse phase column. Water/MeCN with 0.1% (v/v) formic acid was used as the mobile phase at a flow rate of 1 mL/min. Mass spectrometry was performed on a LTQ XL electrospray ionization source-mass spectrometer. The irradiations with γ-rays were performed using a Nordion 220 ^{60}Co gamma cell. The dose rate at the experimental date was around 0.108 Gy/s which is calculated based on the decay law and the half-life of ^{60}Co. The delivered dose was calculated by the dose rate at the date of the experiments multiplied by the exposure time. Radiation was given in one fraction unless otherwise specified.

Synthesis of TE-AMC

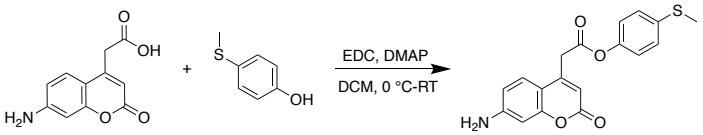

To a 50 mL flask was added 7-amino-4-methylcoumarin (100 mg, 1 eq.), 4-(Methylthio)phenol (64.5 mg, 1 eq.) and 10mL DCM. The solution was cooled to 0 °C using an ice bath followed by adding 1-ethyl-3-(3-dimethylaminopropyl)carbodiimide (EDC, 45 mg, 1.2 eq.). To the mixture was added 4-dimethylaminopyridine (DMAP, 28 mg, 0.5 eq.) and it was stirred at room temperature for 16 hours. After completion of the reaction, the solvent was evaporated under reduced pressure, and the crude product was

purified by silica gel flash column chromatograph eluted with DCM/MeOH (100/1). The product was collected as light yellow powder, yield 54.9 mg (35.5%). ^{1}H-NMR (400 MHz, $CDCl_3$, ***δ***): 7.44 (d, J = 8.84 Hz, 2H), 7.24 (d, J = 8.84 Hz, 2H), 6.97 (d, J = 8.48 Hz, 2H), 6.60-6.58 (m, 2H), 6.21 (s, 1H) 4.20 (s, 2H), 3.90 (s, 2H), 2.46 (s, 3H). ^{13}C-NMR (100 MHz, $CDCl_3$, ***δ***): 167.53, 161.15, 155.97, 150.59, 147.97, 147.58, 136.37, 127.87, 125.64, 121.64, 112.23, 111.96, 110.29, 101.36, 38.26, 16.35. MS (ESI+) *m/z* $[M + H]^+$ calculated 342.07, found 342.08.

^{1}H NMR study of thioether oxidation

4-(Methylthio)phenol (compound **1**) was dissolved in D_2O at a concentration of 50 μM, followed by addition of 2,2,2-trichloroethanol (TCE). The samples were placed in the middle of a gamma cell. For 60 Gy of radiation, the samples were irradiated for 555 seconds (the dose rate of the gamma irradiator was around 0.108 Gy/s at the experimental date).

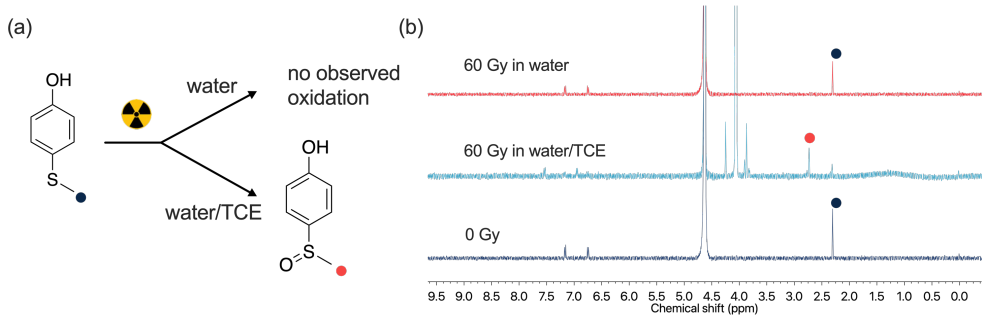

Figure S5.1. (a) The reactions of compound **1** under irradiation in D_2O and D_2O/TCE; (b) ^{1}H NMR spectra of compound **1** (50 μM in D_2O) before and after irradiation (spectra were taken within 3 hours after irradiation, the concentration of TCE was 12 mM if present).

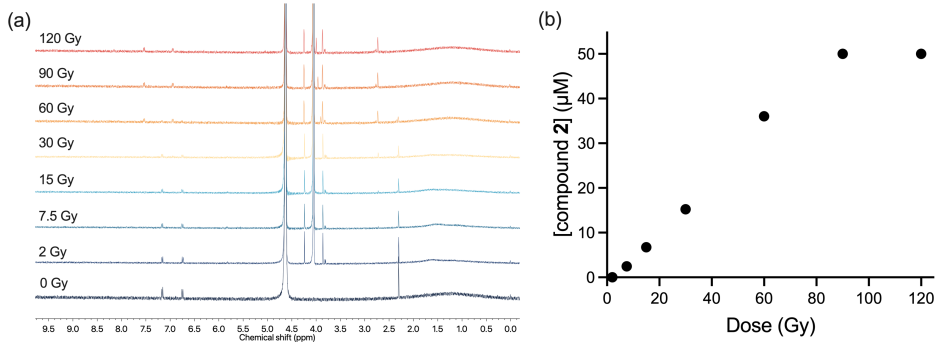

Figure S5.2. (a) ^{1}H NMR spectrum of compound **1** after increasing doses of irradiation in D_2O with 12 mM TCE. (b) The yield of compound **2** vs radiation dose.

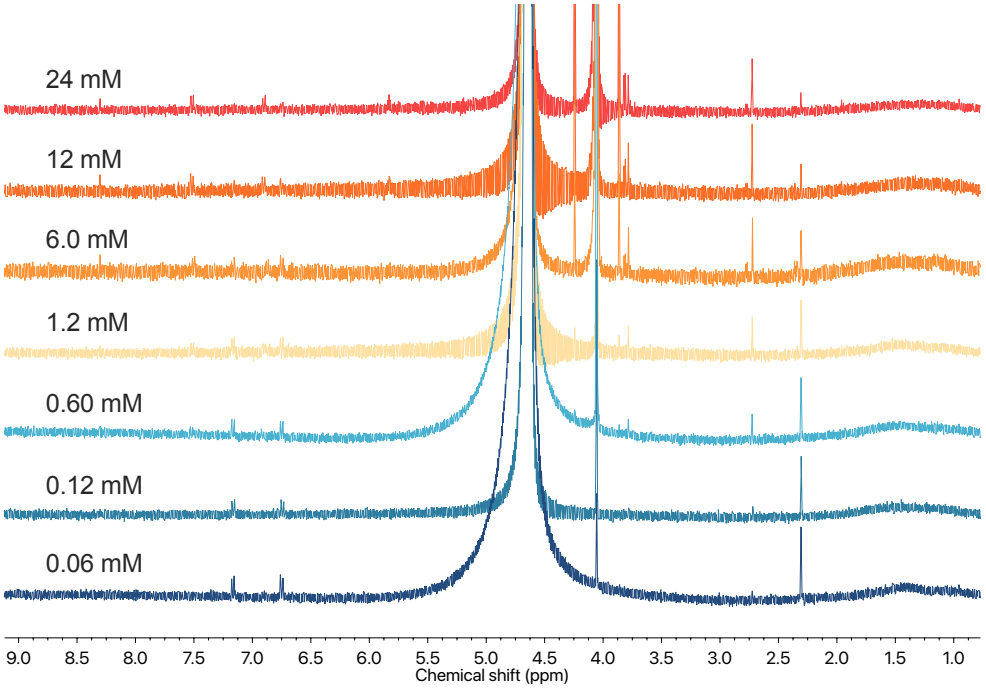

Figure S5.3. ^{1}H NMR spectrum of compound **1** (50 μM in D_2O) after 60 Gy of irradiation. The concentrations of TCE are noted on the corresponding spectrum.

Oxygen determination

To vary the concentration of oxygen in water, we bubbled a mixture of nitrogen and oxygen through the solution for 10 min. The partial pressure of oxygen was adjusted by regulating the flow rates of oxygen and nitrogen via a mass flow controller. Specifically, the nitrogen flow rate was maintained at 15 mL/min, while the flow rate of oxygen was adjusted accordingly to achieve the desired ratio. The exact concentrations of oxygen were determined using a Clark electrode, following the method reported by Pouvreau et al.[1] PBS was stirred under atmospheric conditions for 10 minutes to ensure saturation with air. The air saturated PBS was added to the cell with Clark electrode, and the polarization voltage was recorded. Then, 10 mg sodium hydrosulfite ($Na_2S_2O_4$) was added to the cell and the polarization voltage at 0% oxygen was recorded. The polarization voltages of air-saturated PBS and sodium hydrosulfite contained PBS were calibrated as 0% and 21% oxygen, respectively. The polarization voltages of samples were measured, and the voltages were calibrated to molar concentrations. The concentration of oxygen in air-saturated (21%) PBS at 25 °C (256 μM) was used to convert from molar concentration to partial pressure. The calculated oxygen partial pressures and the concentrations are detailed in **Table S5.1**.

Table S5.1. Calibration of oxygen concentration using Clark electrode.

Partial pressure in gas line (%)	Voltage (V)	Partial pressure (%)	concentration (μM)
5	0.122 ± 0.004	4.45 ± 0.06	54.2 ± 1.2
2	0.022 ± 0.001	2.24 ± 0.01	27.4 ± 0.2
0	-0.059 ± 0.008	0.43 ± 0.10	5.3 ± 2.0
21*	0.868	21	256*
$Na_2S_2O_4$	-0.079	0	0

* Values from Zhang et al. [2]

Irradiation of samples with various oxygen concentration

Samples containing compound **1** (50 μM) and various concentrations of TCE (10 μM, 50 μMm 100 μM and 250 μM) in 1 mL D_2O were prepared in 1.5 mL vials with septum caps. The samples were bubbled with mixed gas of oxygen and nitrogen through needles. For the samples with 21% oxygen, no bubbling process was applied. After regulating the partial pressure, the needles were removed and the septum cap was sealed with grease. The samples were then exposed to γ-rays with a dose of 60 Gy. After irradiation, the vials were

opened and the solution was transferred to NMR test tubes and subjected to NMR measurements (1024 scans per spectrum).

HPLC measurements of TE-AMC

A stock solution of TE-AMC (10 mM) was prepared by dissolving 3.41 mg of TE-AMC in 1 mL DMSO. DMSO/PBS solution was prepared by adding 10 vol% of DMSO to PBS. 1 µL of TE-AMC stock solution was added to 1 mL DMSO/PBS to prepare 10 µM TE-AMC solution. For the irradiation with 12 mM TCE, 1 µL of TCE was added. After preparation, the solution was subjected to HPLC measurement, and the chromatograph was collected as "before irradiation". After irradiation, the sample was analyzed by HPLC and the chromatograph was collected at "5 min" since the transporting time from gamma-irradiator to HPLC was 5 minutes. Then the sample was incubated in water bath at 37 °C for the given time.

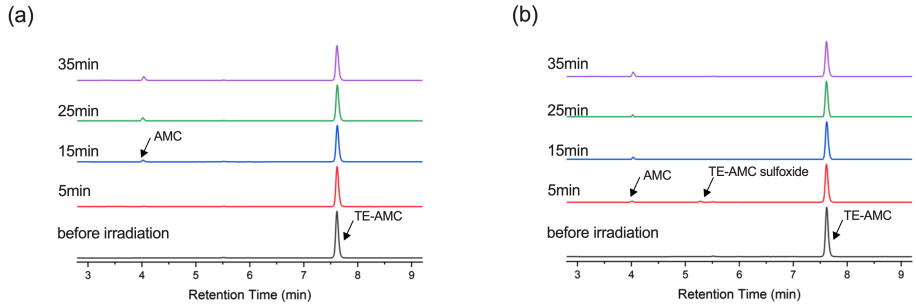

Figure S5.4. HPLC chromatograph at selected wavelength (340-360 nm) of TE-AMC (a) without irradiation in PBS/DMSO and (b) after 60 Gy gamma-irradiation in PBS/DMSO.

References

(1) Pouvreau, L. A.; Strampraad, M. J.; Van Berloo, S.; Kattenberg, J. H.; de Vries, S. NO, N_2O, and O_2 Reaction Kinetics: Scope and Limitations of the Clark Electrode. *Methods Enzymol.* **2008**, *436*, 97-112.

(2) Xing, W.; Yin, M.; Lv, Q.; Hu, Y.; Liu, C.; Zhang, J. Oxygen Solubility, Diffusion Coefficient, and Solution Viscosity. In *Rotating Electrode Methods and Oxygen Reduction Electrocatalysts*, 2014; pp 1-31.

Organochloride Mediated Prodrug Activation Induced by Ionizing Radiation

6

Abstract

Boronic acid and ester-caged prodrugs have been widely investigated in cellular-generated hydrogen peroxide triggered release. Although it is well-known that ionizing radiation generates hydrogen peroxide in aqueous solution, using this approach to activate boronic acid or ester-based prodrugs suffers from low H_2O_2 yields and thus low uncaging efficiency. However, the peroxyl radical formed from irradiating aqueous solution of organochloride may increase the uncaging efficiency. In this study, we used a boronic acid-caged coumarin derivative to quantify the yield of oxidation induced by clinical doses of radiation, and boronic acid-caged gemcitabine to assess the activation of a prodrug upon irradiation. Irradiation of the coumarin derivative in phosphate buffered saline shows a low yield of 0.048 μM/Gy, and the prodrug after irradiation has only limited toxicity to U87 cell line, indicating limited uncaging. The oxidation of boronic acid can be greatly enhanced by the peroxyl radical generated from irradiation of dilute PBS-organochloride solutions, with the yield increasing to 0.13 μM/Gy. Moreover, the oxidation by peroxyl radical can be catalyzed by *N*,*N*-dimethylaniline derivatives, increasing the yield to 0.19 μM/Gy. Clinical dose irradiation of the caged gemcitabine derivative in a solution of PBS with trichloroethanol and 2-(dimethylamino)benzoic acid shows efficient tumor cell killing and a comparable toxicity with that of the parent drug, indicating efficient uncaging.

Availability and Contributions

This chapter is based on an article currently in preparation for submission, in collaboration with Bing Xu, Antonia G. Denkova and Rienk Eelkema.

J.L., A.D. and R.E. developed the project idea. J.L. conducted most of the experiments, designed all the figures and schemes and wrote the first draft. B.X. conducted the cell experiments and helped on radiation experiments. A.D. and R.E. supervised the project, secured funding and corrected manuscript.

Introduction

Radiotherapy and chemotherapy are two common approaches to treat malignant tumors. High-energy X-rays or gamma-rays are applied in radiotherapy to damage the DNA of cancer cells, while cytotoxic drugs are applied in chemotherapy. Combinations of radiotherapy and chemotherapy have shown enhanced treatment effects for a variety of cancer types, but this strategy is still limited by the systemic toxicity of most chemotherapeutics.[1] Targeted prodrug activation is a strategy to reduce systemic toxicity. Prodrugs are chemically modified drugs where a key functional group is caged by a cleavable group. These prodrugs are activated by specific stimuli present in the tumor microenvironment (e.g. oxidative stress[2,3] and enzymes[4]) or by external stimuli such as near-infrared light[5]. Upon activation, the drug is released at the targeted site, enabling precise control over drug delivery. Ionizing radiation-activated prodrugs have been intensively studied in recent years for potential application in combined radiotherapy and chemotherapy with reduced side effects.[6,7] Since most radiation initiated chemical reactions are mediated by species from water radiolysis,[8] radiation-sensitive prodrugs should be designed to react with these species (e.g. hydrogen radical[9], hydroxyl radical[10] and aqueous electrons[11-15]). However, these species have low radiolytic yield (0.30 μM/Gy for aqueous electron and hydroxyl radical) and react unselectively with cellular components, which often results in a low efficiency of drug activation.

Arylboronic acids or esters are widely used as caging groups in prodrug design and chemical sensing systems, owing to their selective oxidation by reactive oxygen species (ROS) such as hydrogen peroxide (H_2O_2) and peroxynitrite,[16,17] leading to phenol formation through hydrolysis of the intermediate (**Figure 6.1**). Since cancerous cells have high levels of H_2O_2 (ranging from 10 μM to 100 μM) compared to normal cells, using intracellularly generated H_2O_2 to activate boronic acid-based prodrugs has been reported in anti-cancer therapy.[3,18,19] Matsushita et al. reported a prodrug where the 4-amino group of gemcitabine was caged with an arylboronate-ester-based carbamate group.[2] Upon oxidation by H_2O_2, the boronate hydrolyses, leaving a phenol group that undergoes quinol-methide elimination to release a molecule of CO_2 and free gemcitabine. However, not all types of cancer overproduce H_2O_2, for instance pancreatic epithelial cell line and human

glioblastoma cell line (U87) are not responsive to boronate ester or acid-based prodrugs.[2,3] Besides, the sluggish reaction rate of H_2O_2 and arylboronates lowers the efficiency of prodrug activation.[17,20] Ionizing radiation, administered during radiotherapy, generates H_2O_2 within tissues, offering potential for the development of radiation-activated prodrugs. However, the practical application of this approach is limited by the low yield of H_2O_2 generated by ionizing radiation.

In chapter 3, we demonstrated the oxidation of stilbene derivatives through irradiation in aerated water containing 0.1 vol% organochloride.[21] Aqueous electrons generated from water radiolysis can react with the organochloride to form a carbon-centered radical and a chloride ion. The radical reacts rapidly with dissolved oxygen to form a peroxyl radical which is a strong oxidant. Here, we present the oxidation of arylboronic acids using ionizing radiation. A fluorescent probe, 7-amino-4-methylcoumarin (AMC), was employed to quantify this reaction since the oxidation of arylboronic acid led to the activation of fluorescence emission. We found that the peroxyl radical generated from the radiolysis of water in the presence of organochloride can efficiently oxidize arylboronic acid (**Figure 6.1**). Furthermore, this oxidation process can be catalyzed by *N*,*N*-dimethylaniline derivatives (**Figure 6.1**). The proposed mechanism suggests that the peroxyl radical oxidizes *N*,*N*-dimethylaniline to form its *N*-oxide, which is known to oxidize arylboronic acids. [22-25] The *N*-oxide is then reduced back to *N*,*N*-dimethylaniline, completing a catalytic cycle. Building on these findings, we synthesized a gemcitabine prodrug in which the 4-amino group is protected by an arylboronic acid-based carbamate group. This prodrug exhibited reduced cytotoxicity toward the U87 cell line. Upon exposure to 6 Gy X-ray in phosphate buffer saline (PBS) containing organochloride and the *N*,*N*-dimethylaniline derivative, the prodrug demonstrated an inhibitory effect comparable to that of native gemcitabine under radiation treatment. Our findings indicate that the activation of a boronic acid-caged prodrug via radiation in the presence of organochlorides is an effective approach for combining chemotherapy with radiation therapy.

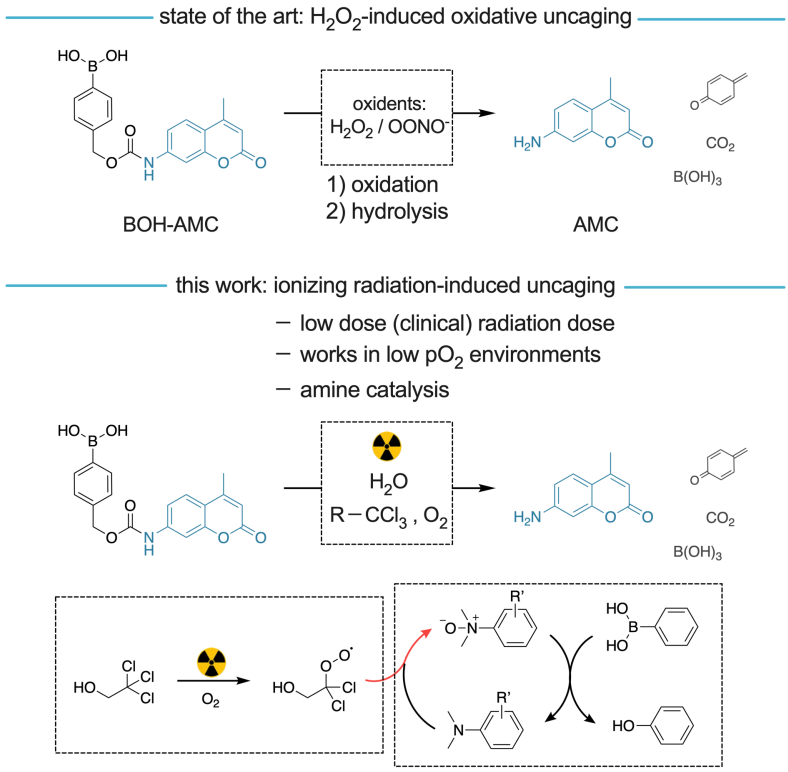

Figure 6.1. Oxidation of boronic acid induces release of amine cargo; state of the art: oxidation induced by hydrogen peroxide or peroxynitrite; this work: oxidation induced by ionizing radiation.

Results and Discussion

To study the oxidation of arylboronic acid, we synthesized a 7-amino-4-methylcoumarin based fluorescent probe, whereas the 7-amino group is protected by a boronic acid based self-immolative linker (denoted as BOH-AMC, **Figure 6.1**). The fluorescence emission of AMC is quenched when the 7-amino is caged by an electron-withdrawing carbamate group. Oxidation of boronic acid will lead to the release of the amino group of AMC, coupled to an increase in fluorescence emission. As shown in **Figure 6.2a**, irradiation (8 Gy) of BOH-AMC in PBS leads to an increase in emission intensity at 441 nm, indicating the release of AMC. We attribute this release to the oxidation of arylboronic acid by H_2O_2 generated from water radiolysis. The introduction of 2,2,2-trichloroethanol (TCE) results in more

AMC activation as evidenced by a higher emission intensity than that in PBS alone, which indicates that the oxidation is likely due to the ROS generated from irradiating PBS/TCE.

It is reported that organic *N*-oxides can oxidize boronic acids or esters selectively and efficiently.[22-25] Meanwhile, *N*-oxide derivatives are commonly synthesized by oxidizing tertiary amines using peroxides such as hydrogen peroxide and peroxybenzoic acid.[26] We were curious if the ROS generated from irradiation of PBS/TCE can oxidize tertiary amines, and if the formed *N*-oxides can oxidize arylboronic acid. As shown in **Figure 6.2a**, more AMC is activated when 2-(dimethylamino)benzoic acid **1** is present in PBS/TCE. The enhancing effect of tertiary amine suggests that the aforementioned mechanism plays a role. In contrast, irradiation of BOH-AMC in PBS/**1** results in much lower AMC activation than observed in PBS/TCE/**1**, meaning that the presence of TCE is crucial in the oxidation process. This conclusion is corroborated by high-performance liquid chromatography (HPLC) measurements (**Figure 6.2b**), where irradiation in water/TCE/**1** results in the highest conversion from BOH-AMC to AMC among all the irradiated groups.

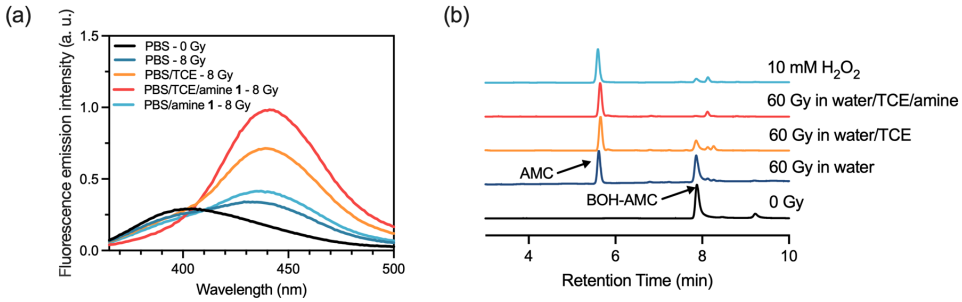

Figure 6.2. (a) Fluorescence emission spectrum of BOH-AMC before and after 8 Gy of gamma-irradiation (excitation at 330 nm; 10 µM probe in PBS, pH 7.4; 12 mM of TCE if present; 100 µM of amine **1** if present; samples were incubated for 30 min after irradiation); (b) HPLC-UV chromatograph determines the oxidation of BOH-AMC (10 µM in water; 0.1 vol% of TCE if present; 100 µM of amine **1** if present; samples were incubated for 30 min after irradiation).

We investigated a series of tertiary amine categories, including derivatives of *N*,*N*-dimethylanilines (compound **1**-**9**), aliphatic amines (compound **10**, **12**,) and heterocyclic amines (compound **11**, **13**) (**Figure 6.3a**). BOH-AMC (10 µM) was prepared in PBS/12 mM TCE with different amines. After irradiation of 8 Gy, the solutions were incubated at

37 ℃ for 30 minutes. The emission intensities of AMC are converted to concentrations according to a calibration curve as shown in **Figure S6.1**. The concentration of all the amines were 100 μM. As shown in **Figure 6.3b**, irradiation in the presence of **1**, **2**, **3**, **5**, **6**, **8**, **9**, **10**, **12** leads to enhanced AMC release, whereas the presence of **7** exhibits inhibitory effects, likely due to the reducing property of the aldehyde group. *N*,*N*-dimethylaniline derivatives (**1**, **3**, **5**, **8**, **9**) show more pronounced enhancement compared to aliphatic amines (**10**, **12**) whereas heterocyclic amines (**11**, **13**) show no enhancement. Our observations align with findings reported by Falck et al., wherein *N*,*N*-dimethylaniline *N*-oxide derivatives exhibit the highest reactivity towards arylboronic acid (with reaction completion within 1 minute in DCM), while aliphatic tertiary amines, such as *N*-methylmorpholine *N*-oxide and trimethylamine *N*-oxide, exhibit sluggish reactivity. To further verify the formation of *N*-oxide after irradiation of water/TCE/amine solution, we used HPLC-mass spectrometry to detect the *N*-oxide. As shown in **Figure S6.2**, the mass spectrum at 2.61 minute suggests the formation of *N*,*N*-dimethyl-*p*-toluidine *N*-oxide after exposure of water/TCE/**9** to 120 Gy gamma-irradiation.

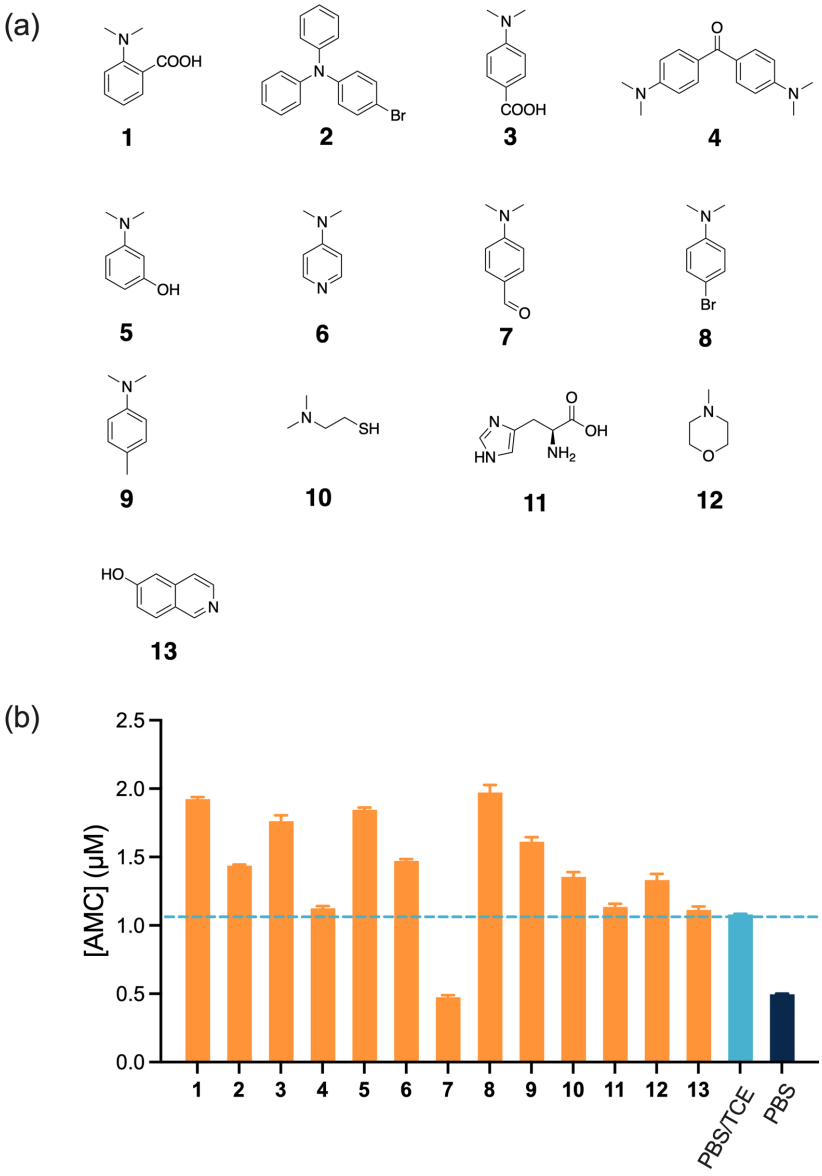

Figure 6.3. (a) Structure screen of tertiary amines; (b) the concentration of released AMC after exposure to 8 Gy gamma-radiation (**1**-**13**, irradiation in PBS/TCE/amines, dashed line presents the AMC release after 8 Gy in PBS/TCE).

We used compound **1** for subsequent studies. **Figure 6.4a** shows the release AMC profiles in relation to absorbed radiation dose. BOH-AMC (10 μM) was irradiated in PBS,

PBS/TCE and PBS/TCE/**1**, and the solutions were incubated for 30 minutes at room temperature. The G-values of AMC are given in **Figure 6.4a**. Irradiation in PBS gives the lowest G-value (0.048 μM/Gy). The presence of 0.1 vol% TCE increases the G-value of AMC to 0.13 μM/Gy, and the G-value is even higher (0.19 μM/Gy) when compound **1** is present with TCE. The significantly higher yield can be attributed to the higher G-value of aqueous electrons (0.30 μM/Gy) compared to that of H_2O_2 (0.07 μM/Gy). The activation profile of AMC after irradiation in PBS/TCE/**1** and PBS/TCE shows a fast fluorescence increase in the first 30 minutes (**Figure 6.4b**), corresponding to the fast kinetics of *N*-oxide and peroxide reaction with the arylboronic acid. In contrast, the kinetic of AMC release after irradiation in PBS is much slower than the other two groups.

We were curious whether *N*,*N*-dimethylaniline served as a catalyst in the oxidation process. To prove this, BOH-AMC solutions were prepared in PBS/TCE with varying concentrations of compound **1**. The release of AMC was monitored following irradiation (8 Gy). As shown in **Figure 6.4c**, the AMC release exhibits an initial increase followed by a decrease with increasing [**1**], peaking at 5 μM. At [**1**] exceeding 5 mM, the activation of AMC goes even below that observed without the presence of compound **1**. Notably, at a concentration of 0.1 μM of **1**, approximately 0.36 μM more AMC is activated compared to that in the absence of the amine, suggesting catalysis by the amine.

The use of organochlorides like TCE raises concerns about potential hepatotoxicity and carcinogenicity.[27] Although the relation between TCE concentration and tissue toxicity has not been fully explored, it is advisable to minimize TCE usage to mitigate any side effects. Considering this, we investigated the oxidation of BOH-AMC in PBS/TCE/**1** with TCE concentrations ranging from 24 mM to 12 μM. As illustrated in **Figure 6.4d**, after exposure to the same dose of gamma-irradiation, low concentration of TCE leads to decreasing release of AMC, while at 24 mM TCE, the release of AMC is slightly lower than that at 12 mM. The strong dependance can be attributed to the short lifetime of aqueous electron, where higher TCE concentrations favor the TCE-aqueous electron reaction over other reactions of aqueous electron such as radical recombination or scavenging by molecular oxygen.

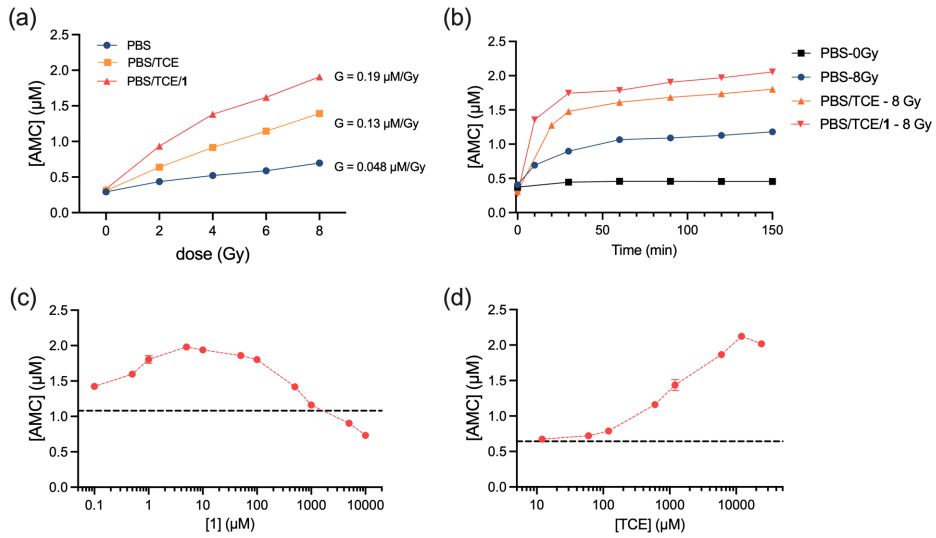

Figure 6.4. Radiation-induced fluorescent probe activation. (a) dose-dependent AMC release (n=3 independent experiments; for some data, error bars are smaller than data markers); (b) time evolution of the probe solutions post-irradiation (radiation dose, 8 Gy; 10 µM probe in PBS, pH 7.4; 0.1 vol% of TCE if present; 100 µM of **1** if present); (c) determination of AMC release against [**1**] (radiation dose, 8 Gy; 10 µM probe in PBS/0.1 vol% TCE; dashed line represents the released AMC without **1**); (d) determination of AMC release against [TCE] (radiation dose, 8 Gy; 10µM probe in PBS/5µM **1**; dashed line represents the released AMC without TCE).

We have discussed the reaction network of peroxyl radical formation in Chapter 5. The network is depicted in **Figure 6.5a**: the organochloride reacts with an aqueous electron to form a carbon-centered radical and a chloride anion. The reaction rate is unknown but is estimated to be diffusion controlled ($k \sim 10^{10}$ M^{-1} s^{-1}).[28] The radical reacts with molecular oxygen to form the peroxyl radical ($k \sim 10^{9}$ M^{-1} s^{-1}).[29] Aqueous electrons can react with molecular oxygen to form superoxide anion ($k = 1.9 \times 10^{10}$ M^{-1} s^{-1})[28] which is known to be unreactive toward organochlorides.[30] The comparable reaction rate of oxygen and organochloride with aqueous electrons makes that the yield of the peroxyl radical strongly dependent on the concentration ratio of organochloride and oxygen. To experimentally investigate this dependence and to test if radiation-induced oxidation can be performed under hypoxic conditions, BOH-AMC solutions (10 µM) were irradiated with 8 Gy g-rays in varying oxygen concentrations. The concentrations of TCE and amine **1** were 120 µM and 5 µM, respectively. Oxygen partial pressure at 2% is the commonly reported value for hypoxic tumors and 5% oxygen is the average for healthy tissues.[31,32] As shown in **Figure**

6.5b, in the group of irradiation in the presence of TCE and amine **1**, the maximum AMC release is observed at 2% (ca. 27.2 µM) oxygen, and higher oxygen concentration results in reduced release of AMC. This result is in line with the proposed mechanism, and means that the oxidation is most efficient under hypoxic conditions. Notably, the release of AMC in the group without organochloride and amine present has a lower total yield which reaches a plateau from 2% oxygen onwards.

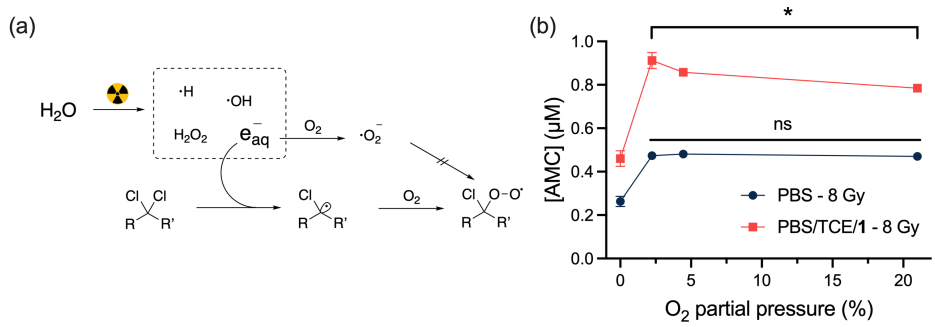

Figure 6.5. (a) Proposed mechanism of the effect of oxygen on the oxidation; (b) relation of coumarin release at hypoxic condition and the enhancing effect of PBS/TCE/**1** at hypoxic irradiation (n = 3, two-way ANOVA, * represents $p<0.5$).

The cytotoxicity of radiation activated prodrugs in a cell environment was tested using gemcitabine (Gem) as the model drug. The combination of Gem and radiotherapy has been investigated to treat a variety of cancers since Gem is a potential radiosensitizer *in vitro* and *in vivo*.[33,34] However, the side effects are unacceptable when Gem is used in combination with radiotherapy or other chemotherapeutics.[35] Inspired by Matsushita et al.,[2] we synthesized a prodrug, BOH-Gem, where the 4-amino group of Gem was caged by a boronic acid-based carbamate group (**Figure 6.6a**). U87, a human glioblastoma cell line, was selected because of the low level of in-cell generated H_2O_2. The half maximal inhibitory concentration (IC_{50}) of BOH-Gem is 90.9 nM against U87 cell line, which is much higher than that of Gem (6.27 nM). We selected the concentration of 20 nM for both Gem and BOH-Gem in the irradiation experiment. As shown in **Figure 6.6c, d**, 5 µM of compound **1** and 500 µM TCE is not toxic toward U87 cells with or without exposure to irradiation, as seen by the non-significant cell viability compared to the control group. Irradiation of cells with BOH-Gem alone does not lead to a high cell killing efficiency

(**Figure 6.6d**), which indicates the H_2O_2 generated by 6 Gy of X-ray is not enough to release significant amounts of Gem and kill the cells. Irradiation of BOH-Gem with addition of compound **1** and TCE results in a similar cell killing efficiency compared to irradiation of Gem, demonstrating the radiation-driven activation of prodrug causes a comparable toxicity as the parent drug.

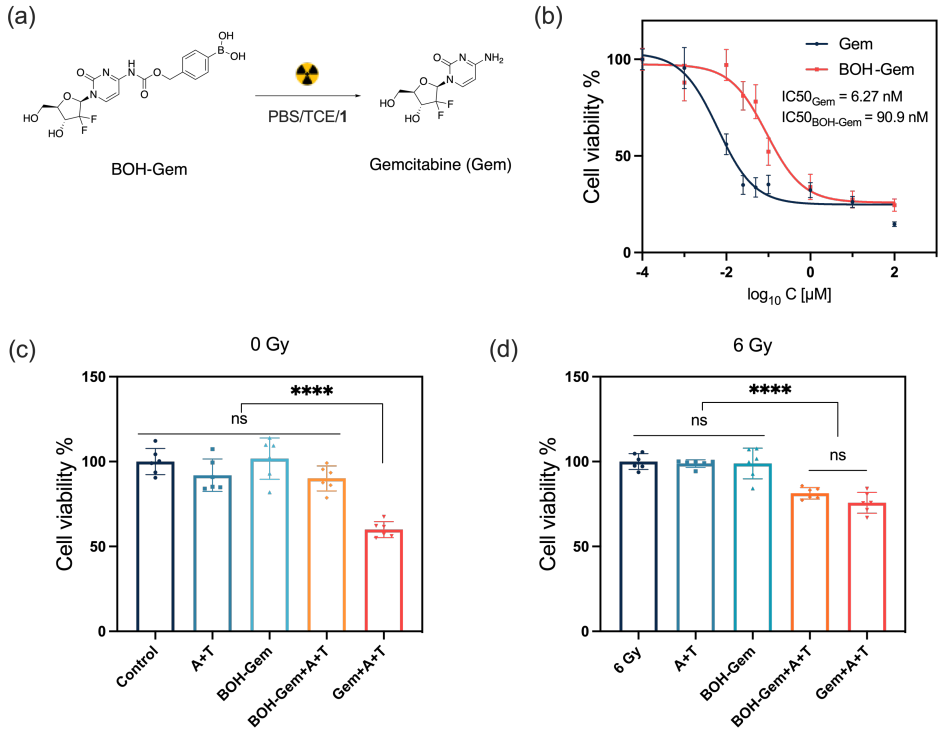

Figure 6.6. (a) Chemical structure of gemcitabine and boronic acid functionalized prodrug BOH-Gem; (b) IC_{50} assays of Gem and BOH-Gem towards U87 cell line; cell viability of U87 cells (c) without irradiation and (d) after 6 Gy of X-ray irradiation (A represents addition of 5 μM amine **1**, T represents addition of 500 μM TCE, n = 6, one-way ANOVA t-test, *P*-values >0.05 show as "ns", *P*-values <0.0001 are indicated with four asterisks).

Conclusions

We show that an arylboronic acid-based probe and prodrug can be oxidized by peroxyl radicals generated from radiolysis of aqueous solutions containing an organochloride

compound. The oxidation is substantially enhanced when *N,N*-dimethylaniline derivative is present. Higher concentration of organochloride results in more oxidation, while at low concentrations of organochloride, the yield of oxidizing product depends on the concentration of oxygen. A boronic acid-caged gemcitabine prodrug shows reduced toxicity compared to parent drug. Exposure of prodrug solutions containing an organochloride and *N,N*-dimethylaniline derivative to clinical doses of radiation results in comparable cell toxicity as the parent drug group. This study presents a promising strategy of using boronic acid-caged prodrugs to achieve radiotherapy-triggered chemotherapy.

References

(1) Denkova, A. G.; Liu, H. H.; Men, Y. J.; Eelkema, R. Enhanced Cancer Therapy by Combining Radiation and Chemical Effects Mediated by Nanocarriers. *Adv. Therap.* **2020**, *3*, 1900177.

(2) Matsushita, K.; Okuda, T.; Mori, S.; Konno, M.; Eguchi, H.; Asai, A.; Koseki, J.; Iwagami, Y.; Yamada, D.; Akita, H.; et al. A Hydrogen Peroxide Activatable Gemcitabine Prodrug for the Selective Treatment of Pancreatic Ductal Adenocarcinoma. *ChemMedChem* **2019**, *14*, 1384-1391.

(3) Skarbek, C.; Serra, S.; Maslah, H.; Rascol, E.; Labruère, R. Arylboronate Prodrugs of Doxorubicin as Promising Chemotherapy for Pancreatic Cancer. *Bioorg. Chem.* **2019**, *91*, 103158.

(4) Lee, B. S.; Cho, Y. W.; Kim, G. C.; Lee, D. H.; Kim, C. J.; Kil, H. S.; Chi, D. Y.; Byun, Y.; Yuk, S. H.; Kim, K.; et al. Induced Phenotype Targeted Therapy: Radiation-Induced Apoptosis-Targeted Chemotherapy. *J. Natl. Cancer Inst.* **2015**, *107*, dju403.

(5) Long, K. Q.; Lv, W.; Wang, Z. H.; Zhang, Y. M.; Chen, K.; Fan, N.; Li, F. Y.; Zhang, Y. C.; Wang, W. P. Near-Infrared Light-Triggered Prodrug Photolysis by One-Step Energy Transfer. *Nat. Commun.* **2023**, *14*, 8112.

(6) Cao, Y. F.; Si, J. L.; Zheng, M. J.; Zhou, Q. H.; Ge, Z. S. X-Ray-Responsive Prodrugs and Polymeric Nanocarriers for Multimodal Cancer Therapy. *Chem. Commun.* **2023**, *59*, 8323-8331.

(7) Liu, H.; Zhao, J.; Xue, Y.; Zhang, J.; Bai, H.; Pan, S.; Peng, B.; Li, L.; Voelcker, N. H. X-Ray-Induced Drug Release for Cancer Therapy. *Angew. Chem. Int. Ed. Engl.* **2023**, *62*, e202306100.

(8) Wardman, P. Factors Important in the Use of Fluorescent or Luminescent Probes and Other Chemical Reagents to Measure Oxidative and Radical Stress. *Biomolecules* **2023**, *13*, 1041.

(9) Tanabe, K.; Ishizaki, J.; Ando, Y.; Ito, T.; Nishimoto, S. I. Reductive Activation of 5-Fluorodeoxyuridine Prodrug Possessing Azide Methyl Group by Hypoxic X-Irradiation. *Bioorg. Med. Chem. Lett.* **2012**, *22*, 1682-1685.

(10) Fu, Q.; Li, H.; Duan, D.; Wang, C.; Shen, S.; Ma, H.; Liu, Z. External-Radiation-Induced Local Hydroxylation Enables Remote Release of Functional Molecules in Tumors. *Angew. Chem. Int. Ed.* **2020**, *59*, 21546-21552.

(11) Ding, Z.; Guo, Z.; Zheng, Y.; Wang, Z.; Fu, Q.; Liu, Z. Radiotherapy Reduces N-Oxides for Prodrug Activation in Tumors. *J. Am. Chem. Soc.* **2022**, *144*, 9458-9464.

(12) Fu, Q.; Gu, Z.; Shen, S.; Bai, Y.; Wang, X.; Xu, M.; Sun, P.; Chen, J.; Li, D.; Liu, Z. Radiotherapy Activates Picolinium Prodrugs in Tumours. *Nat. Chem.* **2024**, *16*, 1348-1356.

(13) Geng, J.; Zhang, Y.; Gao, Q.; Neumann, K.; Dong, H.; Porter, H.; Potter, M.; Ren, H.; Argyle, D.; Bradley, M. Switching on Prodrugs Using Radiotherapy. *Nat. Chem.* **2021**, *13*, 805-810.

(14) Guo, Z. B.; Hong, H. Y.; Zheng, Y. D.; Wang, Z. Y.; Ding, Z. X.; Fu, Q. F.; Liu, Z. B. Radiotherapy-Induced Cleavage of Quaternary Ammonium Groups Activates Prodrugs in Tumors. *Angew. Chem. Int. Ed.* **2022**, *61*, e202205014.

(15) Tanabe, K.; Sugiura, M.; Ito, T.; Nishimoto, S. Synthesis and One-Electron Reduction Characteristics of Radiation-Activated Prodrugs Possessing Two 5-Fluorodeoxyuridine Units. *Bioorg. Med. Chem.* **2012**, *20*, 5164-5168.

(16) Gnaim, S.; Shabat, D. Activity-Based Optical Sensing Enabled by Self-lmmolative Scaffolds: Monitoring of Release Events by Fluorescence or Chemiluminescence Output. *Acc. Chem. Res.* **2019**, *52*, 2806-2817.

(17) Zielonka, J.; Sikora, A.; Hardy, M.; Joseph, J.; Dranka, B. P.; Kalyanaraman, B. Boronate Probes as Diagnostic Tools for Real Time Monitoring of Peroxynitrite and Hydroperoxides. *Chem. Res. Toxicol.* **2012**, *25*, 1793-1799.

(18) Maslah, H.; Skarbek, C.; Gourson, C.; Plamont, M. A.; Pethe, S.; Jullien, L.; Le Saux, T.; Labruere, R. In-Cell Generation of Anticancer Phenanthridine Through Bioorthogonal Cyclization in Antitumor Prodrug Development. *Angew. Chem. Int. Ed.* **2021**, *60*, 24043-24047.

(19) Jourden, J. L. M.; Daniel, K. B.; Cohen, S. M. Investigation of Self-Immolative Linkers in the Design of Hydrogen Peroxide Activated Metalloprotein Inhibitors. *Chem. Commun.* **2011**, *47*, 7968-7970.

(20) Kondengadan, S. M.; Wang, B. Quantitative Factors Introduced in the Feasibility Analysis of Reactive Oxygen Species (ROS)-Sensitive Triggers. *Angew. Chem. Int. Ed.* **2024**, *63*, e202403880.

(21) Liu, J.; Brevé, T. G.; Xu, B.; Hagedoorn, P.-L.; Denkova, A. G.; Eelkema, R. Organochlorides Mediate Oxidation Reactions Induced by Low Dose Ionizing Radiation. *CCS Chem.* **2024**, *6*, 1712-1720.

(22) Gupta, S.; Sureshbabu, P.; Singh, A. K.; Sabiah, S.; Kandasamy, J. Deoxygenation of Tertiary Amine N-oxides Under Metal Free Condition Using Phenylboronic Acid. *Tetrahedron Lett.* **2017**, *58*, 909-913.

(23) Yan, Z. C.; Pan, Y. Y.; Jiao, G. F.; Xu, M. Y.; Fan, D. G.; Hu, Z. W.; Wu, J. R.; Chen, T.; Liu, M.; Bao, X. G.; et al. A Bioorthogonal Decaging Chemistry of N-Oxide and

Silylborane for Prodrug Activation both In Vitro and In Vivo. *J. Am. Chem. Soc.* **2023**, *145*, 24698-24706.

(24) Zhou, Z.; Feng, S.; Zhou, J. J.; Ji, X. Y.; Long, Y. Q. On-Demand Activation of a Bioorthogonal Prodrug of SN-38 with Fast Reaction Kinetics and High Releasing Efficiency *In Vivo*. *J. Med. Chem.* **2022**, *65*, 333-342.

(25) Zhu, C.; Wang, R.; Falck, J. R. Mild and Rapid Hydroxylation of Aryl/Heteroaryl Boronic Acids and Boronate Esters with N-Oxides. *Org. Lett.* **2012**, *14*, 3494-3497.

(26) Gopiraman, M.; Bang, H.; Babu, S. G.; Wei, K.; Karvembu, R.; Kim, I. S. Catalytic N-Oxidation of Tertiary Amines on RuO_2NPs Anchored Graphene Nanoplatelets. *Catal. Sci. Technol.* **2014**, *4*, 2099-2106.

(27) Weber, L. W. D.; Boll, M.; Stampfl, A. Hepatotoxicity and Mechanism of Action of Haloalkanes: Carbon Tetrachloride as a Toxicological Model. *Crit. Rev. Toxicol.* **2003**, *33*, 105-136.

(28) Buxton, G. V.; Greenstock, C. L.; Helman, W. P.; Ross, A. B. Critical Review of Rate Constants for Reactions of Hydrated Electrons, Hydrogen Atoms and Hydroxyl Radicals ($\cdot OH/\cdot O^-$) in Aqueous Solution. *J. Phys. Chem. Ref. Data* **1988**, *17*, 513-886.

(29) Neta, P.; Grodkowski, J.; Ross, A. B. Rate Constants for Reactions of Aliphatic Carbon-Centered Radicals in Aqueous Solution. *J. Phys. Chem. Ref. Data* **1996**, *25*, 709-1050.

(30) Mönig, J.; Krischer, K.; Asmus, K. One-Electron Reduction of Halothane and Formation of Halide Ions in Aqueous Solutions. *Chem.-Biol. Interactions* **1983**, *45*, 43-52.

(31) Harris, A. L. Hypoxia--a Key Regulatory Factor in Tumour Growth. *Nat. Rev. Cancer* **2002**, *2*, 38-47.

(32) McKeown, S. R. Defining Normoxia, Physoxia and Hypoxia in Tumours-Implications for Treatment Response. *Brit. J. Radiol.* **2014**, *87*, 20130676.

(33) Mornex, F.; Girard, N. Gemcitabine and Radiation Therapy in Non-Small Cell Lung Cancer: State of the Art. *Ann. Oncol.* **2006**, *17*, 1743-1747.

(34) Pauwels, B.; Korst, A. E. C.; Lardon, F.; Vermorken, J. B. Combined Modality Therapy of Gemcitabine and Radiation. *Oncologist* **2005**, *10*, 34-51.

(35) Pandit, B.; Royzen, M. Recent Development of Prodrugs of Gemcitabine. *Genes (Basel)* **2022**, *13*, 466.

Supporting Information

General experimental methods

All solvents and chemicals were purchased from commercial suppliers (Sigma Aldrich, Tokyo Chemical Industry and abcr Gute Chemie) and used without further purification. Reactions were monitored by thin-layer chromatography (TLC) on a silica gel plate and visualized by UV light (254 nm). Flash column chromatography was carried out on a 30 cm column loaded with 230-400 mesh silica gel. ^{1}H-NMR and ^{13}C-NMR were recorded on an Agilent-400 MR DD2 at 298 K. Fluorescence spectra were recorded with Spex Fluorolog-3 equipped with a standard 90° setup. HPLC-MS was performed on a LTQ XL electrospray ionization source-mass spectrometer that was connected with a Shimadzu setup with a D2 detector and Discovery C18 reverse phase column. Water/MeCN with 0.1% (v/v) formic acid was used as the mobile phase at a flow rate of 0.2 mL/min. The irradiations with γ-rays were performed using a Nordion 220 ^{60}Co gamma cell. The dose rate at the experimental date was around 0.108 Gy/s which is calculated based on the decay law and the half-life of ^{60}Co. The delivered dose was calculated by the dose rate at the date of the experiments multiplied by the exposure time. The X-ray irradiation was carried out using an X-ray source (Philips MCN 321 variable-energy X-ray tube) performed in a working voltage of 240 keV and a current of 10 mA. The dose rate of the X-ray source was determined using the method as described in literature.[1] The X-ray irradiation was carried out using Philips MCN 321 variable-energy X-ray tube.

Synthesis

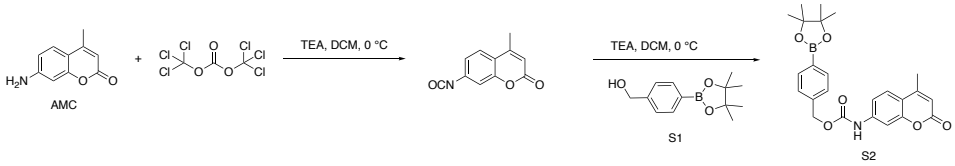

To a flame dried flask was added AMC (1 g, 5.71 mmol, 1.0 eq.), triphosgene (559 mg, 1.88 mmol, 0.3 eq.) and 20 mL DCM. The mixture was cooled to 0 °C using ice bath followed by dropwise adding triethylamine (TEA, 2.37 mL, 17.12 mmol, 3.0 eq.). The reacting mixture was then added compound **S1** (1.5 g, 6.28 mmol, 1.1 eq.) and was allowed to stir for overnight at room temperature. The solvent was evaporated under reduced

pressure. The crude product was purified by flash chromatography over a silica column, eluted with PE: EA from 20:1 to 1:1, to yield compound **S2** as white powder (1.45 g, 58.4%). ^{1}H-NMR (400 MHz, $CDCl_3$, ***δ***): 7.82 (d, *J* = 8.04 Hz, 2H), 7.51 (d, *J* = 8.64 Hz, 1H), 7.43-7.39 (m, 4H), 6.18 (s, 1H), 5.24 (s, 2H), 2.40 (s, 3H), 1.34 (s, 12H). ^{13}C-NMR (100 MHz, $CDCl_3$, ***δ***): 161.00, 154.45, 152.66, 152.13, 141.24, 138.48, 135.11, 127.40, 125.36, 115.60, 114.35, 113.23, 105.95, 83.91, 67.34, 29.69, 24.84, 18.55. MS (ESI+) *m/z* $[M + H]^+$ calculated for $[C_{24}H_{27}BNO_6]^+$, 436.19, found 436.10.

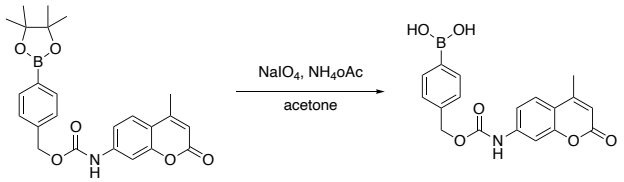

S2 BOH-AMC

Compound **S2** (70.0 mg, 0.16 mmol, 1 eq.) was added to 5 mL acetone followed by adding $NaIO_4$, (172.0 mg, 0.80 mmol, 5 eq.) and ammonium acetate (61.7 mg, 0.80 mmol, 5 eq.) in 2 mL deionized water. The mixture was stirred for 16 hours followed by removal of acetone under reduced pressure. The white precipitate was collected and washed with deionized water 3 times, to yield a white powder (35.0 mg, 61.9%). ^{1}H-NMR (400 MHz, MeOD, ***δ***): 7.66 - 7.60 (m, 4H), 7.42 - 7.36 (m, 3H), 6.17 (s, 1H), 5.21 (s, 2H), 2.42 (s, 3H). ^{13}C-NMR (100 MHz, MeOD, ***δ***): 162.00, 154.21, 154.00, 153.78, 142.97, 137.79, 133.71, 133.34, 126.75, 126.60, 125.31, 114.78, 114.48, 111.54, 104.87, 66.30 MS (ESI+) *m/z* $[M + H]^+$ calculated for $[C_{18}H_{17}BNO_6]^+$, 354.11, found 354.12.

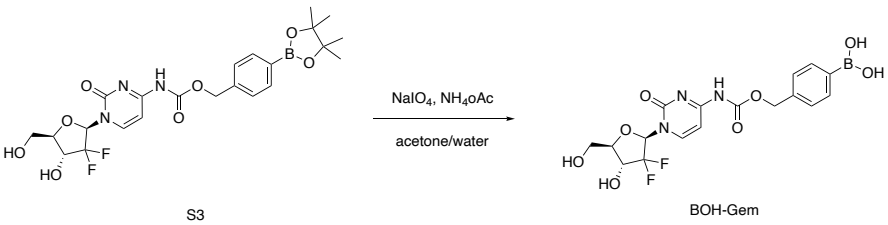

S3 BOH-Gem

Compound **S3** was synthesized using the method reported by Matsushita et al.[2] To a solution of compound **S3** (100.0 mg, 0.19 mmol, 1 eq.) in 5 mL acetone was added $NaIO_4$ (162.5 mg, 0.76 mmol, 4 eq.) and ammonium acetate (58.6 mg, 0.76 mmol, 4 eq.) in 2 mL

water. The mixture was allowed to stir at room temperature for 16 h. After the completion of the reaction, acetone was evaporated under reduced pressure. The precipitate was collected and washed with deionized water 3 times, to yield a white powder (55.0 mg, 65.2%). ^{1}H-NMR (400 MHz, MeOD, ***δ***): 8.30 (d, *J* = 7.68 Hz, 1H), 7.62 (d, *J* = 7.92 Hz, 2H), 7.41 (d, *J* = 7.96 Hz, 2H), 7.34 (d, *J* = 7.64 Hz, 1H), 6.24 (t, *J* = 7.24 Hz, 1H), 5.23 (s, 2H), 4.33-4.25 (m, 1H), 3.97-3.93 (m, 2H), 3.82-3.78 (m, 1H). ^{13}C-NMR (100 MHz, MeOD, ***δ***): 164.01, 156.01, 153.06, 144.23, 133.37, 126.82, 125.06, 122.49, 119.90, 95.62, 85.01, 81.34, 68.77, 67.15, 58.85. MS (ESI+) *m/z* $[M + H]^+$ calculated for $[C_{17}H_{19}BF_2N_3O_8]^+$, 442.12, found 442.01.

Preparation and irradiation of BOH-AMC solutions

A stock solution of BOH-AMC (10 mM) was prepared by dissolving 0.70 mg of BOH-AMC in 0.2 mL of dimethylformamide (DMF). To prepare a 10 μM BOH-AMC solution in phosphate buffered saline (PBS), 1 μL of the stock solution was added to 1 mL of PBS. If required, 1 μL of 2,2,2-trichloroethanol (TCE) was added to 1 mL of the solution to achieve a 12 mM TCE concentration, and 10 μL of a 10 mM amine solution in DMF was added to 1 mL of the PBS solution to reach a final amine concentration of 100 μM. After preparation, solutions are transferred to a Nordion 220 ^{60}Co gamma cell and irradiated for a specific period to reach a targeted dose.

Concentration-emission calibration curve of AMC

A stock solution of AMC (5 mM) was prepared by dissolving 0.28 mg of AMC in 329 μL of DMF. This stock solution was subsequently diluted to the desired concentrations using deionized water. The parameters were set as follows: sensitivity, 600 V; spectrum acquisition starts from 385 nm ends at 500 nm; excited wavelength, 365 nm; response, 4 msec; band width 5 nm; accumulation, 1. The maximum emission intensities at 441 nm were plotted against the concentrations to obtain the concentration-emission calibration curve.

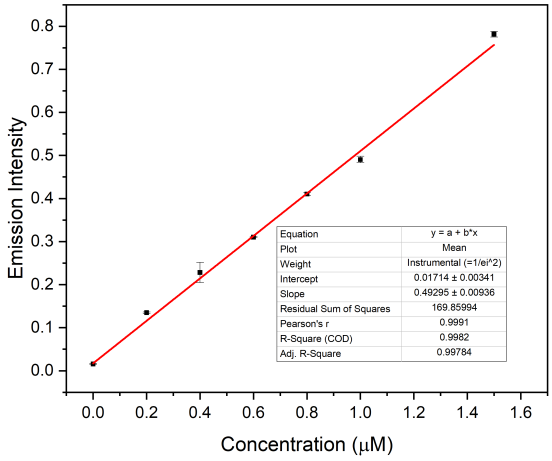

Figure S6.1. The intensity to concentration calibration curve of AMC. Error bars represent experimental variation of three samples.

Detection of N-oxide using HPLC-MS spectrometer

Compound 9 was dissolved in 1 mL water with a concentration of 100 μM. 1 μL of TCE was added to prepare a 12 mM TCE solution. The vials were placed in the center of the Nordion 220 ^{60}Co gamma cell. After irradiation, the samples were subjected to HPLC-MS with the mass spectrum detected in positive mode.

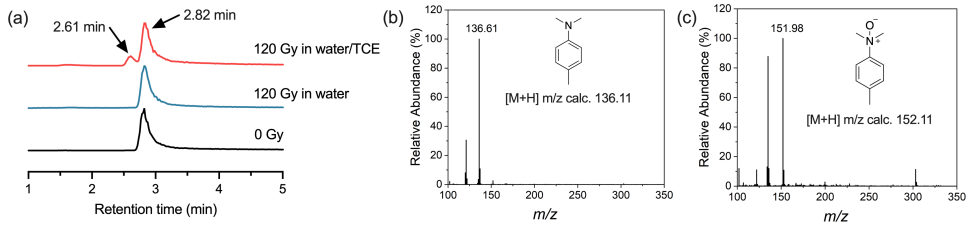

Figure S6.2. (a) HPLC-MS chromatograph (mass channel at selected ions) of amine **9** before exposure to radiation and after irradiation for 120 Gy in water and water/TCE; (b) mass spectrum at 2.82 min; (c) mass spectrum at 2.61 min.

Preparation of BOH-AMC solutions with varying oxygen concentrations

BOH-AMC solution with targeted concentrations of amine and TCE were prepared as described before. The solution was transferred into a 1.5 mL vials with septum cap. The samples were bubbled with controlled flow of oxygen and nitrogen through needles. For

the samples with 21% oxygen, no bubbling process was applied. After regulating the partial pressure, the needles were removed and the septum cap was sealed with grease.

IC50 viability assay

U87 cells (human glioblastoma cell line) were cultured in Dulbecco's modified Eagle's medium (DMEM, Gibco) containing 10% fetal bovine serum (Biowest) and 1% penicillin/streptomycin (VWR) in a cell incubator (Heracell®, Heraeus) with a humidified atmosphere containing 5% CO_2 at 37 °C.

8000 U87 cells were seeded in 96-well plates overnight. Gemcitabine and BOH-Gem were dissolved in DMSO to obtain stock solutions of 10 mM, respectively. Afterwards, the stock solution of Gem and Pro-G were diluted to 100, 10, 1, 0.1, 0.05, 0.025, 0.01, 0.001 μM with DMEM. Subsequently, 100 μL of DMEM containing various concentrations of drug were added into cells. After 48 hours incubation, cells were washed with PBS twice, followed by adding 100 μL Cell Counting Kit-8 (CCK-8, Dojindo Laboratories, Japan)/DMEM = 1:9. The viability of the cells was determined by the absorbance at 450 nm wavelength by a microplate scanning spectrophotometer (PowerWave XS™, Bio-Tek). Each concentration was tested in six replicates.

2D cell viability assay

Gemcitabine and BOH-Gem were dissolved in DMSO to get stock solutions of 10 mM. The stock solutions were diluted to 100 μM using PBS, and subsequently diluted to 20 nM using DMEM or DMEM containing 500 μM TCE and 5 μM amine **1**.

8000 U87 cells were seeded in 96 well plates and incubated overnight. The solutions added to the cells were: control, 100 μL of DMEM; A+T, 100 μL DMEM containing 500 μM TCE and 5 μM amine **1**; BOH-Gem, 100 μL DMEM containing 20 nM BOH-Gem; BOH-Gem+A+T, 100 μL DMEM containing 20 nM BOH-Gem, 500 μM TCE and 5 μM amine **1**; Gem+A+T, 100 μL DMEM containing 20 nM Gem, 500 μM TCE and 5 μM amine **1**. After treatments, cells were exposed to X-ray irradiation (240 kV, 15 mA) for 6 Gy. After 48 hours incubation, cells were washed with PBS twice, followed by adding 100 μL CCK-8/DMEM = 1:9 to test the viability. The viability of non-irradiated groups was normalized

to “control”, and the viability of irradiated group was normalized to “6 Gy” group. Each group was tested in six replicates.

References

(1) Yao, T.; Luthjens, L. H.; Gasparini, A.; Warman, J. M. A Study of Four Radiochromic Films Currently Used for (2D) Radiation Dosimetry. *Radiat. Phys. Chem.* **2017**, *133*, 37-44.

(2) Matsushita, K.; Okuda, T.; Mori, S.; Konno, M.; Eguchi, H.; Asai, A.; Koseki, J.; Iwagami, Y.; Yamada, D.; Akita, H.; et al. A Hydrogen Peroxide Activatable Gemcitabine Prodrug for the Selective Treatment of Pancreatic Ductal Adenocarcinoma. *ChemMedChem* **2019**, *14*, 1384-1391.

Conclusions and Outlook

7

This research focused on developing radiation-initiated chemical reactions for drug release from nanocarriers or prodrug activation, aiming to integrate these processes with combined radiotherapy and chemotherapy. In biological systems, such radiation-initiated reactions are primarily mediated by species generated from water radiolysis. In Chapter 2, we explained the physical and chemical processes of water radiolysis, detailing the products formed, the radiolytic yield of each species, and the reaction mechanisms of these species with various functional groups. Hydroxyl radicals, for example, have been reported to trigger drug release. However, due to their rapid reactivity with sugars and amino acids present at high concentrations *in vivo*, functional groups targeting hydroxyl radical need to be very sensitive. Of all the reactive species from water radiolysis, aqueous electrons have recently drawn researchers' attention for their unique way of generation and reaction: they are produced only by ionizing radiation, so functional groups designed to react with aqueous electrons are less likely to be activated by cellular components. Aqueous electrons are also among the more abundant species from water radiolysis (0.28 μM/Gy), making activation more efficient compared to other species, such as hydrogen peroxide (0.07 μM/Gy). They are strong reductants with a potential of –2.9 V (*vs*. H^+/H_2), and the hypoxic microenvironment of most tumors favors reduction reactions, enabling the reduction of various compounds *in vivo*.

In Chapter 3, we found that irradiating 12 mM chloroform in aqueous solutions generated a strong oxidant, which oxidized a stilbene derivative at its double bond motif, resulting in the formation of two aldehydes. We investigated the reaction mechanism by selectively scavenging oxygen or individual species from water radiolysis. Aqueous electrons and oxygen were identified as key participants in the oxidation, further corroborated by electron paramagnetic resonance (EPR) measurements. We hypothesized that chloroform reacts with aqueous electrons to produce a carbon-centered radical and a chloride ion. This radical then reacts with molecular oxygen to form a peroxyl radical, which subsequently oxidizes the stilbene. An amphiphilic block copolymer was synthesized using stilbene as the linker between two polymer blocks. In aqueous solutions containing chloroform, the polymer formed micelles with high loading efficiency for doxorubicin. Under 15 Gy γ-irradiation, oxidation of the stilbene linker led to polymer cleavage and subsequent drug release. However, this release approach is not compatible with *in vivo* applications because the

chloroform concentration required to initiate oxidation is too high for clinical use. Future research should focus on: (1) identifying other organochlorides that are less toxic and more efficient at oxidizing substrates, (2) determining the minimum effective concentration of organochlorides for oxidation, and (3) discovering substrates or functional groups susceptible to peroxyl radical oxidation, with the goal of applying these in designing drug nanocarriers or prodrugs.

In Chapter 4, we explored whether polymeric organochlorides function similarly to small-molecule organochlorides by attaching 2,2,2-trichloroethanol to polymer backbones. We observed that 4-(methylthio)phenol was oxidized to 4-(methylsulfinyl)phenol upon irradiation in aqueous solution when organochlorides were present. Using 4-(methylthio)phenol as the reducing agent, we found that when the organochloride was bonded to the hydrophobic region of a block copolymer, oxidation was significantly inhibited due to limited accessibility of the organochloride to aqueous electrons. However, when the organochloride was bonded to the hydrophilic block, the oxidation proceeded comparably to that with 2,2,2-trichloroethanol. The possibility of using polymeric organochlorides could help reduce organochloride toxicity. For example, attaching hydrophilic organochloride polymer chains to a tumor-targeting antibody could achieve a locally high concentration of organochloride. Furthermore, as thioether oxidation has been utilized in reactive oxygen species (ROS)-triggered drug release systems, [1-3] the ability to oxidize thioethers could provide additional opportunities for designing radiation-initiated drug release systems.

The fact that the efficiency of organochloride-mediated oxidation depends on the concentration of organochloride was observed in Chapter 3, with higher concentrations resulting in increased oxidation. In Chapter 5, we explored this effect further and found that the yield of the oxidizing product also depends on the concentration of molecular oxygen in the solution. It has been reported that aqueous electrons can react with molecular oxygen to form superoxide, an unreactive species toward organochloride. So, we proposed a competitive mechanism and constructed a model based on the proposed reaction network, calculating peroxyl radical yields at various concentrations of organochloride and oxygen. The model suggested that at low organochloride concentrations (e.g., 250 μM), the yield of

peroxyl radicals peaks at approximately 20 μM oxygen (about 2% partial pressure). The yield gradually decreases as oxygen concentration rises from 2% to 21% and drops sharply to zero between 2% and 0% oxygen. Certain tumors are extremely hypoxic, with oxygen levels below 0.01% in their cores, potentially significantly inhibiting organochloride-mediated oxidation in these areas.

We experimentally measured peroxyl radical yields using 4-(methylthio)phenol as a reducing agent. The experimental results aligned with the calculated trend and supported the proposed mechanism. However, we did not include side reactions in the model, which may account for some discrepancies between the experimental and simulated data. Future research should incorporate side reactions, such as radical recombination and aqueous electron scavenging by cysteine, to provide a more accurate yield of the oxidizing product in biological systems. Additionally, we explored the use of 4-(methylthio)phenol as a caging agent for carboxylic acids, aiming for fast ester hydrolysis following thioether oxidation. We observed greater carboxylic acid recovery after irradiation in the presence of organochloride compared to a control group without organochloride. However, the oxidation yield was lower than expected, likely due to the poor water solubility of the ester. Future research should address the reduction in water solubility of drugs when carboxylic acid groups are caged by 4-(methylthio)phenol.

Boronic acid and its esters have been widely studied as caging groups for prodrugs targeting ROS. In Chapter 6, we demonstrated that boronic acid can also be activated by peroxyl radicals generated during the irradiation of aqueous solutions containing organochloride. Additionally, we found that this oxidation can be catalyzed by *N*,*N*-dimethylaniline derivatives. The oxidation of boronic acid followed the trend observed in Chapter 5, where 2% oxygen yielded the highest oxidation efficiency at 100 μM organochloride. We synthesized a prodrug in which the 4-amino group of gemcitabine was protected by a boronic acid-caged self-immolative linker. Irradiation of solutions containing the prodrug, an organochloride, and an *N*,*N*-dimethylaniline derivative resulted in toxicity toward the U87 cell line comparable to that of irradiated gemcitabine solutions, indicating efficient drug activation. The relatively lower activation of the prodrug at 5% oxygen compared to 2% oxygen could also help reduce drug activation in healthy tissues, which

typically have an average oxygen concentration of about 5%. To make it applicable in clinical, future research should focus on reducing organochloride toxicity, and investigating radiation-induced drug release in realistic environments to include scavenging reactions in the oxidation process.

References

(1) Crielaard, B. J.; Rijcken, C. J.; Quan, L.; van der Wal, S.; Altintas, I.; van der Pot, M.; Kruijtzer, J. A.; Liskamp, R. M.; Schiffelers, R. M.; van Nostrum, C. F.; et al. Glucocorticoid-Loaded Core-Cross-Linked Polymeric Micelles with Tailorable Release Kinetics for Targeted Therapy of Rheumatoid Arthritis. *Angew. Chem. Int. Ed.* **2012**, *51*, 7254-7258.

(2) Luo, C.; Sun, J.; Liu, D.; Sun, B.; Miao, L.; Musetti, S.; Li, J.; Han, X.; Du, Y.; Li, L.; et al. Self-Assembled Redox Dual-Responsive Prodrug-Nanosystem Formed by Single Thioether-Bridged Paclitaxel-Fatty Acid Conjugate for Cancer Chemotherapy. *Nano Lett.* **2016**, *16*, 5401-5408.

(3) Wang, J.; Sun, X.; Mao, W.; Sun, W.; Tang, J.; Sui, M.; Shen, Y.; Gu, Z. Tumor Redox Heterogeneity-Responsive Prodrug Nanocapsules for Cancer Chemotherapy. *Adv. Mater.* **2013**, *25*, 3670-3676.

Summary

Ionizing radiation-induced drug release offers a great opportunity to combine radiotherapy and chemotherapy in cancer treatment. This release is mediated by reactive species generated from water radiolysis. However, the low radiolytic yield of these species limits the amount of drug released, and their high reactivity toward many cellular components make targeted drug release challenging. This thesis aims to explore radiation-initiated reactions and their application in triggering drug release in living systems.

In **Chapter 1**, we provided a general introduction to cancer therapies, focusing on radiotherapy and chemotherapy. We explained the research goals of this Thesis and outline the content of each chapter.

In **Chapter 2**, we presented a literature review of the recent progress in radiation-targeted drug release. We started by briefly introducing the basics of radiation chemistry in aqueous solutions and discussed why reactive species from water radiolysis are suitable for triggering drug release. We then explored the reactivity of these species with specific functional groups and substrates, followed by a discussion of their reactions with cellular components. Finally, we summarized recent developments in reactions used for radiation-induced drug release, aiming to provide readers with a comprehensive guide to designing radiation-sensitive drug release systems.

In **Chapter 3**, we found that irradiation of aqueous solutions containing chloroform or other multi-chloro compounds can generate oxidizing species. Through mechanistic studies, we revealed that the oxidizing species were peroxyl radicals, generated from the reactions between aqueous electrons and chlorinated molecules. An amphiphilic block copolymer with stilbene serving as the linkage between the two building blocks underwent oxidative cleavage when exposed to radiation in PBS with 0.1 vol% chloroform. The cleavage of the block copolymer led to the disruption of micelles, resulting in the release of encapsulated drugs. These findings initiated the study of organochloride-mediated oxidation induced by ionizing radiation.

In Chapter 4, we addressed the issue of applying organochlorides in biological systems, noting their toxicity to the liver at elevated concentrations. We showed that organochloride groups covalently attached to a hydrophilic polymer backbone could mediate the oxidation of thioethers to sulfoxides, similar to small molecule organochlorides. However, if the organochloride was attached to the hydrophobic region of a block copolymer that formed micelles in aqueous solution, the radiation-induced oxidation was significantly inhibited.

In Chapter 5, to further analyze the mechanism of peroxyl radical generation, we developed a reaction network and constructed a mathematical model incorporating key reactions within the network. The calculated yields of peroxyl radicals at various concentrations of oxygen and organochloride were consistent with experimental results, where a thioether was employed as a scavenger of the peroxyl radical. The agreement between the theoretical model and experimental results supported the validity of our proposed mechanism.

In Chapter 6, we demonstrated that an arylboronic acid-based caging group could be oxidized by peroxyl radicals, with a significant enhancement in the presence of *N*,*N*-dimethylaniline derivatives during irradiation. The *N*,*N*-dimethylaniline derivative functioned as a catalyst, undergoing oxidation by peroxyl radicals to form the N-oxide, which was subsequently reduced by arylboronic acid to complete a catalytic cycle. Similar to the findings in Chapter 5, the yield of the oxidation product depended on the oxygen concentration. When prodrug solutions containing organochloride and an *N*,*N*-dimethylaniline derivative were exposed to clinical doses of radiation, they exhibited comparable cytotoxicity to the parent drug group.

In conclusion, we have developed an organochloride-mediated oxidation process induced by ionizing radiation. The formed peroxyl radical can oxidize a wide range of functional groups, some of which are promising as caging agents for chemotherapeutics. Organochloride groups attached to hydrophilic polymers functioned similarly to small molecular organochlorides. We found that the yield of oxidizing agents was higher at low oxygen levels, which could protect healthy tissues (generally higher in oxygen levels) from oxidation-induced drug release. Based on all the findings in this thesis, we believe that

organochloride-mediated oxidation will shed new light on ionizing radiation-induced drug release.

Samenvatting

Ioniserende straling-geïnduceerde medicijnafgifte biedt een uitstekende mogelijkheid om radiotherapie en chemotherapie te combineren bij de behandeling van kanker. Deze afgifte wordt bewerkstelligd door reactieve deeltjes die worden gegenereerd tijdens de radiolyse van water. Echter, de lage radiolytische opbrengst van deze soorten beperkt de hoeveelheid vrijgekomen medicijn, en hun hoge reactiviteit ten opzichte van vele cellulaire componenten maakt gerichte medicijnafgifte uitdagend. Dit proefschrift heeft tot doel straling-geïnitieerde reacties en hun toepassing in het activeren van medicijnafgifte in levende systemen te onderzoeken.

In Hoofdstuk 1 hebben we een algemene introductie gegeven over kankertherapieën, met de nadruk op radiotherapie en chemotherapie. We hebben de onderzoeksdoelen van dit proefschrift uitgelegd en een overzicht gegeven van de inhoud van elk hoofdstuk.

In Hoofdstuk 2 hebben we een literatuuroverzicht gepresenteerd van de recente vooruitgang in stralingsgerichte medicijnafgifte. We begonnen met een korte introductie van de basisprincipes van stralingschemie in waterige oplossingen en bespraken waarom reactieve deeltjes uit waterradiolyse geschikt zijn voor het activeren van medicijnafgifte. Vervolgens hebben we de reactiviteit van deze deeltjes met specifieke functionele groepen en substraten onderzocht, gevolgd door een bespreking van hun reacties met cellulaire componenten. Ten slotte hebben we recente ontwikkelingen in reacties voor straling-geïnduceerde medicijnafgifte samengevat, met als doel de lezers een uitgebreide handleiding te bieden voor het ontwerpen van stralingsgevoelige medicijnafgiftesystemen.

In Hoofdstuk 3 ontdekten we dat bestraling van waterige oplossingen die chloroform of andere multi-chloorverbindingen bevatten, oxiderende deeltjes kan genereren. Door middel van mechanistische studies hebben we kunnen vaststellen dat de oxiderende soorten peroxylradicalen waren, gegenereerd uit de reacties tussen gesolvateerde elektronen en gechloreerde moleculen. Een amfifiele blokcopolymeer met stilbeen als verbinding tussen de twee blokken onderging oxidatieve splitsing wanneer het werd blootgesteld aan straling

in PBS met 0,1 vol% chloroform. De splitsing van het blokcopolymeer leidde tot de verstoring van micellen, wat resulteerde in de afgifte van ingesloten medicijnen. Deze bevindingen waren het begin van de studie naar organochloride-gemedieerde oxidatie geïnduceerd door ioniserende straling.

In Hoofdstuk 4 hebben we de toepassing van organochloriden in biologische systemen behandeld, waarbij we hun toxiciteit voor de lever bij verhoogde concentraties benadrukten. We hebben aangetoond dat organochloridegroepen die covalent zijn gebonden aan een hydrofiele polymeerketen de oxidatie van thioethers tot sulfoxiden kunnen mediëren, vergelijkbaar met kleine moleculaire organochloriden. Echter, als de organochloride was gebonden aan het hydrofobe deel van een blokcopolymeer dat micellen vormde in een waterige oplossing, werd de door straling geïnduceerde oxidatie aanzienlijk geremd.

In Hoofdstuk 5, om het mechanisme van peroxylradicaalvorming verder te analyseren, hebben we een reactienetwerk ontwikkeld en een wiskundig model opgesteld waarin de belangrijkste reacties binnen het netwerk zijn opgenomen. De berekende opbrengsten van peroxylradicalen bij verschillende concentraties zuurstof en organochloride waren consistent met experimentele resultaten, waarbij een thioether werd gebruikt als opvanger van het peroxylradicaal. De overeenstemming tussen het theoretische model en de experimentele resultaten ondersteunde de geldigheid van ons voorgestelde mechanisme.

In Hoofdstuk 6 toonden we aan dat een arylboorzuur-gebaseerde beschermgroep kon worden geoxideerd door peroxylradicalen, met een significante verbetering in aanwezigheid van *N*,*N*-dimethylaniline derivaten tijdens bestraling. Het *N*,*N*-dimethylaniline derivaat fungeerde als een katalysator, onderging oxidatie door peroxylradicalen om het N-oxide te vormen, dat vervolgens werd gereduceerd door arylboorzuur om een katalytische cyclus te voltooien. Vergelijkbaar met de bevindingen in Hoofdstuk 5, was de opbrengst van het oxidatieproduct afhankelijk van de zuurstofconcentratie. Wanneer prodrugoplossingen met organochloride en een *N*,*N*-dimethylaniline derivaat werden blootgesteld aan klinische doses straling, vertoonden ze vergelijkbare cytotoxiciteit als de oorspronkelijke geneesmiddelengroep.

Samenvattend hebben we een organochloride-gemedieerde oxidatieproces ontwikkeld dat wordt geïnduceerd door ioniserende straling. Het gevormde peroxyl radicaal kan een breed scala aan functionele groepen oxideren, waarvan sommige veelbelovend zijn als afschermingsagenten voor chemotherapeutica. Organochloridegroepen gebonden aan hydrofiele polymeren functioneerden vergelijkbaar met kleine moleculaire organochloriden. We ontdekten dat de opbrengst van oxiderende agentia hoger was bij lage zuurstofniveaus, wat gezonde weefsels (doorgaans hoger in zuurstofniveaus) zou kunnen beschermen tegen oxidatie-geïnduceerde medicijnafgifte. Gebaseerd op alle bevindingen in dit proefschrift geloven we dat organochloride-gemedieerde oxidatie nieuw licht zal werpen op ioniserende straling-geïnduceerde medicijnafgifte.

List of publications

Publications

Related to this Thesis:
Liu, J.; Brevé, T. G.; Xu, B.; Hagedoorn, P.-L.; Denkova, A. G.; Eelkema, R. Organochlorides Mediate Oxidation Reactions Induced by Low Dose Ionizing Radiation. *CCS Chem.*, **2024**, *6*, 1712-1720.
Liu, J.; Xu, B.; Denkova, A. G.; Eelkema, R. Organochloride Mediated Prodrug Activation Induced by Ionizing Radiation, in preparation.
Liu, J.; Xu, B.; Uslamin, E.; Li, Z.; Denkova, A. G.; Eelkema, R. Reaction Network Analysis of Organochloride Mediated Oxidation Induced by Ionizing Radiation, in preparation.
Liu, J.; Piergentili, I.; Xu, B.; Denkova, A. G.; Eelkema, R. Polymeric Organochloride Mediated Thioether Oxidation Induced by Ionizing Radiation, in preparation.
Liu, J.; Denkova, A. G.; Eelkema, R. The Role of Ionizing Radiation-Initiated Reactions in Targeted Delivery of Chemotherapeutics, in preparation.

Others:
Liu, J.; Lu, H.; Liu, Y.; Zhang, J.; Li, C.; Xu, X.; Bo, Z.; Efficient Organic Solar Cells Based on Non-Fullerene Acceptors with Two Planar Thiophene-Fused Perylene Diimide Units. *ACS Appl. Mater. Interfaces*, **2020**, *12*, 10746-10754.
Liu, J.#; Xie, S.#; Feng, S.; Li, M.; Wu, L.; Xu, X.; Chen, X.; Li, C.; Bo, Z. A Propeller-Shaped Perylene Diimide Hexamer as a Nonfullerene Acceptor for Organic Solar Cells. *J. Mater. Chem. C*, **2018**, *6*, 9336-9340. (#authors contributed equally)

Oral presentations

Juncheng Liu, Activating prodrugs by X-rays and gamma rays. 19th Radiochemical Conference, Marianske Lazne, Czech Republic, 2022.
Juncheng Liu, Organochlorides mediate oxidation reactions induced by ionizing radiation. Dutch Symposium on Organic Chemistry 2024, Lunteren, The Netherlands, 2024.

Acknowledgements

First of all, I would like to thank my promotors **Dr. Rienk Eelkema** and **Dr. Antonia Denkova** for providing me the chance to work on this interesting yet challenging project. I enjoyed every *Thursday* meeting with you. **Rienk**, your expertise in chemistry surprised me in our first interview, when you asked a crucial question on my master's topic after a 5 minute presentation. From that time, I knew the PhD journey would not be boring. Your door was always open when I need help. I appreciate your enlightening suggestions over the 4 years, especially when my research went into "dead end". Thanks for your detailed explanation on the reaction mechanisms. Thanks for your patience in correcting my manuscripts and slides. **Antonia**, it was very delightful to work with you since your were always open to my ideas and tried your best to help with all the experiments. Thanks for creating a relaxing working environment. Thanks for speaking to me when I was in trouble with SBE.

Also, my great gratitude goes to the whole defence committee for their time on correcting my thesis and giving comments. Thanks for my ISE neighbours since I received from you not only lab supporting but also scientific inputs from you. Thanks to **Prof. Dr. Evgeny Pidko** for the meaningful discussion on the oxidation mechanism of stilbene and the reaction network of peroxyl radical generation. Thanks for **Dr. Evgeny Uslamin** on the coding of reaction networks. Thanks for **Dr. Georgy Filonenko** for the straightforward suggestions at the beginning of my PhD; thanks for your "patient" guidance on the usage of LCMS, your tolerance of me stealing countless syringes, needles, filters, chemicals form your lab, and your tutorial in the gym. Thanks for taking care of each other on all the late experiments. Thanks for **Dr. Robin de Kruijff** for your suggestions on the cryo-EM analysis. Thanks for **Dr. Peter-Leon Hagedoorn** for your kindness explanation on the EPR measurements

Most of the experiments in this thesis would be extremely difficult without the help of technicians. **Sietse**, thank you for taking care all the lab issues, giving tutorial, ordering stuff, repairing instruments. Thanks for ordering drinks and pizzas on our Thursday borrel. **Stephen**, thanks for your help on the NMR instrument. Every time I got problem, I sent a message and you came in minute. Thanks for your suggestions when I got ugly spectrum,

and your support on setting up the Bruker one. **Aleksandra**, thanks for organizing lab cleaning. You always do much more than us and make sure our lab is clean and well-organized. **Marcel**, thanks for taking care of lab safety and your suggestions on using lab goggles. **Liliana**, thanks for your help on all the LC experiments. **Astrid**, thanks for your help on the LC instrument in reactor, also for your help on the cell experiments. **Baukje**, thanks for giving tutorial in the reactor labs. We had nice chat in lab and conferences. **Wiel**, thanks for preparing cryo-EM samples and measuring them, I enjoyed our chat during those experiments. **Marc**, thanks for the guide on the Clark electrode.

Thanks for all the "old legends" of ASM and ARI group. **Yongjun**, thanks for your suggestion when I was looking for a PhD position, and for introducing me to Rienk. **Qian**, thank you for your treat when I visited Guangzhou, and for your suggestions on my future career. **Tobias**, thanks for your lab tour on my first day in ASM. Thanks for your help on the beginning of my PhD, and for your suggestions on the stilbene paper. **Reece**, **Irene**, **Benj**, **Hendrik**, **Mark**, **Peggy** thanks for your help on the lab works. I do enjoyed our time making videos and having pizzas after lar cleaning. **Bowen**, **Bohang**, **Yu**, **Jianan**, I will never forget our time playing football and board games, and our travel to Texel! **Min**, thanks for setting up the synthetic gas line for me in your working place! One of the chapter would not be there without your help! **Huanhuan**, you are like an elder sister taking care of me. You always cheer me up when I'm upset about my work or life. Thanks for your suggestions on my experiments. Thank for organizing hotpot night at the beginning of my PhD, which made me feel like home. I wish you and your daughter all the best. **Chao**, thanks for nominating me as your neighbour. I could have nowhere to live without it. **Qi**, thanks for your help on the lab work in reactor, also for bring delicious snacks! **Gauri**, thanks for bring India snacks and sweets. **Benni**, it was great to work with you on supervising LO2 students, I learnt a lot from you! Thanks for bringing chocolate and home-made coffee! **Guotai**, thank for your help and suggestions on synthesis, and your suggestions on choosing future career, and for the discussions on publishing papers. Thanks for your treat when I was visiting Qindao. **Suellen**, I enjoyed our chat a lot! I like your laugh, it's very unique. **Anand**, we started close to each other, thanks for being with me in the big office downstairs! **Dennis**, it was great to work and talk with you, both in lab and in office. I like your jokes although sometimes I can't get them at first. **Sereno**, it was

happy to work with you. I also enjoyed our time together. Hope to see you in China. For all the office mate, **Sarah**, **Elmira**, **Gijs**, **Fabiana**, **Tamar**, **Dnyandevi**, **Ardshir**, **Daniel**, **Rogier**, **Robin**, **Svenja** and **Ester**. I appreciated our time together. Thanks for all the students who worked with me, **Jisca**, **Taihong**, **Rebecca**, **Kees** and all the LO2 students!

Runze, it was you who encouraged me when I was not so confident to myself to peruse a PhD outside China. Thanks for your warm welcome when I first arrived in the Netherlands, to make me feel home on the other side of the continent. Thanks for hearing me complaining about failed experiments (sure you were also complaining yours). Thanks for your patience answering every simple question, so that you gave us a feeling that "Runze knows everything". I'll never forget our travel to Koln, Berlin, Croatia etc. I wish you a great success in your career.

Bing, you're the best collaborator! Appearing in every chapter and paper of my thesis. Thanks for elaborate all the cell experiments. I appreciate the time we discussing the experimental setups. Thanks for providing suggestions while I was sick! You will be an excellent doctor!

Zichao, I really enjoyed our road bike journey all over Netherlands, not only for the view on the road, but also for the in-depth discussion about general science, technology, philosophy and politics, which happened on the train. We've circled more than half of Netherlands, with more than 1000 miles on road! It was great to have you. I wish you a great success in your career.

最后，我要感谢我的家人们对我的支持与陪伴。感谢我的妻子在我最孤单的时候来荷兰陪我读书，在实验失败的时候安慰我，在失落的时候鼓励我，在压力大的时候带我出去逛。感谢你的陪伴，信任与支持，在这一刻，以及今后的每一刻，所有的欢呼都是属于我们俩的。感谢我的爸爸，妈妈，岳父，岳母，哥哥对我们小家的支持，我爱你们！

Curriculum Vitae

Juncheng Liu was born in 1995 in Tianjin, China. After graduating from high school in 2013, he pursued his studies at Beijing Normal University, China, and got his B.Sc. in Chemistry in 2017. He got a postgraduate recommendation to the group of Prof. Zhishan Bo and continued his master studies in polymer chemistry. His researched perylene diimide based materials used in polymeric organic solar cells. After three years study, in 2020 he obtained M.Sc. degree in chemistry with the honor of Excellent Graduate of Beijing. Subsequently, he joined the group of Dr. Rienk Eelkema and Dr. ir. Antonia G. Denkova at Delft University of Technology. His research focuses on the application of ionizing radiation-initiated reactions in the design of radiation sensitive drug delivery systems.